AN ABSTRACT OF THE THESIS OF

Sri Sai Kameswara Mullapudi for the degree of Master of Science in Electrical and Computer Engineering presented on March 17, 2016

Title: Fabrication of Cost-effective Flexible Glucose Sensor for Continuous Glucose Monitoring

Abstract approved:

_____

John F. Conley, Jr.

Diabetes is a pandemic that affects nearly 29.1 million Americans and the fourth leading cause of mortality in the US. Type 1 diabetes is a chronic condition which occurs due to little to no production of insulin by the pancreas. This form of diabetes requires constant monitoring of blood glucose and administration of insulin, necessitating the need for an artificial pancreas. This work is aimed towards creating an artificial pancreas and focuses on fabrication process of a glucose sensor on a titanium clad polyimide flexible substrate. In particular, controlled laser ablation as a novel process to pattern titanium is discussed, which has broader potential applications in the field of flexible substrate processing for other bio-sensing applications.

Fabrication of Cost-effective Flexible Glucose Sensor for Continuous Glucose Monitoring

by
Sri Sai Kameswara Mullapudi

A THESIS

submitted to

Oregon State University

in partial fulfillment of
the requirements for the
degree of

Master of Science

Presented March 17, 2016
Commencement June 2016

Master of Science thesis of Sri Sai Kameswara Mullapudi presented on March 17, 2016

APPROVED:

Dr. John F. Conley Jr., Major Professor, representing Electrical and Computer Engineering

Dr. V John Mathews, Director of the School of Electrical Engineering and Computer Science

Brenda McComb, Dean of the Graduate School

I understand that my thesis will become part of the permanent collection of Oregon State University libraries. My signature below authorizes release of my thesis to any reader upon request.

Sri Sai Kameswara Mullapudi, Author

ACKNOWLEDGEMENTS

I would like to first express sincere gratitude to my parents for their encouragement and support, while I continue my education in a new country.

I have nothing but sincere appreciation and respect for Dr. John Conley for aiding my transition to graduate school and will remain a role model for me for many years to come. Dr. Xuebin has contributed immensely to this project and helped me discover my passion for process design and Dr. Nishit Murari was instrumental in helping me shape my professionalism and uplifting me emotionally. Dr. Greg Herman, Dr. Yajuan Li, and Dr. Xiaosong Du all contributed to the development of this work.

The team of Pacific Diabetes Technologies Inc., have been exceptionally helpful in the planning and execution of this project. In particular, I would like to thank the CEO, Dr. Robert Cargill and the MD, Dr. Kenneth Ward for providing direction, inputs and feedback throughout this endeavor. Joe Kowalski, Chad Knutsen and Tyler Milhem have provided exceptional help during the technology transfer. I sincerely wish them the best in their mission to make continuous glucose monitoring affordable and hope they will be successful in continuing their work.

Primary funding for this project was provided by Leona M. and Harry B. Helmsley Charitable Trust Grant #2015PG-T1D046. The OSU Materials Synthesis and Characterization Facility (MaSC), the Microproducts Breakthrough Institute (MBI) and Electron Microscopy Facility (EMF) at OSU provided the tools and facilities that made this work possible. I would like to thank Chris Tasker and Rick

Presley of MASC and Neill Thornton of MBI for training me on process tools and their valuable inputs.

I would also like to thank Dustin Austin, Sean Smith and other members of Dr. Conley's group for providing me help and valuable inputs throughout my project. Finally, I would like to express sincere appreciation for each of the professors that I took classes from and Drs. Greg Herman, Larry Cheng, Adam Higgins and again, Dr. John Conley for serving on my thesis committee.

TABLE OF CONTENTS

Page

TABLE OF CONTENTS (Continued)

Page

TABLE OF CONTENTS (Continued)

Page

LIST OF FIGURES

LIST OF FIGURES (Continued)

Figure Page

LIST OF FIGURES (Continued)

LIST OF TABLES

1. Introduction

Healthcare costs of glucose monitoring for diabetic patients are increasing every year [1]. The section of people worst affected by this are people who suffer from type I diabetes, who suffer hyperglycemic and hypoglycemic condition many times a day due to failure of pancreas functioning. Hence, they require continuous glucose monitoring systems, which can keep track of these conditions and administer appropriate hormones when necessary. Such a device is also known as an artificial pancreas. Though the field of artificial pancreas development has seen great technological evolution over the years [7], much work needs to be done in reducing patient discomfort, especially in the area of implantable glucose sensing. A reduced durability of such technology also greatly influences the cost of these sensors.

Flexible electronics show huge promise for applications in many fields with their recent developments. Implantable biomedical devices can benefit from the advantages flexible substrates have to offer, in terms of improving patient comfort. The aim of this work is to apply flexible processing techniques to achieve a realization of an artificial pancreas. Four main functions need to be satisfied for its proper functioning. First, it must be able to accurately and continuously monitor blood glucose within the body. Second, it must be responsive enough to dispense insulin or glucagon necessary for maintain normal blood sugar levels. Third, it must be able to decide accurately when there is need for dispensing. Lastly, it should provide high durability to make it more cost-effective and affordable.

Though this work does not intend to address all of the above functions, it attempts to focus on building a reliable and cost-effective sensor to detect glucose levels. The organization of this thesis is given below.

Chapter 2 begins by motivating the need for continuous glucose monitoring for type 1 diabetes patients. Though new innovations in glucose sensing technology are being reported every year, the rising costs of healthcare make many of these still unaffordable to a vast majority of these patients. The operating principles of an electrochemical glucose sensing technology is described, followed by a brief mention of previous work that was done on this project, that was done as collaboration between Prof. Greg Herman and Prof. John Conley of Oregon State University (OSU) and Pacific Diabetes Technologies (PDT). This work then picks up on addressing new motivations for modifying the established process flows to improve yield and reduce fabrication costs and help facilitate a successful technology transfer from OSU to PDT.

Chapter 3 describes the process steps adapted at the start of the study to aid animal studies by PDT. Each process step was initially designed at OSU using conventional semiconductor processing tools. Motivations for reducing and combining process steps and improving yield are introduced, which are then addressed in the next chapter using alternate process developments.

Chapter 4 introduces alternate patterning techniques such as shadow masking and controlled laser ablation to pattern different layers of the sensor. The potential for implementation of these process steps is discussed. A later section discusses the

integration of these process steps into the existing process flow of chapter 3 and provides a direction for innovation.

Chapter 5 briefly discusses reliability aspects of different surface treatments and compares it with laser ablated substrates, highlighting the potential for adopting alternate patterning techniques introduce in chapter 4. Also a brief section on animal studies performed on pigs is discussed to demonstrate working of fabricated sensors.

Chapter 6 summarizes the current work and provides recommendations for future work and direction of this project.

2. Background

Section 2.1 of this chapter intends to provide a history of continuous glucose monitoring for type 1 diabetes patients and concludes with a motivation of the necessity for a reliable and cost-effective sensing technology. Section 2.2 attempts to discuss briefly the working and components of a subcutaneously inserted amperometric glucose sensor, the main device developed in this work with an aim to construct an artificial pancreas. Section 2.3 focuses on flexible substrates and their importance in this work. Finally section 2.4 discusses the previous work done on this project, concluding with the groundwork laid for the current study.

2.1 Continuous glucose monitoring: Motivation and history

Diabetes mellitus is a condition that is diagnosed due to the body's inability to metabolize elevated blood sugar levels. This condition results in three main scenarios: a type 1 diabetes where insulin (the hormone produced by the pancreas to promote absorption of blood glucose to skeletal muscles and fat) is not produced in sufficient quantities; type 2 diabetes where the body's cells fail to respond appropriately to naturally produced insulin; and gestational diabetes, which occurs during pregnancy. Though both type 1 and type 2 diabetes are chronic conditions, type 2 diabetes can be controlled with medication and restricted diet intake. Type 1 diabetes poses a much higher risk for control since insulin needs to be administered daily. In-fact many people born with this condition need a reliable continuous glucose monitoring system to keep track of their hourly glucose levels [1].

A report by released by Center for Disease Control and Prevention (CDC) released in 2014 [2] shows at-least 21 million Americans have been diagnosed with some form of diabetes, with 5% of these cases belonging to type 1 category. Estimated direct treatment costs in 2012 totalled $176 billion, with average medical expenditure almost 2.3 times higher than people without diabetes. Diabetes was the seventh leading cause of death, though it can be underreported. This is because it can lead to other complications such as amputations, kidney disease, high LDL cholesterol and heart strokes.

Such facts establish a necessity, not just for the development of technology to treat or control existing diabetic conditions but also to invent cost effective and reliable monitoring techniques to prevent other complications that can arise from untreated diabetes. Hence, the development of a cost-effective artificial pancreas is desired to control and treat type 1 diabetes condition.

A natural pancreas regulates the blood sugar level through timely administration of two hormones (i) insulin – which works to reduce the concentration of glucose in the blood stream and, (ii) glucagon - which works to increase the blood glucose concentration. Glucokinase, an enzyme that occurs in the cells of the pancreas, acts as a natural glucose monitoring system, which shifts metabolism or cell function in response to rising or falling blood glucose levels [3]. In a similar way, an artificial pancreas [6, 7] consists of a continuous glucose monitoring unit (CGM), which feeds back glucose levels to an insulin or glucagon pump to regulate glucose levels in the blood stream.

One of the earliest artificial pancreas was developed in 1974 by Advanced Diabetes technology [4] and involved automatic insulin administration. However, the sensing and administration were done intravenously, which causes significant patient discomfort and could not be used outside the medical facility. Modern advances in glucose sensing technologies has opened up many avenues for the construction of a portable and comfortable artificial pancreas.

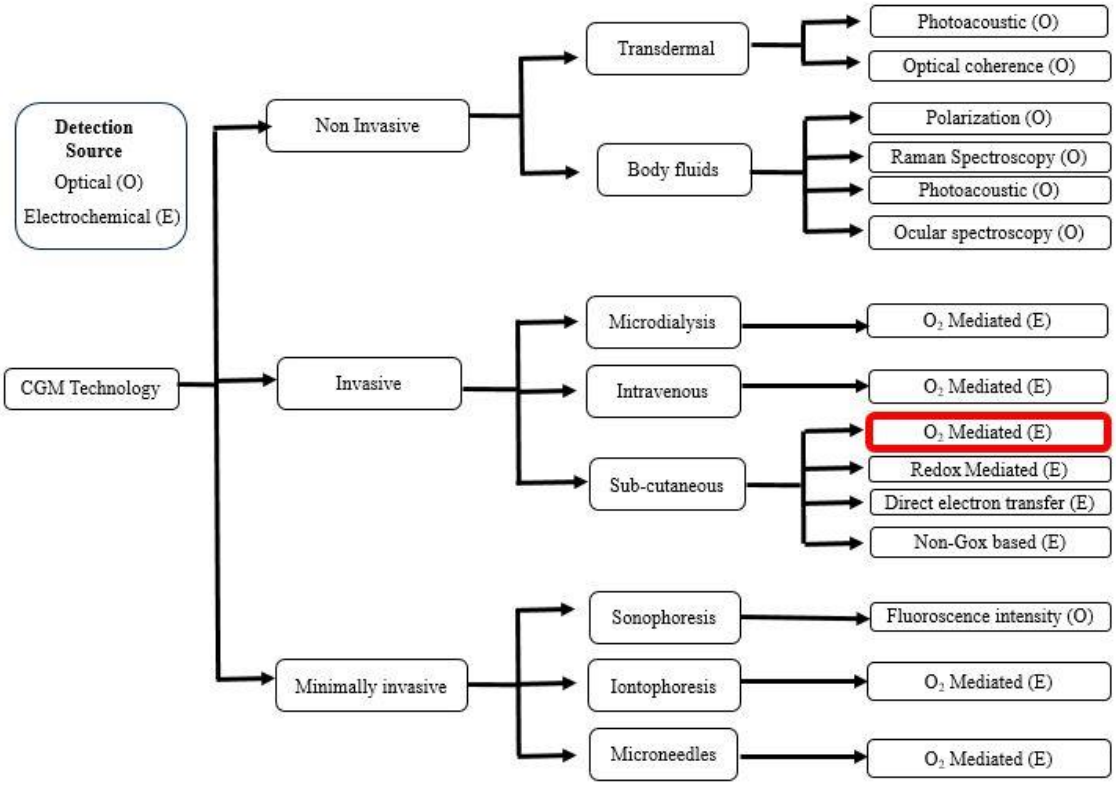

Figure 2.1: Classification of CGM technologies based on their mode of sensing [6]. The technology used in this study is highlighted in red.

Figure 2.1 provides a tree of classification for CGM technologies developed over the years. CGMs in the market usually rely on electrochemical glucose sensing. Sub-cutaneous glucose sensing [5] which involves insertion of a sensing catheter consisting of an electrochemical cell is inserted into the sub-cutaneous fat tissue provides a lesser amount of patient discomfort and is a common technology for accurate and reliable CGM. In-fact a recent review of artificial pancreas development efforts [7] focuses on advancement of reliability, cost-effectiveness and accuracies of CGM technologies. Dexcom® has recently reported its G6 sensors which have an improved wear time of 14 days, and other companies look to integrate glucose sensing data to the cloud. Dominant issues appear to be cost, due to the affordability of such technology, followed by reliability.

2.2 Device working mechanism

Clark and Lyon [8, 9] proposed the basic principle for glucose sensor operation in 1962, which is still used by many modern devices, including the one employed in current work. The sensor technology used in this study is a 1st generation device [6], in which glucose oxidase reacts with glucose in the blood to form gluconic acid (hydrolyzed gluconolactone) and hydrogen peroxide. The produced hydrogen peroxide is oxidized at a catalytic electrode such as platinum, which produces a measurable current [10]. A reference electrode is used to maintain a steady reference voltage to sense this current. The chemical reaction that occur during this process are summarized in equations 2.1, 2.2 and 2.3.

$$Glucose + GO_x(FAD) \rightarrow Gluconolactone + GO_x(FADH_2) \quad (2.1)$$

$$GO_x(FADH_2) + O_2 \rightarrow GO_x(FAD) + H_2O_2 \quad (2.2)$$

$$H_2O_2 \overset{Ag/Ag^+}{\longleftrightarrow} 2H^+ + O_2 + 2e^- \quad (2.3)$$

Glucose oxidase (GOx) works along with its cofactor enzyme, flavin adenine dinucleotide (FAD) to help catalyze oxidation of β-D-glucose into D-glucono-1,5-lactanone, which upon hydrolysis produces gluconic acid (equation 2.1).The reduced FAD (or $FADH_2$) utilizes molecular oxygen present in the blood stream to oxidize back to FAD, forming hydrogen peroxide (H_2O_2) in the process. The formed H_2O_2 then oxidizes to O_2 and protons, which produces excess electrons, thereby producing a measurable current at the electrode. This process is catalyzed by the use of a transition metal surface such as platinum, gold or silver [11], which ensures that the reaction occurs at its surface upon biasing the metal electrode at a fixed voltage.

2.2.1 Structure of CGM sensor

In this work, we employ the use of a platinum electrode coated with GOx as the sensing electrode. This biased at +0.6 V with reference to Ag/AgCl standard electrode using an external source to obtain spontaneous oxidation of H_2O_2 at the platinum surface, thereby detecting the glucose signal. This voltage was chosen for

maximum oxidation rate of H_2O_2 and is consistent with previously reported values employed in biosensors [20, 89, 90, 91].

Figure 2.2 (a) & (b) illustrate a top and cross-section view of a CGM sensor. The bottommost layer of the sensor is called its foundation. To reduce tissue trauma after sensor implantation and improve patient comfort, a flexible foundation for the sensor is necessary. The layer immediately on top of the foundation comprises of conductive traces, which connect the sensor electrodes electrically to the outside world through external contacts. The platinum/GOx sensing electrode and Ag/AgCl reference electrode are fabricated on top of the conductive trace region.

Metals in contact with an aqueous solution such as the subcutaneous fluid generate an electrochemical potential. Though this phenomenon forms the basis of the working of the sensing and reference electrodes, it however also causes unwanted artifacts in case of the conductive traces. Moreover, the conductive trace area is the most susceptible region of the sensor for reliability issues, due to its high aspect ratio structures. Hence, to mask this region, a coverlay is used to protect the conductive traces. Finally, a diffusion barrier is coated on top of the region that is to be implanted inside the body, to regulate the concentration of glucose near the vicinity of the electrodes.

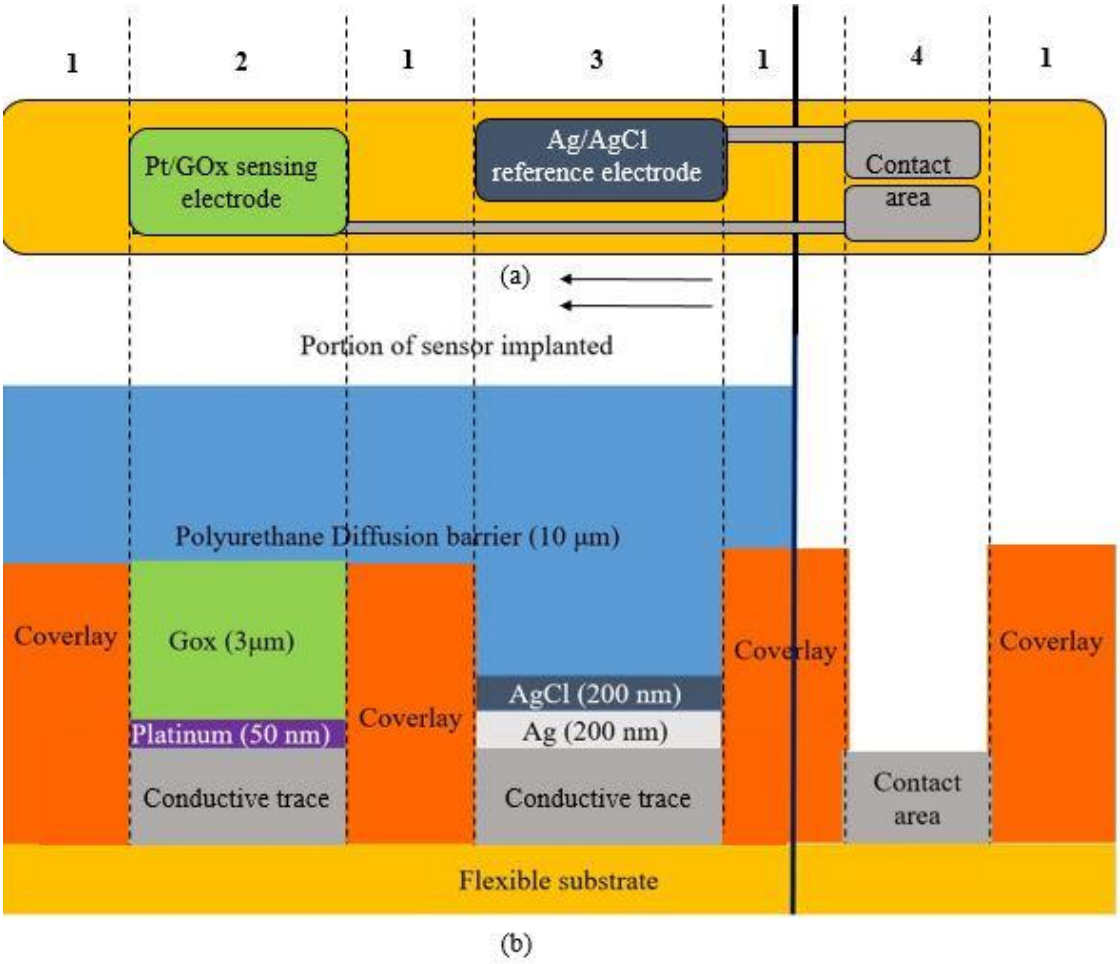

Figure 2.2: (a) Top view of CGM sensor indicating a sensing and reference electrode fabricated on top of a flexible substrate and connected to the contact area through conductive traces (b) Cross-sectional schematic of the same CGM sensor (along red-dash line) with different layers and their estimated thicknesses (not to scale).

Numbered regions (dashed lines): 1) Polyimide coverlay, 2) sensing electrode, 3) reference electrode and 4) contact area. Bold line separates the portion of the sensor implanted inside the body from the contact area which slightly outside.

2.2.2 Glucose detection and diffusion barrier

The use of glucose oxidase (GOx) to determine glucose concentration was first suggested by Keilin & Hartee [12] in 1948. It remains to date, one of the most employed enzyme in detecting glucose levels due its high stability and low costs. The success of GOx oxidizing glucose and detecting a glucose signal as discussed in section 2.2 depends on its affinity towards glucose. GOx is highly selective to β-glucose [12] however, it is also known to oxidize other species present in the subcutaneous fluid such as acetaminophen [13]. This interference can pose a challenge to the detection of the true glucose signal.

This work also refers to the use of an inactivated GOx electrode (iGOx) which is no longer catalytically active, to enhance selectivity towards glucose. iGOx, which can be synthesized by inactivating GOx through chemical reaction [14], UV exposure [15] or thermal treatment [16] results in loss of sensitivity towards glucose detection. However, iGOx is still able to oxidize other unwanted species, which generates a current on its own. This signal can be subtracted from the original GOx signal to obtain a noise free glucose signal. Region 2 of the sensor shown in figure 2.2 is used for implantation of iGOx.

Diffusion barrier is an important and integral part which determines the dynamic range of the signal detected by the sensor. Commercially available glucose sensors are designed to respond to a glucose range of 0 to 20 mM (360 mg/dL) to sense both hypo and hyperglycemic conditions [17-19]. However, it is important to have a linear relationship between the input glucose concentration and output current

sensed. Diffusion barrier achieves this linearity and avoiding signal saturating conditions by limiting total glucose and oxygen concentrations at the sensor.

Previous work carried by Dr. Xiasong Du and Chris Durgan investigated the use of perfluorosulfonic acid (PFSA) as a diffusion barrier due to its enhanced selectivity for glucose over acetaminophen [13]. Latest work that is being investigated at Pacific Diabetes Technologies (PDT) by Dr. Kenneth Ward involves a proprietary polyurethane diffusion barrier. Polyurethane barrier has been used to enhance oxygen to glucose permeability ratio and obtain a better signal to noise ratio output [23]. The diffusion barrier occupies all the regions except region 4 involving contacts in figure 2.2.

2.2.3 Silver/silver chloride reference electrode

As discussed in the previous sections, the glucose sensor requires an internal voltage reference to maintain a reliable glucose signal. This is accomplished using a silver /silver chloride reference electrode [21-22], whose steady state electrochemical cell reaction is given by equation 2.4.

$$AgCl_{(s)} + e^{-} \leftrightarrow Ag_{(s)} + Cl^{-}{}_{(aq)} \qquad (2.4)$$

This reference electrode has a constant and well known potential (*E*) for a given chloride concentration provided by the Nernst equation 2.5 [92].

$$E = E^0 - 2.303\left(\frac{RT}{nF}\right) log_{10}\alpha[C_{Cl^-}] \qquad (2.5)$$

Where E^0 is the standard electrode potential (+0.2223 V for a Ag/AgCl electrode [25]), R is the molar gas constant (8.314 J/K.mol), T is the absolute temperature (in K), F is the Faraday constant (96,486 C/mol), $[C_{Cl^-}]$ is the concentration of chloride ions in the solution (mol/L), n is the number of electrons involved and α is the activity co-efficient for chloride ions. Equation 2.5 reduces to equation 2.6 when a simplification of n=1 and α = 1 are applied. From equation 2.6, it is apparent that the electrode potential depends logarithmically only on the chloride concentration, given by equation 2.6.

$$E = E^0 - 0.0591 log_{10}[Cl^-] \qquad (2.6)$$

Chloride being an important electrolyte in human blood, its concentration is maintained in a narrow range of 96-106 mM [24]. This constant regulation of chloride concentration helps to maintain a constant potential of E^0 (0.22 V) and hence makes it a reliable reference electrode. Region 3 of figure 2.2 indicates the area where the reference electrode is employed.

2.3 Towards an Artificial Pancreas

The previous section 2.2 presents a brief description of the working of the glucose sensing element used for an artificial pancreas. The sensing element (Pt/GOx) along with an insulin/glucagon infusion element (not discussed in this work) together form the typical artificial pancreas system. An ideal realization of this system would consist of a single catheter with a sensor, inserted at a single point in the body, which performs both glucose sensing and administration of insulin and glucagon at the same site, making this system compact and comfortable for day-to-day use. However, the problems associated with this setup such as, hinder accurate monitoring of glucose at the site of hormone infusion. Though the problem of glucose monitoring at the site of infusion is a challenge in itself is not addressed by this work.

Also, monitored glucose signal can be affected by artifacts introduced due to body fluids [93, 94], or even insulin preservatives [95]. These artifacts can be filtered by using multiple sensing elements [7, 96]. CGM units currently available in the market consist of usually four points of insertion (two for glucose sensing and the other two for hormone infusion), with one sensing electrode at each of the two sensing points [97, 98]. This arrangement can boost the overall glucose signal SNR by capturing glucose signals from different locations, avoiding interference from hormone infusion and output an accurate count of blood glucose reading. Also, in the event that one of the sensor fails, the other inserted sensing element still provides a reliable glucose signal count, thereby providing a window to replace the failed sensor

while performing CGM. However, the main drawback associated with this design id increased patient discomfort due to the use of multiple insertion points.

One of the main goals of PDT towards an artificial pancreas aims at reducing patient discomfort by employing multiple sensing elements on the same catheter. This reduces the overall design to a single point of insertion, with the current work's designs employing three sensing electrodes on the same catheter for the best noise filtering performance [96]. However, this design would require improved durability over multiple insertion element design, since a physical failure of the sensor might not provide CGM tracking until it is replaced.

Hence, the main goal of this work in this thesis is to improve the sensor durability using conventionally available process technologies, while striving to keep the cost per sensor low.

2.4 Previous Work

Previous work on this project by Dave Matthews [26] aimed towards establishing a stable process flow. An investigation of materials involved the adoption of PMDA-ODA polyimide flexible substrate due to its well established literature and durability. Gel-pak™ DGL X8 film by Vichem was observed to be chemically and physically compatible for its use as a rigidization layer to hold the flexible polyimide flat onto a glass substrate. The above work also investigated the use of Al_2O_3 as a supporting layer to titanium, a well-known adhesion layer, on top which electrodes of silver and platinum were deposited and patterned. This was found to be in-effective as the alumina dielectric could not survive the bend radius constraints offered by 21 gauge (21ga) needles (diameter = 0.724 mm). Finally, a gold coated polyimide flexible substrate was deemed most suitable for the substrate necessary for device construction.

Later work done on this project involved investigation of e-jet printing by Dr. Xiasong Du and Dr. Chris Durgan as an alternative to conventional patterning and chemical chloridization [27]. Parallel investigation led by Dr. Xuebin Tan uncovered adhesion and reliability problems with a gold foil substrate, laying the motivation and foundations for this study on investigating using a titanium foil substrate.

The current work focuses on continuing to build a working glucose sensors by improving throughput and alternatively, investigating process flows to improve the reliability of the sensors.

3. Process design

The previous work done on this project focused on prototyping a working glucose sensor and hence involved the usage of a 1” x 1” size substrate on a 12 μm thick titanium foil laminated onto an acrylate adhesive coated DuPont polyimide. Once a working sensor was obtained, there was an inherent need in scaling up the production of these sensors by using bigger substrates and also make them more reliable and suitable for human studies. This chapter starts with section 3.1 addressing the drawbacks of this substrate and a motivation for transition onto a 5μm thick titanium clad polyimide substrate of 3” x 2” size. Sections 3.2, 3.3, 3.4, 3.5 and 3.6 address the evolution of process changes and optimizations.

3.1 Substrate analysis and preparation

The substrate is the starting material for the manufacturing process. For the substrate to be flexible, it has to be thin enough to bend around a small radius, offering durability at the same time. Previous generation of sensors made the use of gold as a base layer. This was to utilize its ability to help catalyze the decomposition of H_2O_2 [28, 29]. Gold was also an attractive candidate for its electrical conductivity. However, it was later found out by our collaborators (Dr. Xiasong Du with OSU Dept. of Chemical Engineering) that the determined catalytic activity of gold was not enough for application [26].

3.1.1 Substrate development

Titanium was investigated again for its use as a conductive trace forming material at the beginning of this work. The benefits offered by titanium foil are (1) lower galvanic current in salt solution compared to gold , which is better for improving the sensitivity of glucose current signal [31], (2) a well-known bio-compatibility, widely used for many biomedical applications [30], (3) well known adhesion layer properties and can aid in better adhesion of Ag and Pt electrodes onto substrate. Though the use of titanium was previously investigated in this project by Dave Matthews [26], its development was halted due to constraints posed by the form in it which it was used. Attempts were made to deposit titanium through sputtering directly onto polyimide surface and with the aid of an adhesive Al_2O_3, none of which were effective from a reliability stand point of view. Pre-treating the surface of polyimide using plasma cleaning also did not support the cause.

Hence, PDT proposed the use of a titanium foil as a new substrate material for making the flexible substrates, when gold was concluded to be ineffective from a reliability and cost point of view. The availability of cost-effective and standard titanium foils, also offers an attractive cost-benefit alternative to the existing gold evaporation process. For the purpose of our study, we employed the use of a 12 µm thick titanium foil (grade 1) from Baoji Tongrun metal materials for better durability as opposed to a thinner titanium layer investigated in previous work [26]. However, the usage if titanium foil as an underlying layer presents two innate issues (1) unlike gold, titanium has a thin native oxide layer, which can pose challenges for electrode

adhesion [31, 32], (2) the usage of 12 µm thick titanium foil creates huge under-cuts during the trace patterning step due to isotropic nature of wet-etch (figure 3.1).

Initial studies using this substrate were designed to overcome these challenges. A pre-clean step was employed (discussed more in detail in section 3.2) to remove the native oxide. However, the undercut problem remained as it was not possible to obtain a completely directional etch using wet etch processing. This created further problems into transitioning from 21ga design trace masks to a 25ga trace mask, where the trace width was reduced by more than a factor of 50% so that the under-cut severely impacted the durability of the sensors. SEM studies performed by Dr. Xuebin Tan, indicated an undercut area of almost 41% of the electrode area, leaving too little titanium remaining under the electrode, leading to its collapse in subsequent processing steps and loss of adhesion (figure 3.1).

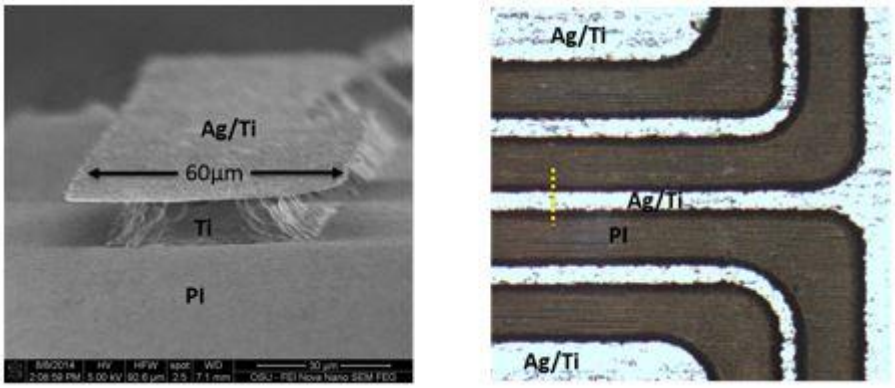

Figure 3.1 (a) SEM cross section image indicating ~41% electrode area of under-cut titanium leading to electrode collapse seen in the anterior region (b) top view of Ag/Ti trace of 60 µm width in trace pattern.

In addition to the problem of under-cutting, thicker titanium electrode delaminated when 25ga sensors were wrapped around a 25ga needle. This prompted a transition from a 12 µm titanium foil to a 5 µm foil. Hence the expected undercut for a 5µm thick titanium for a 60µm linewidth was calculated to be a total of 10µm, which amounts to 16% of the electrode, a significant improvement in under-cut loss of titanium. Moreover, this transition of foil thickness eliminated electrode delamination upon bending the flex sensor around a thinner 25ga needle. However, it also ushered in the issue of hydrogen embrittlement of titanium, which existed for 12µm titanium foil but was not significant enough to affect the sensor's durability. This is discussed in detail in section 3.2 of surface preparation.

3.1.2 Rigidization

Rigidization is an important step in which the flexible substrate is made flat enough for subsequent processing steps. Flatness of substrates is a crucial parameter in process development as many conventional process steps are designed on the assumptions of a flat substrate. For example, the usage of photolithography as a patterning step can be severely impacted if the substrate is not flat enough. Spin-coating of a non-flat substrate can result in comets and shadow regions with too little resist and affect pattern resolution, where some regions may be over-developed and some, under-developed.

The previous generation of substrates developed by Dave Matthews [26] were rigidized using an DGL-40 X8 Gel-Pak™ film, due its process compatibility,

adhesion strength and facilitates easy removal of flexible substrate form glass slide after processing. The Gel-pak™ material used consists of a “Process B” gel material sandwiched between a releasable polycarbonate sheet and a polyethylene substrate.

Glass slides from VWR International were pre-cleaned with de-ionized (DI) water, followed by an acetone/isopropyl alcohol (IPA) rinse, to remove any particulate contamination. The cleaned glass slides are blown dry with nitrogen (N_2) and stored in clean poly-styrene boxes. In the next step, the gel-pak material is cut into the required dimensions of the substrate and the polycarbonate film is removed. The exposed “process B” get is then carefully adhered to cleaned glass slide, followed by removing any trapped air-bubbles to remove non-uniformities. The polyethylene substrate is released from the gel material by heating the substrate on a hot-plate at 85°C for 30 seconds. Now, the gel material is again exposed onto which the substrate (titanium clad polyimide foil) is adhered carefully and trapped air-bubbles are removed. Excess gel around the outline of the substrate is carefully removed using a blade. The final substrate obtained after rigidization is flat and ready for subsequent process steps.

3.2 Surface preparation

Surface preparation is a crucial step for any substrate before introducing it in a manufacturing process. Practically, no two substrates are the same. Hence, the aim of surface preparation should be to reduce or eliminate external but uncontrollable process variables such as substrate to substrate variability and keep them in check by minimizing their effect on the subsequent process steps. Another important goal of surface preparation techniques is to make the substrate into a reliable foundation onto which subsequent process steps can benefit. Hence, this steps plays as important as a role in the stability of a process flow.

The substrate composition discussed in the previous section 3.1.1, employs the usage of a titanium clad polyimide flexible substrate, rigidized onto a glass with the assistance of gel-pak™. The titanium foil part of the substrate plays the role of a physical and a chemical foundation onto which subsequent process steps need to be designed. Titanium's bio-compatibility is well known [30]. However, from a process point of view, it also offers an added benefit of serving as a well-known adhesion layer [30, 31]. The aim of surface preparation hence is to produce a clean and uniform titanium surface that can aid in designing subsequent process steps.

Adhesion is the tendency of dissimilar particles to cling onto each other. The forces that cause adhesion between two materials fall into four broad categories (1) chemical adhesion (2) dispersive adhesion (3) diffusive adhesion and (4) mechanical adhesion [34]. Adhesion between metal layer systems such as Ti/Ag and Ti/Pt can be modeled as a combination of multiple adhesion factors such as surface wettability,

method of thin-film deposition and electrostatic charge adhesion. However, in our process the adhesion studies performed (discussed in chapter 3.2.2) show mechanical adhesion and surface wettability of titanium as two important factors in trying to model adhesion of these metal interfaces. Hence, the effectiveness of titanium as an adhesion promoting substrate depends on two factors (1) physical and chemical purity of titanium surface and (2) surface roughness [34, 35].

The substrate after rigidization consists of an electro-polished and annealed titanium foil, which is macroscopically smooth and has a thick oxide layer (1-1.5μm). This surface is not ideal for good adhesion of electrodes (Ag and Pt) that are deposited in the subsequent process steps. Hence, a surface preparation or pre-clean is necessary in achieving good adhesion between electrodes and the substrate.

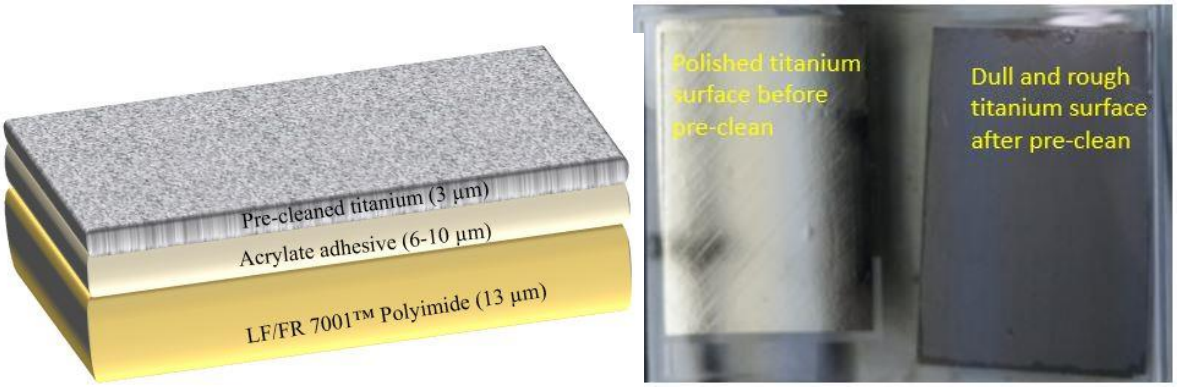

Figure 3.2: (a) Schematic of substrate after pre-clean step. The titanium thickness reduces to ~3μm due to loss of oxide and some titanium thickness. (b)Top view of a rigidized titanium clad polyimide substrate (left) before acid pre-clean (right) after pre-clean.

Surface preparation using acid pickling is an important process step commonly used to prepare titanium surfaces in the dental [30] and aviation [44] industries. Common etch solutions for titanium involve hydrofluoric acid (HF) as the primary etchant and an oxidizing counterpart (such as hydrogen peroxide, nitric acid, etc.) to oxidize the pure titanium surface and pave a pathway for the etchant to remove the generated oxide. In the following sections 3.2.1 and 3.2.2, we investigate the use of different pre-clean solutions and their effect on surface preparation of titanium.

3.2.1 Hydrogen embrittlement of titanium

The shift from 12µm thick titanium foil to a 5µm thick titanium foil as previously discussed, carried its issues along with its benefits. The main issue surrounding this transition was the reduced trace reliability of 5µm thick titanium in comparison to 12µm titanium due to the effects of hydrogen embrittlement [36, 37]. Though this was inferred to have existed even in 12µm generation of devices, its effects were not significant to affect the sensor durability. However, transition to 5µm generation completely changed this picture.

The various advantages 5µm generation devices discussed in previous section 3.2, such as reduced electrode delamination, easier transition to 25ga designs, lesser undercuts and etch times were endangered with two main issues (1) loss of relatively significant thickness of titanium during surface pre-preparation (2 – 2.5µm) and (2) cracking of electrode areas. The loss of titanium thickness during the pre-clean step is

inevitable since this portion comprises of the shiny oxide, which needs to be removed for a better adhesion performance. However, this can be circumvented though the use of controlled laser ablation of titanium and its integration in a new process flow discussed in chapter 4.3.

Cracking of electrodes happened due to hydrogen embrittlement of titanium [37], which is a common problem observed during the pickling of titanium using wet etch solutions. Free hydrogen ions in the solution diffuse through titanium metal and are trapped beneath its surface. These ions then recombine and form gaseous H_2, which tries to free itself from these traps and as a result creates cracks slightly below the surface of the metal. These cracks can then propagate if the metal is too thin and result in failure of the metal during reliability tests.

Absorption of hydrogen by titanium is exacerbated through formation of a surface hydride [36], which forms on the surface of titanium for HF based pre-clean solutions. Also, the temperature of the solution is important in controlling hydrogen absorptivity since it controls the diffusion co-efficient. Hydrogen diffusion into titanium at low temperatures ($<100^0$C) surface controlled. Though it would be expected of hydrogen absorptivity to be lesser at lower temperature, Brauer et al. [39] used an electrochemical method to measure the diffusion of hydrogen in titanium at lower temperatures ($< 100^0$C) and found it to be 2×10^{-7} cm^2/sec, which was 5 orders of magnitude higher than previously published studies [40]. This shows that even solutions at room temperature are susceptible at embrittiling titanium. Hence, it is

important to concoct a pre-clean solution, which can control the amount of free hydrogen generated in the solution.

The effects of H_2 embrittlement were observed from the first lot of arrays produced using 5µm generation substrates through electrode cracking (figure 3.3), the result of crack propagation of an already embrittled titanium underneath the electrodes (figure 3.3). Since, the surface properties of this titanium was altered during the pre-clean step, it was necessary to find alternate surface preparation solutions to overcome this issue.

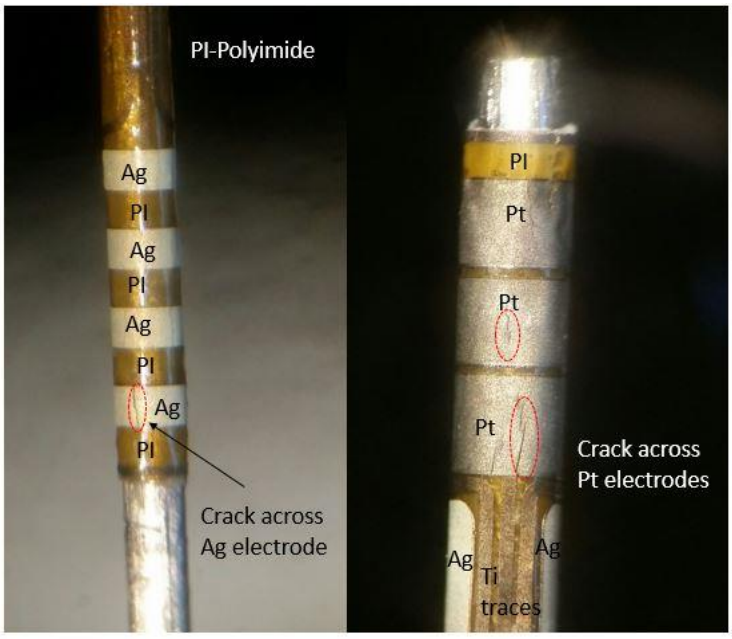

Figure 3.3: Image showing instances of electrode failure of a sensor with 5µm thick titanium foil wrapped around 21ga needle, due to crack propagation formed due to hydrogen embrittlement of underlying titanium. Image credit: Pacific diabetes technologies, Inc.

This problem required a necessary quick and long term solutions. A faster way to solve hydrogen embrittlement using a HF based etchant was to limit the amount of free hydrogen contain in the pre-clean etch solution. A solution of HF and nitric acid (HNO_3) with mixture ratios of HNO_3 greater than 10 parts to 1 part of HF was recommended to contain hydrogen embrittlement [30, 39]. HF etches titanium oxide forming soluble and stable titanium fluoride complexes [39, 86] and liberating hydrogen (equations 3.1 and 3.2).

$$2Ti + 10\,HF \rightarrow 2\,[TiF_6]^{2-} + 3H_2 + 4H^+ \qquad (3.1)$$

$$2Ti + 12\,HF \rightarrow 2\,[TiF_6]^{3-} + 3H_2 + 6H^+ \qquad (3.2)$$

The nitric acid component then reacts with the liberated hydrogen to from nitrous oxide and water, thereby reducing hydrogen available to embrittle titanium as in equation 3.3. The remaining nitric acid then proceeds to oxidize titanium and form TiO_2, which is further etched by HF by the above process in equation 3.1.

$$3H_2 + 2\,HNO_3 \rightarrow 4\,H_2O + 2NO \qquad (3.3)$$

Another etch chemistry that was found to alleviate hydrogen embrittlement was pre-clean using concentrated sulfuric acid [38, 87]. This was investigated further in section 3.2.2 as a long term solution for both pre-clean and etch of titanium.

3.2.2 Pre-clean etch optimization

The pre-clean solutions employing HF introduced hydrogen embrittlement in the titanium foil (discussed in the previous section 3.2.1). Two pre-clean solutions were investigated to alleviate hydrogen embrittlement (1) a 1:10:100 solution of $HF:HNO_3:H_2O$ and (2) a 33% solution of sulfuric acid (H_2SO_4) heated to 120^0C.

First, a surface preparation test was performed to calibrate the oxide breakthrough time for the above test solutions. Next, an adhesion test comprising of 400 nm of thermally evaporated silver (discussed in section 3.3.1) was performed on substrates with the above pre-cleans using an ASTM scotch tape test to test adhesion [45].

Samples pre-cleaned with 33% H_2SO_4 heated to 120^0C, performed exceptionally well compared to $HF:HNO_3:H_2O$ (1:10:100) solution in terms of adhesion due to a more hydrophilic titanium surface formed after a sulfuric acid pre-clean [38]. However, sulfuric acid etch solution displayed a strong dependence on bath temperature, in particular, the etch rate of the solution increased with an increase in temperature. Also, the time taken by sulfuric acid solution to break the initial oxide was found to be around 4 minutes 30 seconds at 120^oC, which was longer than that of 40 seconds of HF and nitric acid solution.

Further optimization of sulfuric acid etch solution resulted in a final pre-clean solution of 50% H_2SO_4 at 65^0C, which allowed for the survival of photoresist required for final titanium etch. Higher temperature baths also contained the disadvantage of removing too much titanium after initial oxide break through, which

reduced the titanium foil thickness to below 2 μm, affecting the reliability of conducting traces. This was also one of the drawbacks observed using a HF and nitric acid pre-clean, which despite the dilution ended up etching through almost 4 μm of titanium due to a faster etch rate [41, 42].

Subsequent lots of sensors were pre-cleaned with 50% H_2SO_4 at 65^0C, which remained a favorable long term alternative with PDT, due to extra investment and safety regulations needed for adopting a HF based etch process, thereby facilitating a cheaper and safer technology transfer from OSU.

3.3 Thin film deposition

Thin film deposition is the process of growing metal or insulator thin films on substrates. This process can be classified into two broad categories: physical and chemical vapor deposition. Physical vapor deposition techniques rely on imparting kinetic energy to the material source to deposit a thin film on the substrate, whereas chemical vapor deposition grows a thin film through chemical reaction with the substrate. Two methods of physical vapor deposition were investigated in this study (1) thermal evaporation and (2) sputtering.

3.3.1 Silver electrode deposition

Silver electrode is an integral part of forming the reference electrode for the glucose sensor. To ensure better electrochemical durability of the sensor, a high quality silver electrode is required, which shows properties such as (i) good adhesion onto the substrate, (ii) high purity film and (iii) good surface uniformity. Hence, the aim of this section is to investigate the methods of depositing the silver electrode onto the sensor and their corresponding film quality.

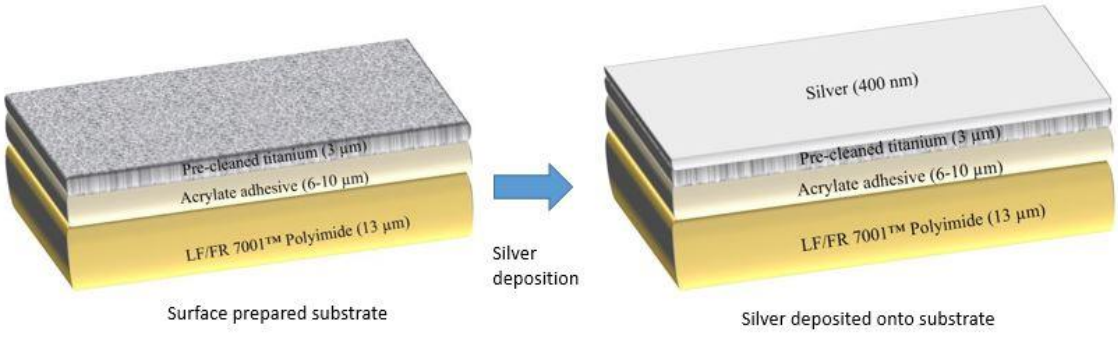

Figure 3.4: Schematic showing the substrate (left) before deposition and (right) after silver deposition.

Thin film deposition of silver was performed initially using thermal evaporation technique using a Veeco™ thermal evaporator and later, sputtering as a technique to deposit silver was adopted using an ATC Orion tool. Later in this process flow, this silver is partially chloridized at PDT to form the Ag/AgCl reference electrode.

Thermal evaporation of silver was initially preferred due to low costs associated with producing thermally evaporated thin films. The source material consisted of 2-3 pellets of 50 grams silver supplied by Kurt J. Lesker, which are loaded into the source 2 and 1 pellet of 50gm titanium into source 1. Each source consists of a tungsten basket, which heats up during operation due to current flow, and melts the source material to its vaporizing point. This vapor then rises in the bell jar cavity of the thermal evaporator and deposits onto the substrates, which face downwards. The rate of deposition is measured using a quartz-crystal monitor which vibrates acoustically at a specific frequency, a frequency which changes as material is

deposited onto the sensor, allowing one to estimate the thickness of material deposited using an external thickness monitor connected to this sensor.

The thermal evaporator is then loaded with substrates through orifices located above the sources at a fixed throw distance. The jar is then sealed and then cavity is pumped down to an operable base pressure of medium vacuum range (~10^{-6} Torr) using a diffusion pump backed by a mechanical roughing pump. This pressure range achieves a long mean free path (~5 meters) for the air molecules inside the bell jar, which helps avoid in-situ oxidation of deposited film and negligible scattering of material deposition due to air. This also lower the boiling point of the source material in the cavity (due to lower vapor pressure being exerted on the molten metal) and hence, lesser current needed to achieve this. The power supply is turned on, with a current controlling knob that can switch between source 1 and 2 if needed. 20nm of titanium is first deposited through source 1 followed by silver deposition using source 2, without breaking vacuum.

Since, evaporation is a line-of sight based deposition [46], the rate of film deposition varies inversely with increase in throw distance, and hence the substrates at the center of the cavity ended up with a more accurate thickness prediction compared to the substrates at the periphery. This caused inter-thickness uniformity issues with variance as high as 50 μm for 1” x 1” substrate size and thickness non-uniformity within a 3” x 2” substrate. However, the problem of inconsistent adhesion performance of thermally evaporated silver ultimate led to investigation of replacing it with sputtering.

Sputtering of silver was investigated to improve adhesion of the silver electrode to the substrate. The process of sputtering involves ejection of target atoms (in our case, silver) with the help of electrically ionized plasma (mostly argon ions), that imparts kinetic energy to the ejected target atoms [46]. This kinetic energy is more than two orders of magnitude larger than that of thermally evaporated silver atoms, and hence can penetrate into the substrate for a depth of a few monolayers. The subsequent piling up of sputtered silver atoms maintain a good cohesion between each other up-to the required film thickness and result in a good adhesion performance of sputtered silver [34]. No adhesion layer of titanium was required before sputtering of silver. Another advantage of sputtering includes a better control on deposition rate as opposed to thermal evaporation, which can be used to advantage for better feature resolution using shadow masking, discussed in chapter 4.

Consistent adhesion performance of sputtered silver facilitated in obtaining better yields and was later adopter as a process technology transfer from OSU to PDT.

3.3.2 Platinum electrode deposition

Platinum electrodes were deposited onto a pre-patterned layer of photoresist on the substrate preceding a lift-off process. Sputtering was chosen as the deposition method due to reliable adhesion performance found in previous studies [26]. A 5 nm thick titanium layer preceded the 50 nm thick platinum electrode deposition, both of which were sputtered without breaking vacuum for the best adhesion performance.

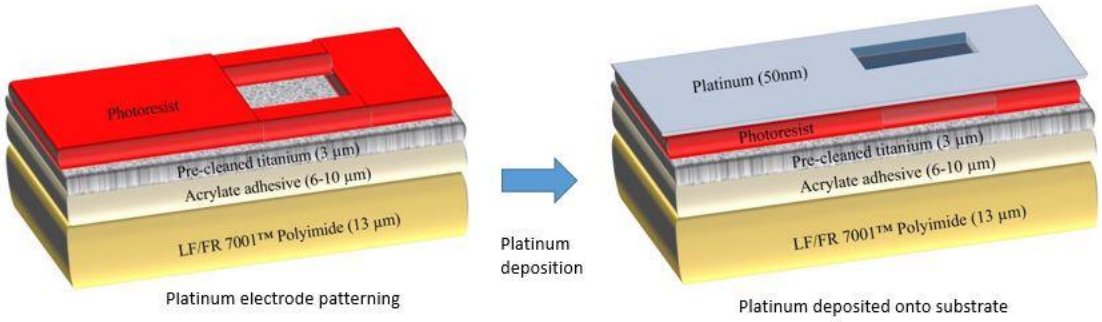

Figure 3.5: Schematic showing a pre-patterned substrate (left) before deposition and (right) after platinum deposition.

Platinum deposition was carried out using an ATC Orion V6 sputter tool at MBI. The sputter chamber with titanium and platinum sputter targets was pumped down to a stable base pressure of 5µ Torr to remove gaseous contaminants. The substrate was then loaded into the sputter chamber using a fork and load lock mechanism of the sputter tool. The substrate is then set at a rotation of 40 rpm to ensure uniformity of sputter coat. The chamber was then filled with argon, the gas used for striking plasma using a flow rate of 20 sccm to reach an operating pressure of ~10m Torr. An argon pre-strike clean was performed before deposition at 100W power for 5 min. Titanium was then deposited at 300 W target power for 60 sec to

achieve ~5nm thickness followed by platinum deposition at 100 W for a 700 sec coat time to achieve ~50 nm platinum. The substrates were then unloaded from the sputter chamber using the load-lock mechanism and were verified for thickness using a KLA Tencor Alpha-Step 500 surface profilometer on a dummy wafer piece placed close to the substrate.

Though sputtering is a well-controlled process, problems can arise with the film quality and purity (due to cross-contamination) depending on the metal sputtered previously. This was one of the potential causes of reduced platinum electrode sensitivity reported by PDT on some lots. This can be kept in control by pre-coating the sputter chamber with the metal to be sputtered so that the ionized argon atoms can deposit platinum as opposed to other metal that was previously sputtered, on the off chance that the plasma strikes the chamber walls. This was also an issue observed in sputtering silver electrode, though the tolerance level on silver electrode sensitivity was much higher than those required by the platinum electrode.

3.4 Electrode patterning

The simplest way to realize a pattern in a material is to deposit the material as the pattern itself and is the integral way to achieve an additive manufacturing process. For thin films, this is realized using shadow or stencil masking technique, which is discussed in detail in chapter 4. However, conventional processes are designed using subtractive manufacturing techniques, the most common of which involves patterning of a blanket material using patterned photoresist. The patterned photoresist protects the regions in the pattern which are required, leaving the remaining areas to be removed through an etch process.

Photoresists are of two categories (1) positive resist (2) negative resist [46]. The former type forms patterns through selective exposure to a conventionally, UV lamp source, the exposed areas of the resist being weakened by photo-assisted dissociation. This exposed region is then dissolved using a developer, usually an alkaline solution, forming a photoresist pattern. The latter type of photoresist hardens upon exposure to light source though photo-assisted polymerization. The remaining unexposed areas are soluble in the developer.

In this study, we use S1818 – a positive photoresist to pattern our substrates [47]. Positive photoresists are hydrophobic and usually require a priming step, involving a HDMS (hexamethyldisilazane) solution. This solution makes the surface of the substrate hydrophobic and aids in binding the photoresist to the substrate during spin-coating step [46, 47]. A 5% NaOH based developer (developer 351) dissolves the exposed photoresist. Pattern transfer is then performed using an etch or

a lift-off process, depending on the material to be patterned, the etch effectiveness and selectivity between the material and the layer beneath it.

3.4.1 Silver electrode patterning

The silver thin film deposited in the previous step (section 3.3.1) is patterned using a photoresist. The recipe describing the pattering step parameters is described in table 3.1.

Process step	Parameters
Adhesion promoter	2ml of HDMS primer. Spin dry for 30 sec at 4000 RPM
Bake	85ºC for 3min
S1818 Photoresist	Dispense 3ml, 3000RPM, 5000RPM/s, 10s, 4000RPM, 5000RPM/s, 20s
Pre-exposure bake	85ºC for 3 min
Exposure	10s, 350 W/cm^2
Develop	(1:4) 351 developer: DI water, 1min 10sec
Silver Etch	(8:8:75) NH_4OH:H_2O_2:DI water , 30 sec

Table 3.1: Process recipe for silver reference electrode patterning

Priming is done for this patterning to ensure the photoresist bonds well to the silver areas that need to be protected throughout the etch process. The substrate is then spin-coated with the photoresist and then soft baked. The spin speed and duration decides the final thickness of the photoresist that can be realized on the

substrate, and is given by spin-speed curves, which are a part of technical datasheet for the photoresist. Ramp rate is crucial in determining the uniformity of the photoresist spread [46, 47]. The soft-bake temperature and duration are important for two reasons, they (1) remove excess solvent in the photoresist and make sure it does not stick to the mask during contact exposure and (2) activates photoactive compound in the resist for exposure and ensure good development quality.

The substrate is then loaded into the mask aligner (Karl Suss MJB3), a broad-line contact aligner, which is loaded with a light field mask and alignment is performed. The substrate is then brought to contact with the mask, to register patterns precisely and avoid any edge diffraction effects followed by a limited time exposure to UV light. After exposure, the substrate is removed from the aligner and immersed in the prepared developer solution, following an immersion developing process. The solution needs to be agitated continuously during development to make sure there is no local saturation of photoresist dissolved.

The main advantage of patterning silver first in this process flow is to utilize the good optical reflectivity of silver to register reference alignment marks on the substrate. These alignment marks can be easily viewed compared to a duller platinum or titanium and tremendously aid subsequent patterning steps, especially the steps which utilize a dark field mask. The pattern is then transferred onto the silver film by immersing the substrate in a diluted version of base piranha solution which is a mixture of 8 parts a 30% solution of ammonium hydroxide (NH_4OH) and 8 parts of 30% solution of hydrogen peroxide (H_2O_2) in 75 parts of DI water [46, 47].

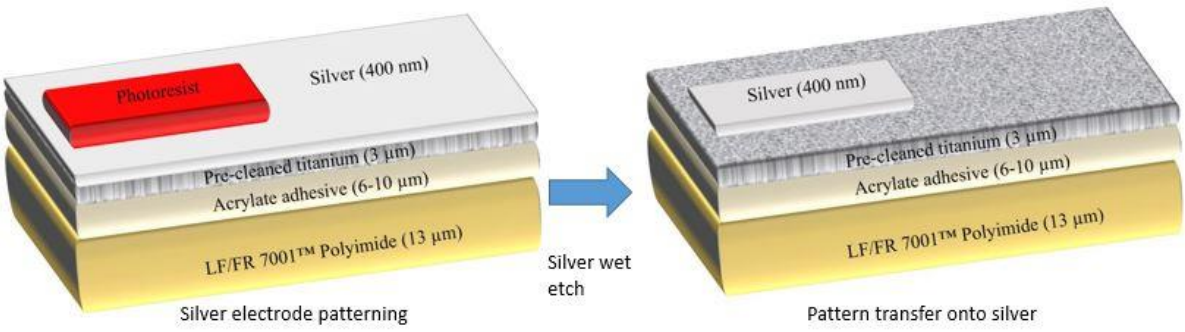

Figure 3.6: Schematic showing (left) step of patterning silver with photoresist followed by a wet etch (right) and pattern transfer onto silver.

Even though in a diluted form, the base piranha is a dangerous mixture to handle and readily oxidizes organic compounds including skin upon exposure. Hence, careful handling and disposal (the solution must be exposed to air to dissipate oxygen formed) before it is mixed with other waste and disposed. The containers containing piranha or its waste should always be stored with a vented cap to avoid pressure build up due to oxygen formation. Piranha solutions are only effective when freshly prepared and cannot be stored in large quantities. These issue beckon for an alternative method for patterning silver, instead of a wet etch. An alternative process involving the use of a shadow mask is discussed in chapter 4.

Figure 3.7 shows the final pattern of silver electrodes after pattern transfer following silver etch. The substrate was stripped of photoresist using a short rinse in acetone after the etch step. Adaptation of the silver etch process to a 3” x 2” foil was relatively easy and just required an increase in volume of the etchant used while keeping the same proportions.

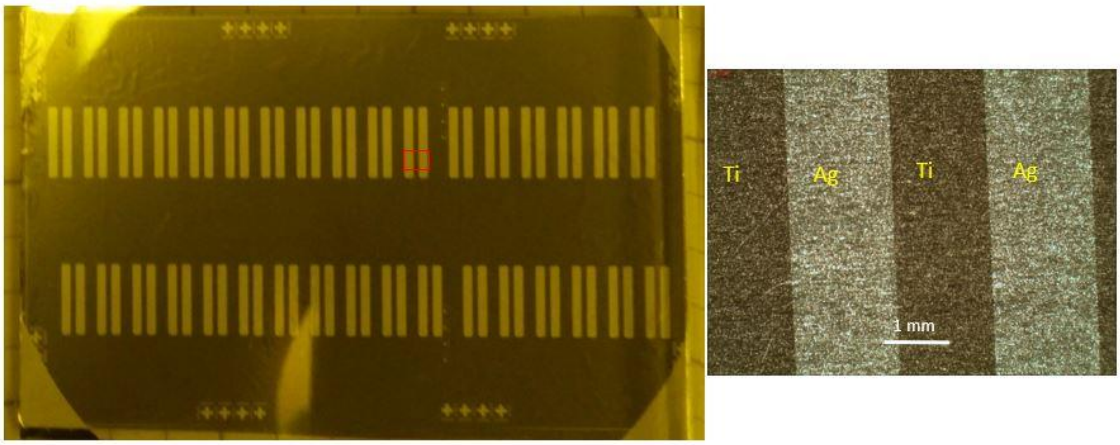

Figure 3.7: (left) Pattern transfer onto 3” x 2” substrate after silver etch (right) zoomed light field image of section indicated by a red box showing the patterned silver electrodes. This step registers the alignment marks used for aligning subsequent masks.

3.4.2 Platinum electrode patterning

This section deals with the patterning of the platinum electrode. Since the role of platinum electrode is to assist oxidation of hydrogen peroxide to detect blood glucose, care must be taken to maintain the purity of the electrode during its fabrication. Platinum presents a challenge compared to silver in the domain of finding a suitable etchant, since no appropriate wet etch chemistry exists. Slow etch rates of platinum have been reported using aqua-regia (1:3 mixture of nitric: hydrochloric acid) [41, 42] and was studied previously [26]. However, it was observed that this etchant did not create enough etch activity to effectively etch platinum. Finally, a lift-off process was adopted to pattern platinum.

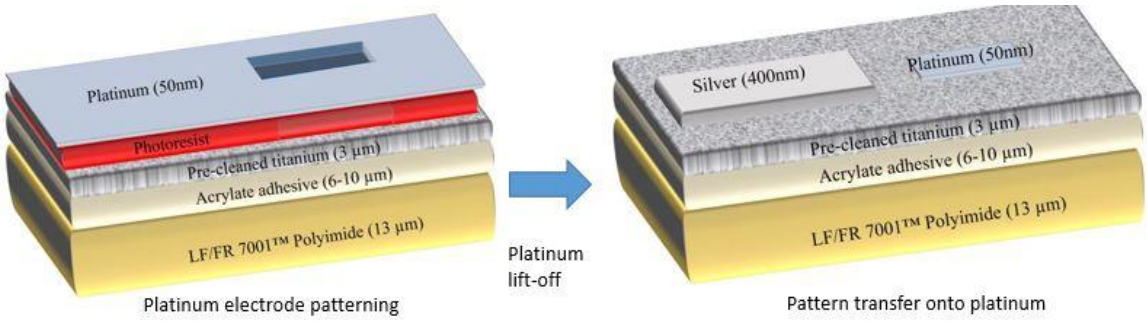

Figure 3.8: Schematic summarizing lift-off process. The metal deposited on a pre-patterned photoresist (left) is sonicated a solution of acetone to dissolve the underlying photoresist and lifting-off the section of metal not needed in the pattern (right).

Lift-off process involves patterning of a thin-films for which etch chemistries are hard to find, or exhibit poor selectivity between the film and substrate [46]. The film is deposited onto a pre-patterned layer of removable material (usually a photoresist) followed by removal of this material. S1818 photoresist was used to realize this removable and patternable material and then platinum was sputtered on top of the patterned photoresist. The substrate is then sonicated in a beaker of acetone until the pattern is transferred completely onto the substrate. Sonication aids the removal of photoresist which helps acetone seep under the deposited thin film and dissolves the photoresist, hence “lifting-off” the film. The process recipe parameters for the lift-off process are highlighted in the table 3.2 below.

Process step	Parameters
S1818 Photoresist	Dispense 3ml, 3000RPM, 5000RPM/s, 10s, 4000RPM, 5000RPM/s, 20s
Pre-exposure bake	85ºC for 1 min
Exposure	10s, 350 W/cm^2
Develop	(1:4) 351 developer: DI water, 1min 10sec
Deposit	Platinum sputter (50nm)
Lift-off	Immerse in 300ml of acetone, sonicate for 10min

Table 3.2: Process recipe for platinum sensing electrode patterning

However, there were many issues that were observed with such a process. First, lift-off process in itself is considered dirty and contaminates the substrate with photoresist residues, which caused problems due to variability in platinum electrode sensing during animal studies. Secondly, the process carried many unknown and uncontrollable process variables, such as the resist integrity pre and post deposition due to exposure to white light, sputtering chamber conditions and the presence of surface contaminants. This caused platinum lift-off residues on the substrate, sometimes even causing shorts between small the small gaps between adjacent platinum electrodes.

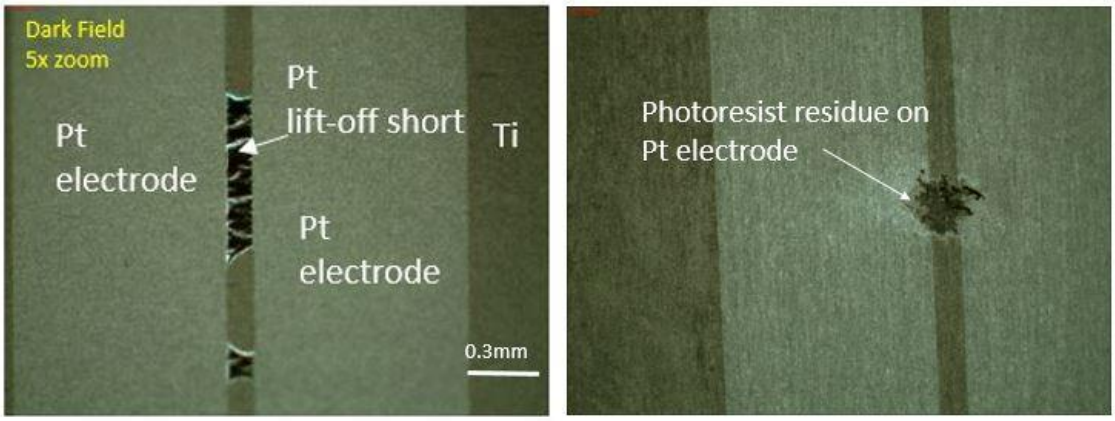

Figure 3.9: Dark field optical image showing lift-defects resulting in loss of yield and variability in sensors (left) platinum lift-off shorts remaining due to improper acetone penetration (right) photoresist residue causing contamination of sensing electrodes.

Figure 3.10 discusses a bilayer lift-off process which involves adding a blanket layer of exposed photoresist before coating another layer of photoresist, which is to be patterned. This extra layer of photoresist causes a bigger undercut (figure 3.10) which is hard and remote to cover, even using an isotropic deposition method such as sputtering, allowing room for acetone to penetrate the thin-film cover and dissolve underlying photoresist with more ease. However, this process adds to an extra step and wastage of photoresist (for bigger substrates) and also increases photoresist residue contamination during lift-off [48].

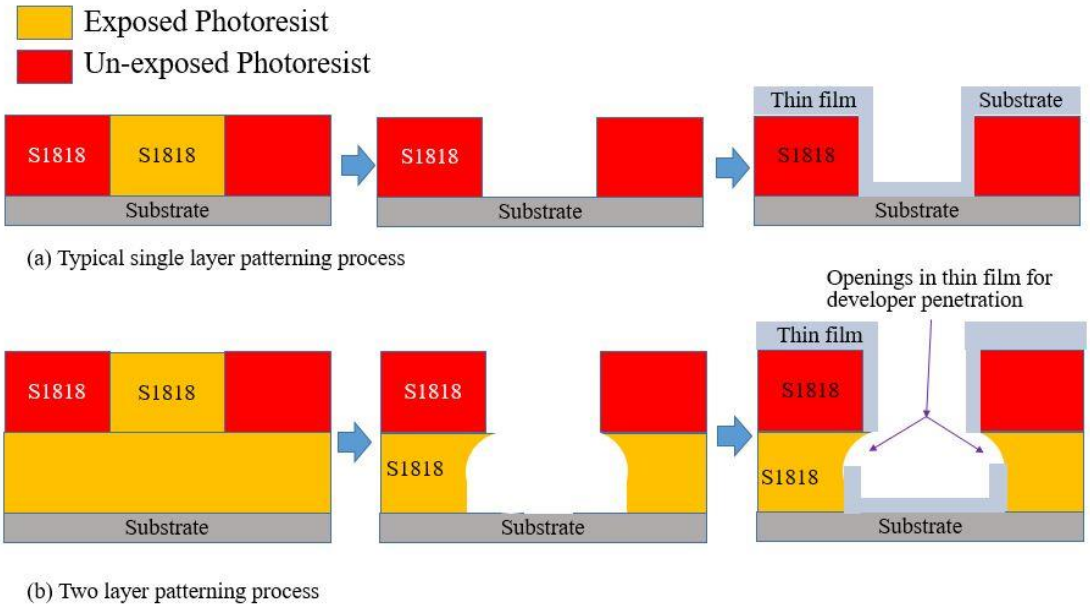

Figure 3.10: Schematic illustrating (a) lift-off residues resulting due to inability of developer to penetrate thin film (b) two layer patterning process used to create an extra undercut to ensure discontinuity in thin film to facilitate developer penetration.

A scotch tape aided removal of left-over platinum shorts was needed to achieve measureable yields in some cases, which led to contamination residues on adjacent platinum electrodes. These defects usually arise from many variables such photo-resist viscosity, exposure dosage, substrate non-uniformities, handling and pre-process contamination

Figure 3.11 shows an image of the patterned platinum electrodes after lift-off process. To overcome the yield loss through lift-off, an alternate step of platinum shadow masking as a replacement to lift-off is investigated in chapter 4.

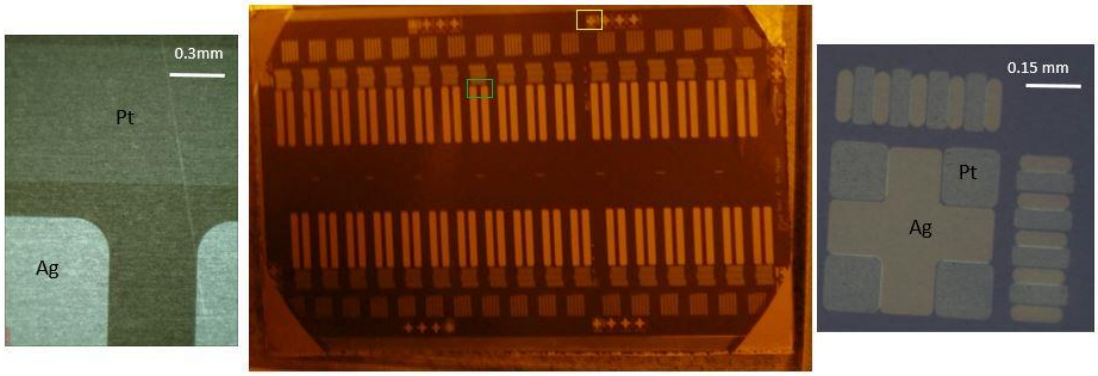

Figure 3.11: (left) Light field optical image of patterned platinum electrode (green box) (center) Image of 3” x 2” substrate after platinum lift-off patterning (right) Optical image of platinum alignment mark aligned with silver registration alignment mark (red box).

3.5 Contact-to-electrode trace masking

Conductive traces are an integral part of any sensor, which interface it to the outside world. This section focuses on patterning titanium layer to (1) electrically isolate platinum and silver electrodes and to (2) form connecting traces for these electrodes to contacts that interface the sensor to the real world.

.

3.5.1 Titanium trace patterning

The pattern connecting reference and sensing electrodes to their respective contact areas is formed using a photolithography step involving an S1818 photoresist. The process parameters for this step are provided in table 3.3.

Process step	Parameters
Adhesion promoter	2ml of HDMS primer. Spin dry for 30 sec at 4000 RPM
Bake	85ºC for 3 min
S1818 Photoresist	Dispense 3ml, 3000RPM, 5000RPM/s, 10s, 4000RPM, 5000RPM/s, 20s
Pre-exposure bake	85ºC for 3 min
Exposure	10s, 350 W/cm^2
Develop	(1:4) 351 developer: DI water, 1min 10sec
Hard bake	85ºC for 5 min

Table 3.3: Process recipe for titanium patterning

The evolution of titanium pattern over many mask revisions was aimed at achieving etch uniformity, fitting contact areas into custom made sockets at PDT for electrical testing and improvisation from issues related with reliability that cropped up from wrapping the sensor around 21ga, and later a 25ga catheter for animal studies. This study focuses only on the changes in masks from a process perspective.

Initial designs involving 21ga sensors were modelled with thicker titanium traces of trace width of 150 μm. The trace widths in the later designs were reduced to 100 μm to facilitate a transition from 21ga to 25ga catheters. However, some mask designs retained or rather increased the aspect ratios (1:400) which made the traces as a weak link that can compromise the reliability of the sensor. Using hydrogen embrittiling solutions (discussed in section 3.5.2) further reduced reliability. Though, the transition to a bigger 3" x 2" substrates improved throughput by more than factor of 5 (8 sensors per 1" x 1" design and 45 sensors for a 3" x 2" design), the yield was compromised due to etch non-uniformities arising from unequal etch windows in titanium etch mask design. Wet etching is a surface reaction controlled process [46], which results from diffusion of etchants across a thin boundary layer to the metal surface. Bigger etch windows reduce diffusion time of reactants and these areas end up over-etched compared to smaller window areas. Hence, an equal etch window mask design was adopted from subsequent lots, which eliminated the problem of etch uniformity.

Finally, a hard bake step was introduced in the process to improve etch uniformity and photoresist durability during etching process [47], especially when involving corrosive etch solutions such as 50% H_2SO_4 at 65^0C.

3.5.2 Titanium wet etch

This step involves the pattern transfer of titanium pattern formed that connect both the Ag and Pt electrodes to the contact area. A schematic of pattern transfer onto titanium after wet etch is shown in figure 3.12.

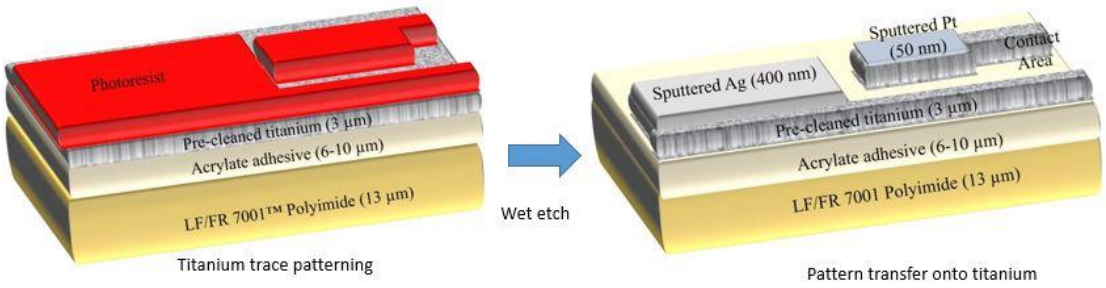

Figure 3.12: Device stack after titanium etch step. This step attempts to pattern titanium traces to connect the electrodes to the contact area. The silver and platinum electrodes fabricated in the previous steps (not seen) are protected by photoresist.

The etch step is carried out after patterning with titanium pattern in section 3.5.1 followed by removal of flexible substrate from gel-pak and immersing it in the etch solution. This is done since glass is incompatible with an HF based solution since it can etch through SiO_2, the composition of glass. Initially a 1:1:20 solution of $HF:H_2O_2:H_2O$ was used as titanium etchant solution. However, hydrogen

embrittlement of titanium lead to investigating if an alternate etch could be found. Though pre-clean solutions such as $HF:HNO_3:H_2O$ (1:10:100) that were investigated for containing hydrogen embrittlement in section 3.1.3, it was impractical to prepare etch solutions of such compositions for a bigger 3" x 2" substrates. Hence, the use of original HF and peroxide based solution was continued, though this did not compromise reliability of titanium traces as badly as with using it as surface preparation. Also, the use of bigger substrates consumed more reactants per substrate, and hence the etch solution needed to re-prepared after every four substrates etch.

The transition from a 12μm titanium foil to a 5μm foil reduced the etch time from 7 minutes to 2 min 30 sec. This contributed to a faster processing time and also a smaller undercut (section 3.1). However, etch defects still resulted from defects arising from previous process steps such as platinum lift-off defects, substrate point defects and sometimes even due to bubble clotting that happens if the solution is not agitated well (figure 3.13).

Sulfuric acid (50%) at 65^0C had also been investigated as a final etch solution. A hard bake of at-least 5 minutes was observed to be necessary for the patterned photoresist to survive the corrosive environment provided by this solution. Since the effectiveness of sulfuric acid etch of titanium depends on temperature, proper regulation of bath temperature was necessary throughout the etch process. The etch time for this solution was found to be ~ 35 minutes and etch rate found to be 85nm/min, which was observed to increase with increase in bath temperature.

The maximum temperature that the photoresist pattern on the substrate survived was found to be 110^0C, above which the photoresist ends up charred. Also, higher temperatures were observed to affect the brittleness of the polyimide substrate, making it more papery with increased temperature.

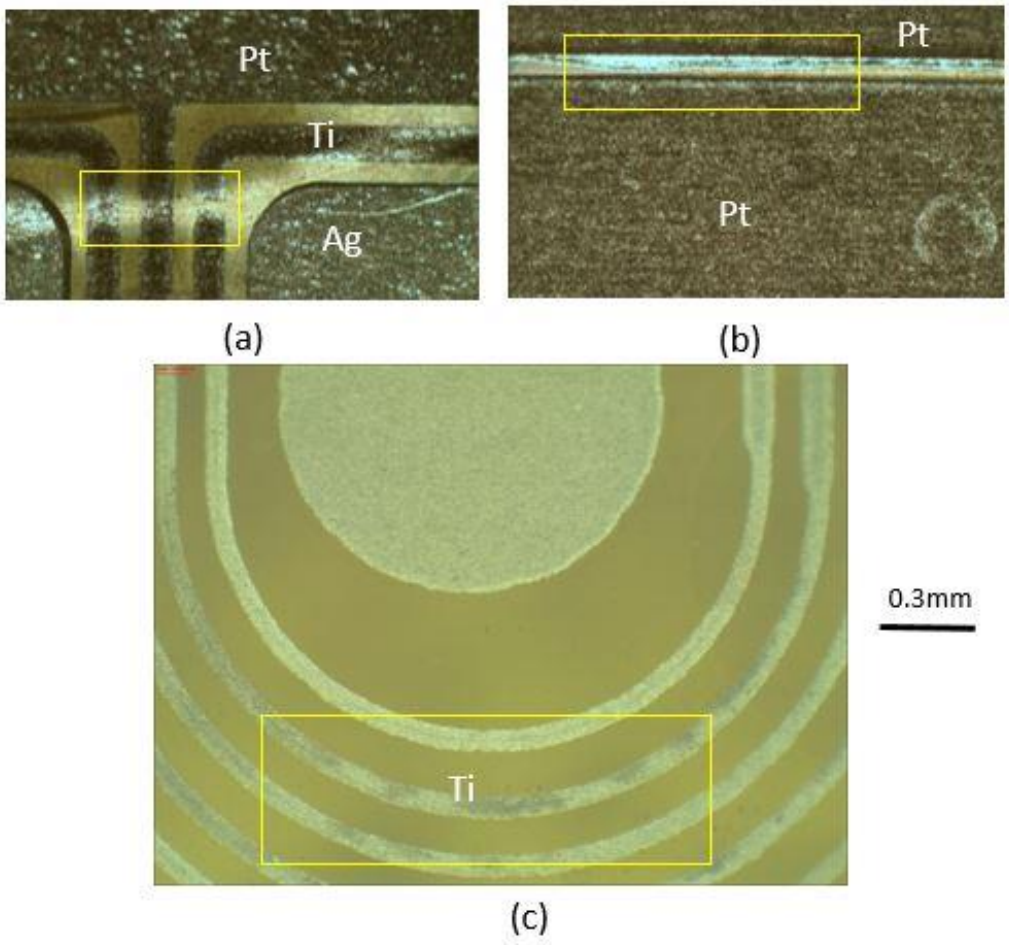

Figure 3.13: Titanium etch defects (highlighted in yellow boxes) occurring due to (a) over etch of trace due to substrate point defect, (b) under etch or etch short between platinum electrodes due to platinum lift-off residue, and (c) over etch of thinner traces compared to thicker traces due to unequal etch windows.

However, the durability tests conducted in chapter 5 showed much better durability of sulfuric acid pre-cleaned and etch substrates compared to HF based etched. Hence, sulfuric acid etch technology was adopted by PDT for the future lots. Figure 3.14 shows a 3” x 2” substrate after titanium wet etching.

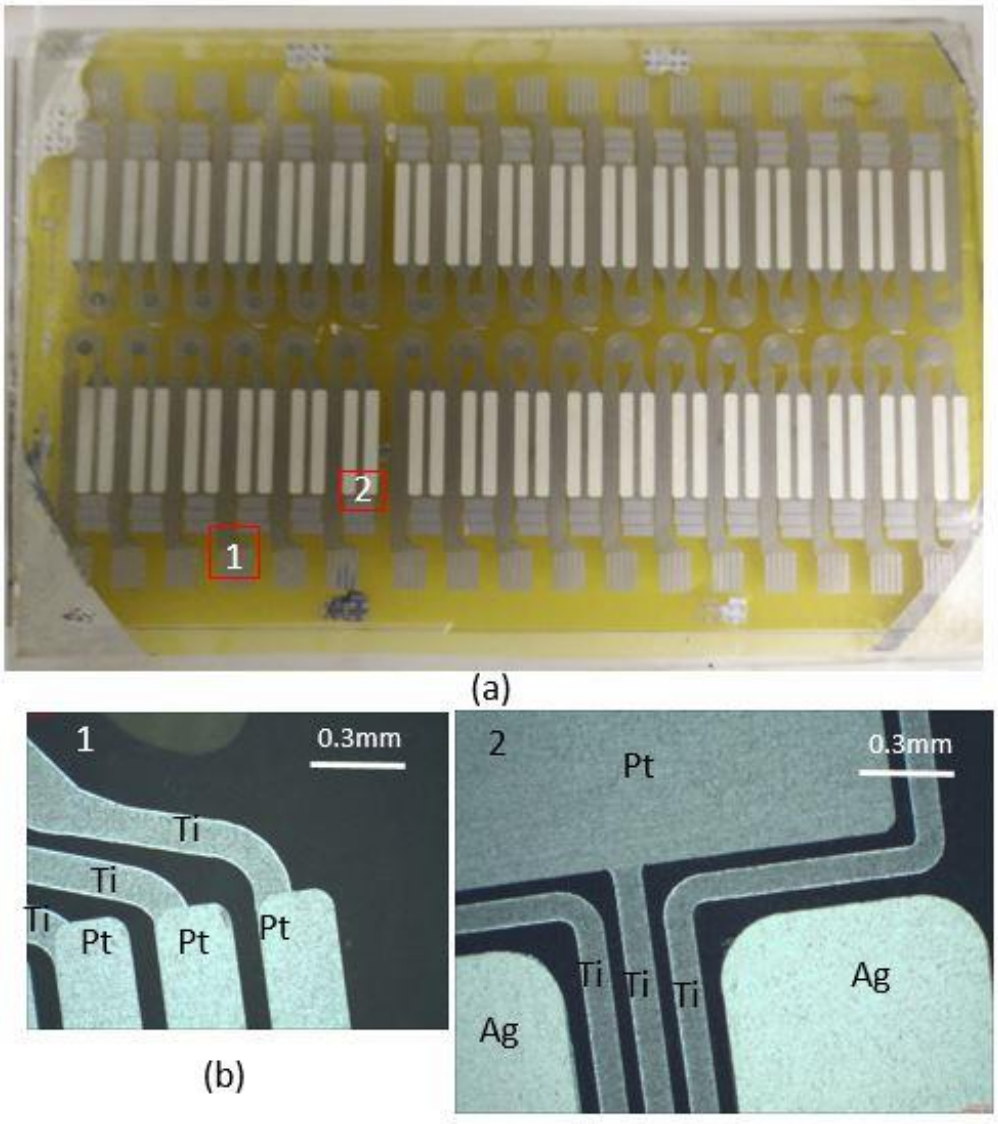

Figure 3.14: (a) A 3” x 2” substrate after titanium wet etch. Boxes in red highlight specific areas of a sensor show in (b) Region 1- titanium traces connecting contact pads, region 2- center area of the sensor showing reference and sensing electrodes.

3.6 Coverlay

A coverlay (or) cover-layer is a final protection layer for any electrical circuits. Cover-lays are ubiquitous any PCB manufacturing process flow as they help in shielding underlying conducting metal layers from the vicissitudes of the external environment [49]. Polyimide is a common choice for a cover lay material since it serves as a perfect flexible insulator all the while being temperature and chemically resistant. Other materials like polyurethanes, SU-8, poly-carbonyls, etc. are also used as cover-lays in many applications. Figure 3.15 shows a schematic of application and patterning of a coverlay to protect titanium traces of the sensor.

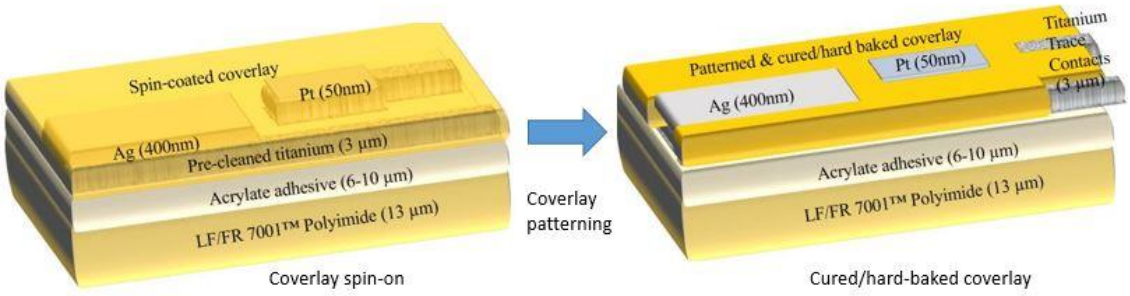

Figure 3.15: Schematic of process steps involving (left) spin-coating of coverlay on top of patterned titanium trace sensors flowed by a pattern step and a curing process (right) which produces a final coverlay exposing the electrodes and contacts, protecting the thin and vulnerable traces.

3.6.1 SU-8 coverlay

SU-8 is an epoxy based negative photoresist that is widely used in MEMS (micro-electro mechanical system) fabrication for features involving high aspect ratio structures such as micro-channels, ink-jet components and micro arrays for bio-analysis [50-52]. Aspect ratios as high as 1:20 have been achieved using SU-8 [50], however the main advantages of SU-8 lies in its biocompatibility, chemical resistance and good thermal and mechanical properties [50, 51]. This coupled with its inherent patterning capability make it an excellent candidate for a coverlay. The process recipe used in SU-8 coverlay patterning has been describe in table 3.4.

Process step	Parameters
SU-8 photoresist	2ml of SU-8 photoresist, 500RPM, 10s, 2000RPM, 30s
Soft bake	95ºC for 3min, 65ºC for 1min
Exposure	20s, 350 W/cm^2
Pre-exposure bake	85ºC for 3 min
Exposure	10s, 350 W/cm^2
Post-exposure bake	95ºC for 1min, 65ºC for 1min
Develop	SU-8 developer, 1min followed by 15 sec soak

Table 3.4: Optimized SU-8 process flow for coverlay

However, two major issues haunt this application of SU-8, cracking and delamination, which have been found in previous studies involving SU-8 films [53]. These phenomenon have been found to occur due to residual stress, which consists of two parts: (1) intrinsic stress due to cross-linking of epoxy resist during post-exposure and (2) extrinsic stress mostly due to thermal heating. SU-8 negative photoresist was previously used as a cover-lay for protecting the sensor traces [26].

The challenge of using an SU-8 coverlay was to obtain a uniform and smooth cover layer of the SU-8. The spin coating of SU-8 was difficult on top of the etched titanium foil since SU-8 thickness varied inside the region that was surrounded by the patterned titanium foil. This further affected the hard bake time and exposure time, which makes the exposure dose inconsistent across the substrates. Array lots utilizing SU-8 as coverlay suffered high yield losses due to cracks and delamination (figure 3.16), which could be attributed to the poor quality of SU-8 after spin coating.

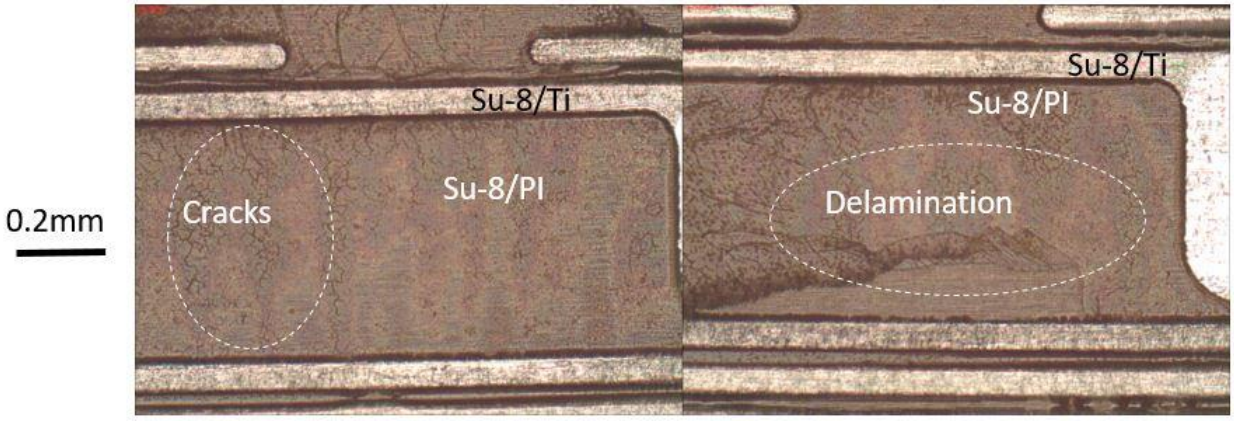

Figure 3.16: SU-8 cover-lay exhibiting many surface cracks and de-lamination issues.

PDT also reported a silver reference electrode contamination possibly caused by residual SU-8 during development. Hence, SU-8 was found to be unreliable as a layer to protect high aspect ratio titanium traces and a cover-lay which can withstand higher tensile stresses was needed. An alternative coverlay consisting of a polyimide was researched to overcome these issues.

3.6.2 Polyimide coverlay – A case study of PI-2525

Polyimide coverlays are the prime choice for printed circuit board passivation, and are known for their mechanical, chemical, electrical and thermal durability [54] and biocompatibility [55, 57]. Commercially available polyimides are mainly of three classes (i) photosensitive polyimides – which come as negative photoresists with photoactive compounds, (ii) wet-etch pattern transfer polyimides – onto which a pattern be transferred using a common developing solution and (iii) dry coverlays. The first two varieties of polyimides offer the advantage of patterning and good feature resolution though they need a curing process to attain the characteristics of a durable coverlay. Curing of polyimide is a high temperature process during which imidization of polyamic acid occurs from an N-Methyl-2-Pyrrolidone (NMP) / polyamic acid complex [56].

PI-2525, a wet-etch pattern transfer polyimide supplied by HD-Microsystems was identified for this study [58]. In comparison to a photo-sensitive polyimide it was found to be more durable and cost-effective for usage. It is also a low temperature cure polyimide, which has solvents that can help initiate imidization reaction at low

temperature of even 180^{0}C unlike usual polyimide cures at 400^{0}C, offering a benefit for our substrate compatibility. It has a final cured film thickness range of 5-13 µm and is used as an internal dielectric for IC and for stress buffer applications [59]. Unlike photoimageable polyimides, which are expensive and have lesser mechanical reliability, wet etch pattern transfer polyimides have superior strength, can be cured at lower temperatures, and can also be used for dry etch processing recipes [58]. A wet etch transfer process for patterning this polyimide is illustrated in figure 3.17.

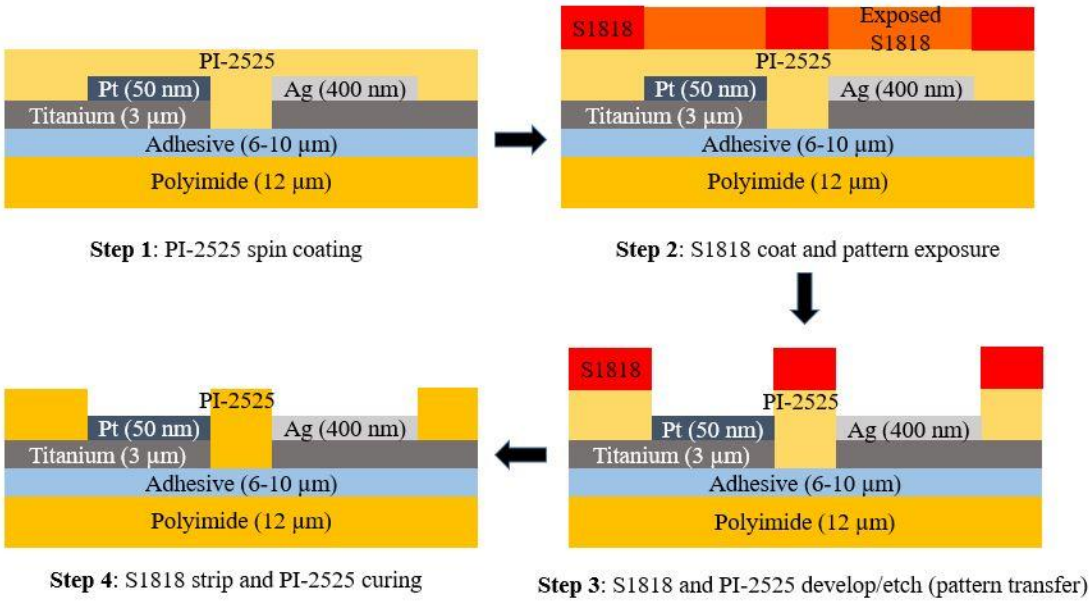

Figure 3.17. Process flow outlining wet pattern transfer of PI-2525. The pattern from S1818 is transferred onto the polyimide layer underneath using a common develop/etch stage.

The process steps begin once the titanium etch stage has been completed on the substrate. The first step involves the use of an adhesion promoter, an organo-silane compound (VM 651) to prime the substrate. This step is recommended for

metallic or silicon substrates .Since these substrates usually have an oxide/hydroxyl termination, they are hydrophilic and this organo-silane adhesion promoter makes the surface hydrophobic and increases cohesion between surfaces. However, this step was found not to be necessary since it involved coating PI-2525 over a 70% polyimide substrate area, which is already hydrophobic and a necessity to etch PI-2525 from metal surfaces, where we do not want really good adhesion of PI-2525.

The next step involves spin-coating of PI-2525, which is a very viscous solution and require careful dispensing to avoid any trapping of bubbles. The spread cycle should be done by ramping slowly such that PI-2525 reaches every corner. The spin cycle determines the final film thickness. PI-2525 can harden easily during extended soft bakes, so the time was optimized to achieve a better etch performance.

Once PI-2525 was coated onto the substrate, a patterning layer needs to be deposited to facilitate pattern transfer. S1818 photoresist was used to pattern, which did not require further priming as it exhibited a good adhesion onto the PI-2525 layer. An important metric in this step is the thickness of the photoresist which needs to be as thick as possible to ensure that it survives though an extended development time. PI-2525 starts to develop only when the photoresist has developed and this requires S1818 to survive longer developing times. A slow spin speed of 2500 RPM was used to achieve maximum possible S1818 thickness.

The patterned photoresist was then developed using a 25 % solution of a sodium hydroxide based developer (351 developer) [58] which develops the photoresist followed by etching of the underlying PI-2525, facilitating pattern

transfer. Pattern resolution was then inspected under a KLA Tencor optical microscope followed by a photoresist strip by immersing it in a bath of acetone.

The curing step was modified for the substrates which contained a modified B-stage acrylate adhesive layer. Acrylate adhesives are rated for use only around 200^0C and start to darken and char for longer durations at temperatures higher than 200^0C [59]. So a 300^0C cure for 1 hour, as recommended by HD Microsystems for curing PI-2525, charred the whole substrate, thereby rendering it unfit for final use (figure 3.18(a)).

To circumvent this problem, lower temperature & longer duration cures were experimented as suggested by HD Microsystems. Figures 3.18(b) & (c) show samples cured at 225^0C for 2 hours and 180^0C for 3 hours respectively. However, it was necessary to test if enough imidization occurs at these lower temperatures. Partial imidization of the film was a major concern, as it can compromise the biocompatibility of the sensor. To verify the imidization content at different temperatures, a Fourier Transform Infrared Spectroscopy (FTIR) study was performed using a Nicolet 6700 FTIR Spectrometer at Oregon Process Innovation Center (OPIC) using attenuated total reflectance mode (ATR) [60]. Glass slides spin coated with PI-2525 and cured at (a) 300^0C for 1 hour (b) 225^0C for 2 hours and (c) 180^0C for 3 hours were analyzed. Figure 3.19 shows an FTIR spectra of these samples.

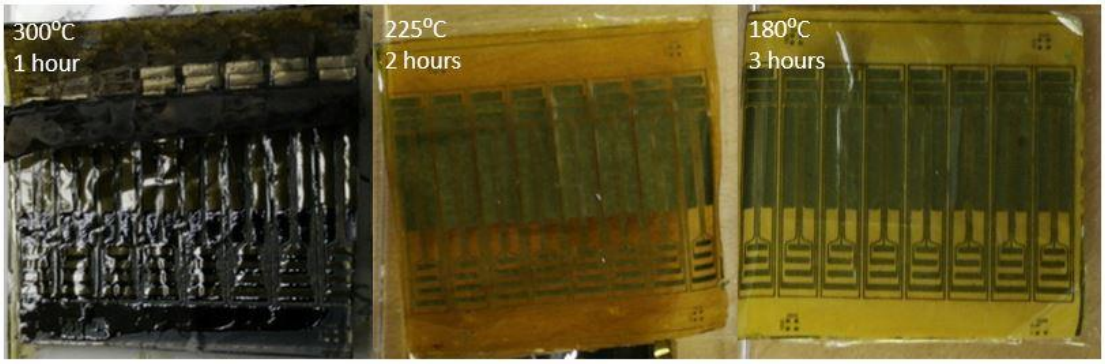

Figure 3.18: (a) Sample cured at 300^{0}C for 1 hour. The acrylate adhesive between the polyimide substrate and PI-2525 charred and severely affected trace reliability. (b) Sample cured at 225^{0}C for 2 hours. This looked promising in reliability aspects but still was papery and slightly dark. (c) Sample cured at 180^{0}C for 3 hours. This sample retained excellent flexibility and mechanical characteristics of a good coverlay.

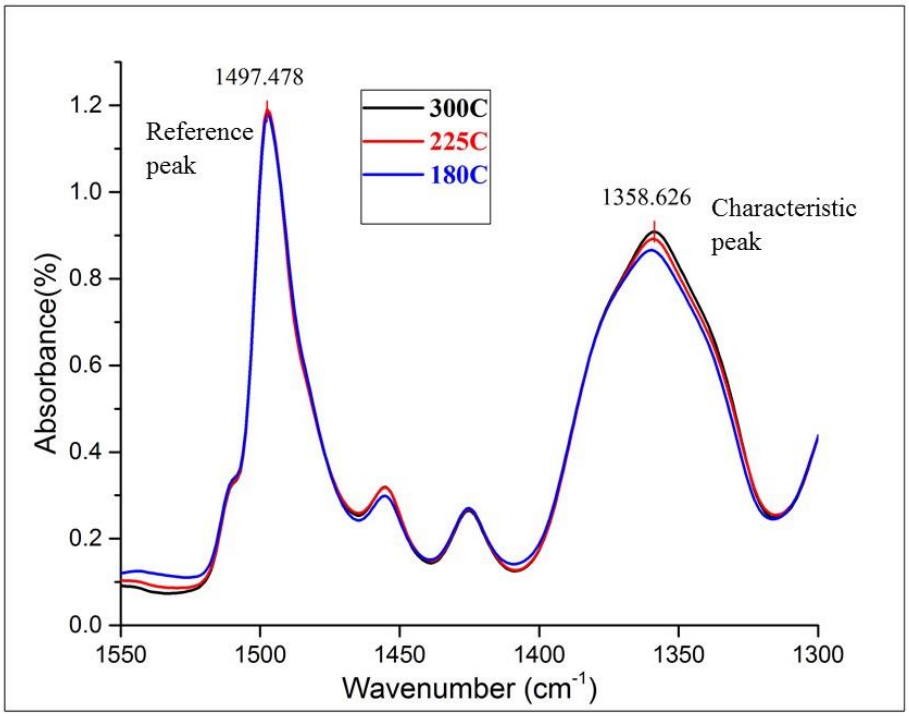

Figure 3.19: An FTIR spectra of PI-2525 cured at temperatures and durations of (i) 300^{0}C for 1 hour (ii) 225^{0}C for 2 hours, and (iii) 180^{0}C for 3 hours, spin-coated on a glass slide. Sample (i) is used as a reference to measure imidization content of other samples

The percentage imidization is measured using standard reference peaks (either carbonyl at 1720 cm^{-1} or aromatic at 1502 cm^{-1}) and comparing them with characteristic peaks of 1379 cm^{-1} of an FTIR. The % imidization (I) can be calculated using equation 3.4 [61, 62].

$$\%\ Imidization = \frac{Area\ of\ peak_{sample}^{1379\,\mathrm{cm}^{-1}}\ /Area\ of\ peak_{sample}^{1502\,\mathrm{cm}^{-1}}}{Area\ of\ peak_{reference}^{1379\,\mathrm{cm}^{-1}}\ /Area\ of\ peak_{reference}^{1502\,\mathrm{cm}^{-1}}} \qquad (3.4)$$

The sample cured at 300°C is considered as reference. The samples cured at other temperatures are evaluated for their imidization against this fully imidized reference sample.

It was found that both the samples cured at 180^0C and 225^0C were fully imidized in comparison with the 300^0C sample used as a reference. Also, both these samples performed well in terms electrical isolation after the curing stage. However, 180^0C cure was selected for further use as it showed the best mechanical reliability performance. The final optimized recipe for PI-2525 process is shown in table 3.4.

Pattern resolution was also tested for features as small as 100 μm with gaps a small as 50 μm being resolved. Figure 3.20 shows optical images of features resolved using PI-2525 after curing.

Process step	Parameters
Adhesion promoter	2ml of 0.5% of VM-651 solution. Spin dry for 30 sec at 3000 RPM
PI-2525	Dispense 3ml, 500 RPM, 100RPM/s, 10s ; 5000 RPM, 500RPM/s, 35s
Pre-exposure bake 1	150ºC for 45sec
S1818 photoresist	Dispense 2ml, 500 RPM, 100RPM/s, 10s ; 2500 RPM, 500RPM/s, 35s
Pre-exposure bake 2	90ºC for 1min
Exposure	10s, 350 W/cm^2
Photoresist develop and PI-2525 etch	1:4 solution of 351 developer for 2min 30sec
Photoresist strip	Dip and rinse with acetone
Curing	RT to 180ºC, 4ºC/min, 180ºC dwell (3 hours), 180 C → RT 4ºC/min (N_2 flow 5-10 sccm)

Table 3.4**:** Optimized PI-2525 coverlay process flow for protecting titanium traces

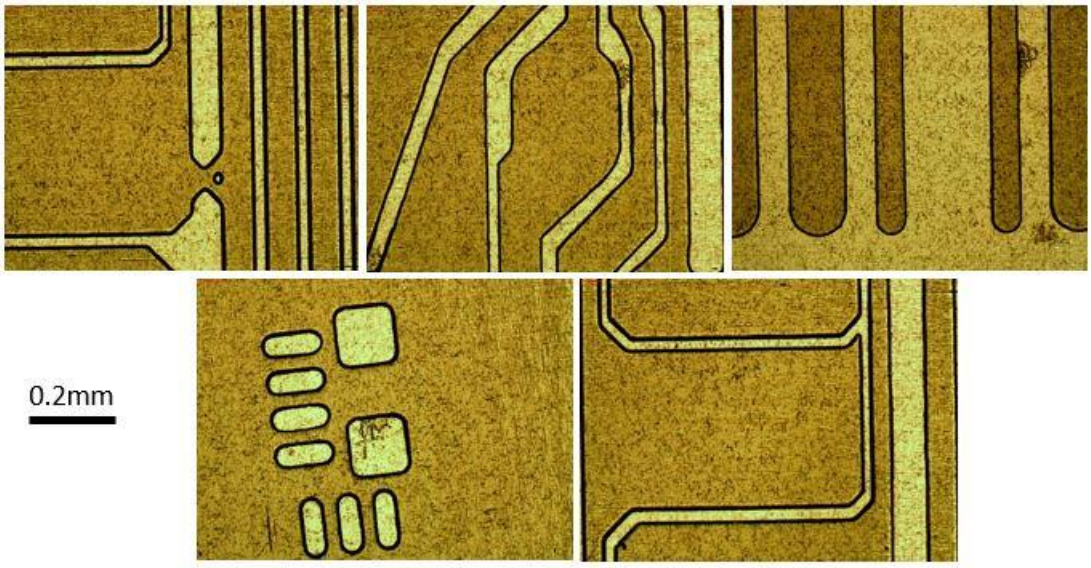

Figure 3.20**:** Optical light field image showing feature resolution for a 3” x 2” coverlay design indicating different parts of the sensors such as contact traces, alignment marks, and electrode region.

Hence, PI-2525 was found as a suitable alternative coverlay to SU-8. The process was optimized for a 3” x 2” substrate size and transferred to PDT for future use.

4. Development of alternate patterning approaches

The original process design discussed in the previous chapter employs a total of eleven process steps to manufacture the sensor electrode base, which include four photo-mask steps. The original process flow, though easier to realize using conventional manufacturing methods, still suffers from a number of issues.

The photo-patterning steps were observed to contaminate the electrode response during animal studies conducted by PDT. In particular, the lift-off process used to pattern platinum electrodes resulted in contamination of platinum with photoresist and introduced artifacts in sensitivity of the final sensors. Moreover, sonication on the substrate during lift-off process weakened the adhesive layer bonding titanium foil to the polyimide base. This reduced the reliability of the sensors significantly, and even resulted in titanium foil peel-off after sonication for about 40 minutes in acetone. Spatial variability was also an issue within a given lot or between lots. Photo-patterning of Ag electrode also introduced issues with etch residues that can impact further process steps and involved handing of dangerous base piranha solution.

This chapter discusses a few alternate process approaches, their integration into the existing process flow, and the benefits they offer if successfully adopted. Section 4.1 discusses the principle of shadow masking, their fabrication and concludes with their integration in the process flow. Section 4.2 discusses the process of controlled laser ablation of titanium as a patterning method alternative to titanium

wet etch discussed in section 3.5. Section 4.3 concludes with a new process flow and tests for integration done to accommodate the above mentioned process steps.

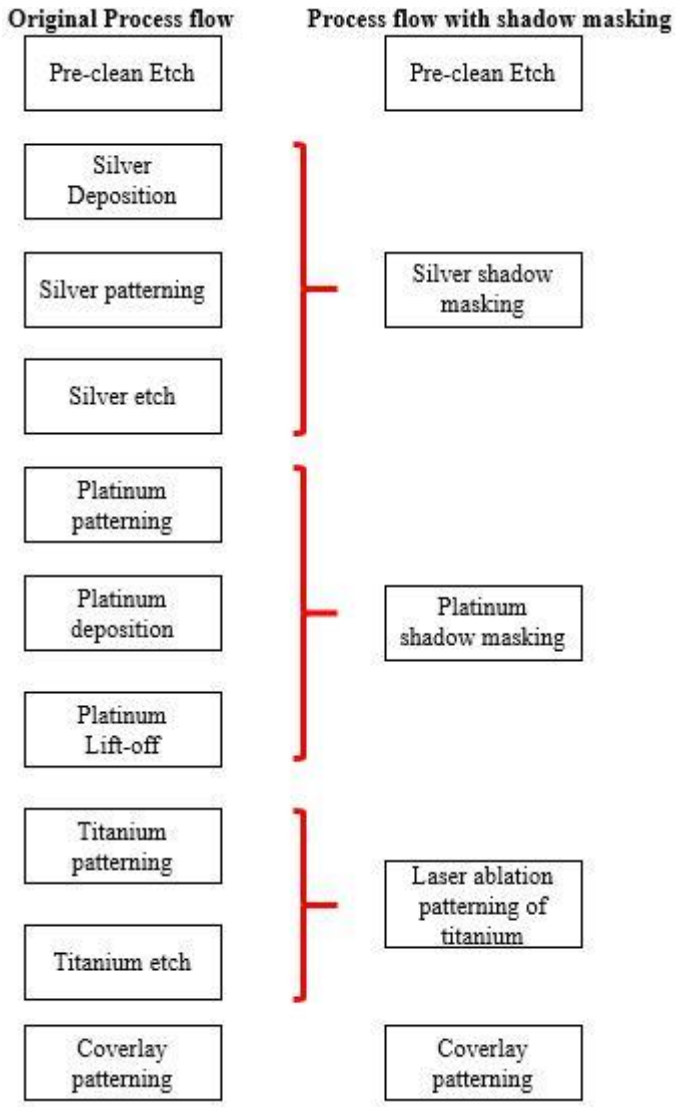

Figure 4.1: Comparing original process flow discussed in previous chapter 3 to a modified process flow using shadow masking and laser ablation patterning. The number of process steps can be significantly reduced from 11 steps to 5 steps, if successfully implemented.

4.1 Shadow masking electrodes

Shadow/stencil masking is a method of realizing patterned structures on substrates through depositing over selective area openings defined by a mask [63]. This mask is usually a hard mask i.e. made of a permanent material or metal and overlaid on a substrate. The mask is then secured onto the substrate using an appropriate substrate holder. The goal was to ensure that there is no significant gap between the mask and the substrate. This set-up is then loaded into a thin film deposition chamber, which deposits the required thin film in the openings defined by the mask. The mask can be easily removed or peeled off after the deposition, containing the thin-film only in the areas required to realize a given pattern. Figure 4.2 summarizes some inherent problems associated with shadow masking [64].

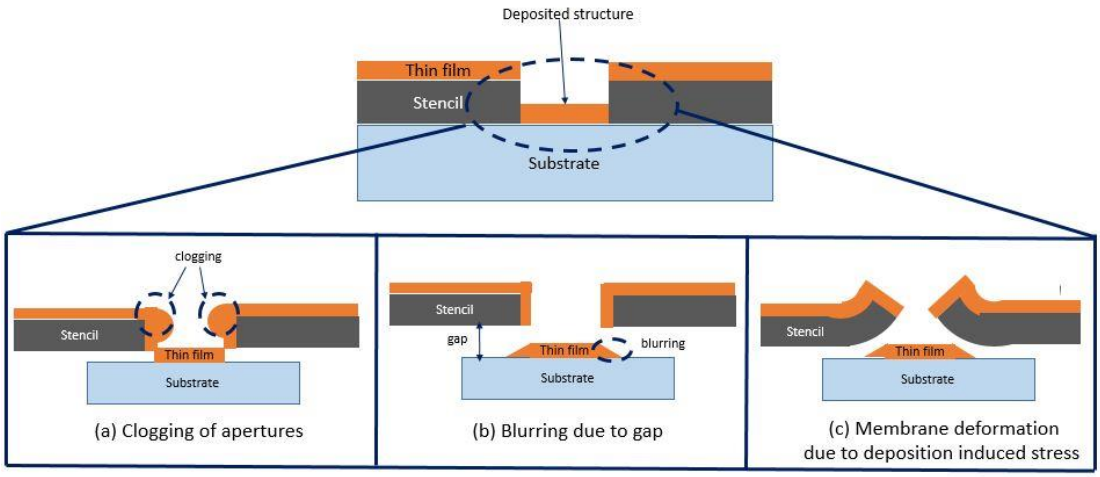

Figure 4.2: Process of realizing patterned structures using a stencil/shadow mask with practical issue that can result (a) clogging of apertures to repeated usage (b) blurring of structures due to finite gap between substrate and stencil mask (c) mask deformation due to thermal or film induced stresses [64].

Subsequent sections discuss the fabrication of shadow masks, attempts to pattern silver and platinum patterns and conclude on recommendations for improving pattern resolution of shadow masking and its integration in the existing process.

4.1.1 Fabrication

Shadow masks can made from a wide variety of materials, each offering its own benefits and issues. An ideal shadow mask offers (i) excellent pattern resolution, (ii) surface planarity or conformity, (iii) durability for long-term repeated usage, and (iv) easy manufacturability. However in practice, it can be very difficult to realize a shadow mask with all ideal qualities and many times depends on the choice of material.

Silicon shadow masks are popular in realizing high precision features (close to 2 μm) [64, 65]. The silicon is usually patterned with a photoresist on both the sides, and a directional wet etch in KOH [66] of silicon is performed to realize very accurate feature resolution. However, silicon masks are brittle and often fail or crack upon repeated usage.

Metal shadow masks are known for their durability for repeated usage. Aluminum shadow masks are perhaps the most common of this variety, benefitting from their low cost and easy machinability. However, a higher co-efficient of linear thermal expansion (CTE) of aluminum (22.2×10^{-6} m/m.K) [67] limits its usage for feature sizes < 200 μm. Also, thinner masks are required to realize smaller feature

sizes. Aluminum becomes very fragile in 2 mil (1 mil = 1/1000 inch) thickness range, the thickness usually used to pattern feature sizes around or less than 100 μm.

Stainless steel is better alternative and relatively inexpensive to use as a starting material to machine shadow masks due its lower CTE (18.7 X 10^{-6} m/m.K) [67]. In this study we use stainless steel shadow masks fabricated using a 2 mil thick 304 grade stainless steel provided by Trinity Brand Industries (TBI). The shadow masks were fabricated using an ESI 5330 μVia Nd:YAG laser of 355 nm wavelength and 10 nanosecond pulse width [68]. The operation of this laser are discussed in detail in section 4.2. Mask designs were made using CAD (computer aided design) software SOLIDWORKS™, which created a drawing exchange format file (.dxf). This file was then loaded into a CAM (computer aided manufacturing) software SMARTCAM™, which defines the tool path for the pattern. The CAM software then outputs a g-code, which defines laser coordinates for movement and is loaded into the laser. The process parameters used to machine the shadow masks and their significance in design the recipe are summarized in table 4.1.

Laser Parameter	Function	Range	Value used
Laser power (Watts)	Overall laser power in a pulse of the laser beam.	0.3-5.8 W (for Gaussian beam) 0.3-1.9 W (for flat top beam)	2.481 W
Laser velocity	Very crucial in pattern definition and heat transfer statistics along the masks.	50-400mm/sec	200 mm/sec
Z-offset	Controls the efficiency of the ablating laser beam (power used to ablate/power wasted as heat) and concentration of power at point of focus. Crucial in reducing warping of material.	-5.0 mm to 5 mm	-0.05mm
Repetitions	No. of times the laser traces the whole pattern. Changes with change in pattern, as heat transfer varies and so the no. of repetitions to totally ablate the material from the cavity	Any number desired	13(for Ag)/15 (for Pt)
Laser beam profile	The shape of laser beam power. Determines the profile of the cut achieved.	Gaussian/Top hat	Gaussian
Laser rep rate	The time between laser pulses. Can affect the energy delivered per pulse and hence the ablation depth and efficiency.	30 kHz-70 kHz	30 kHz
Spot size	The diameter of the cylindrical beam (only for flat top profile)	55 -140 μm	Not applicable

Table 4.1: Process parameters of a laser used for machining shadow masks out of 2 mil thick grade 304 stainless steel along with their significance, range and optimized values.

Initial attempts to fabricate shadow masks ended up warping stainless steel due to high pattern density and increased local heating. This problem was later circumvented by using a copper backing mesh to conduct away local heating due to

laser heating during machining process. The machined masks contained oxidized slag around corners of features, which was removed by an overnight sonication in a 5% solution of Citranox™. The final shadow masks fabricated for silver and platinum electrode patterns are shown in figure 4.3.

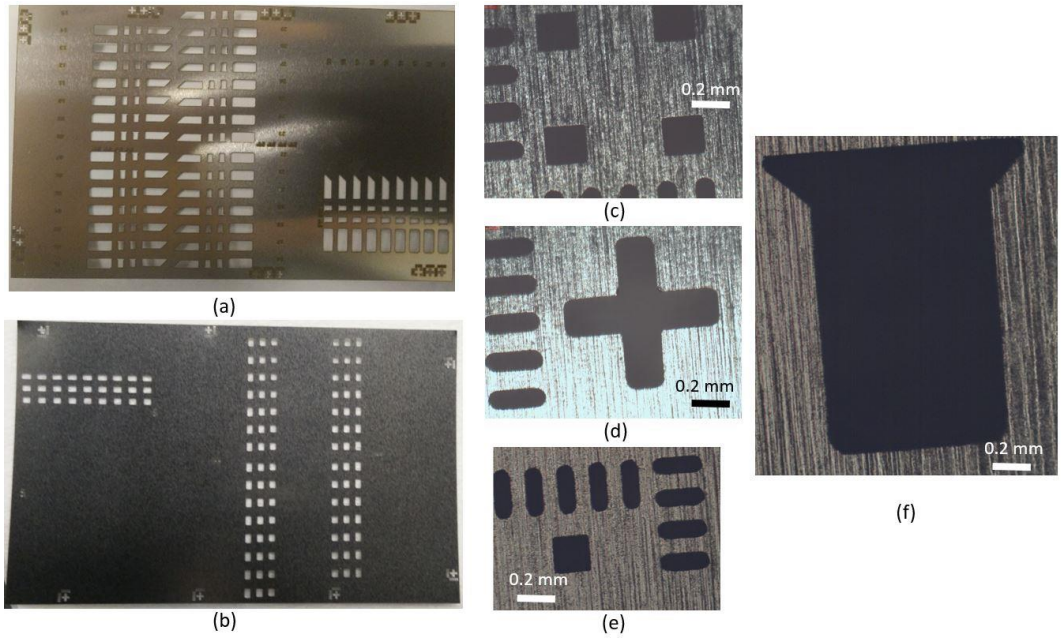

Figure 4.3: Images of fabricated shadow masks for (a) silver pattern, (b) platinum pattern, (c) optical image of dark field alignment mark, (d) optical image of light field alignment mark, (e) optical image of smallest feature (smaller light field alignment mark of 100μm apertures), and(f) optical image of silver electrode aperture

4.1.2 Electrode masking

The shadow masks fabricated (discussed in the previous section) were aimed towards replace photo-patterning steps to realize Ag and Pt electrodes. This requires a pattern resolution as good as or better than photolithographic patterning. Masks patterned in the previous section 4.1.1 were used to shadow mask silver and platinum patterns in two different scenarios (i) thermal evaporation of 400 nm silver for silver

pattern (ii) sputtering of 50 nm molybdenum for platinum pattern (platinum sputter runs were found to be very expensive for process tests). Pre-cleaned 3” x 2” substrates and aluminum substrate holders were used. This study was conducted to analyze the effect of mask pattern density, and thin film deposition method on shadow mask pattern resolution.

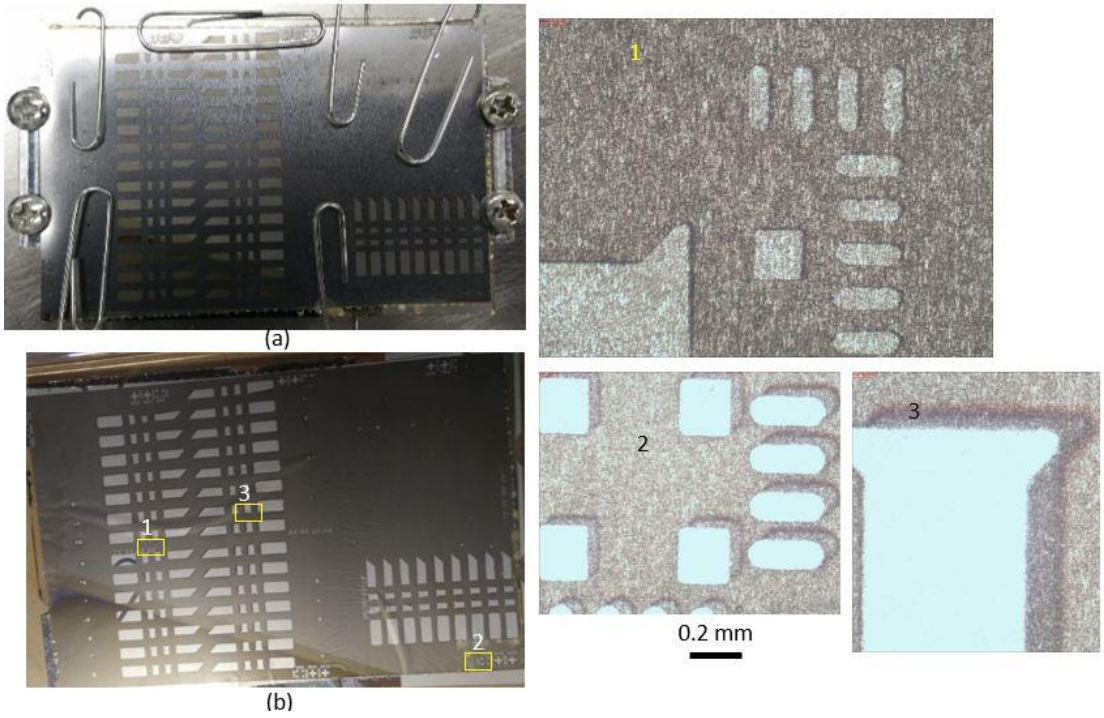

Figure 4.4: (a) Substrate holder arrangement to hold shadow mask to substrate before loading into thermal evaporator. (b) Pattern after shadow masking 400nm silver. Regions 1, 2 and 3 indicate specific areas of the substrate in yellow boxes. Region 1- region with excellent pattern registration due to proximity to holding clip, Region 2 & 3 – poor pattern resolution due to gap between substrate and mask. The aura seen is called “shadow”.

Thermal evaporation, being a line of sight of deposition method, was able to register patterns well at places where the mask was in contact with the substrate.

These were the areas in the close proximities of the paper clips in figure 4.4(a). Line of sight deposition also requires the substrate to lie exactly in line with the source. This can be a problem with bigger substrates where patterns near the periphery can exhibit large shadowing even for a small gap.

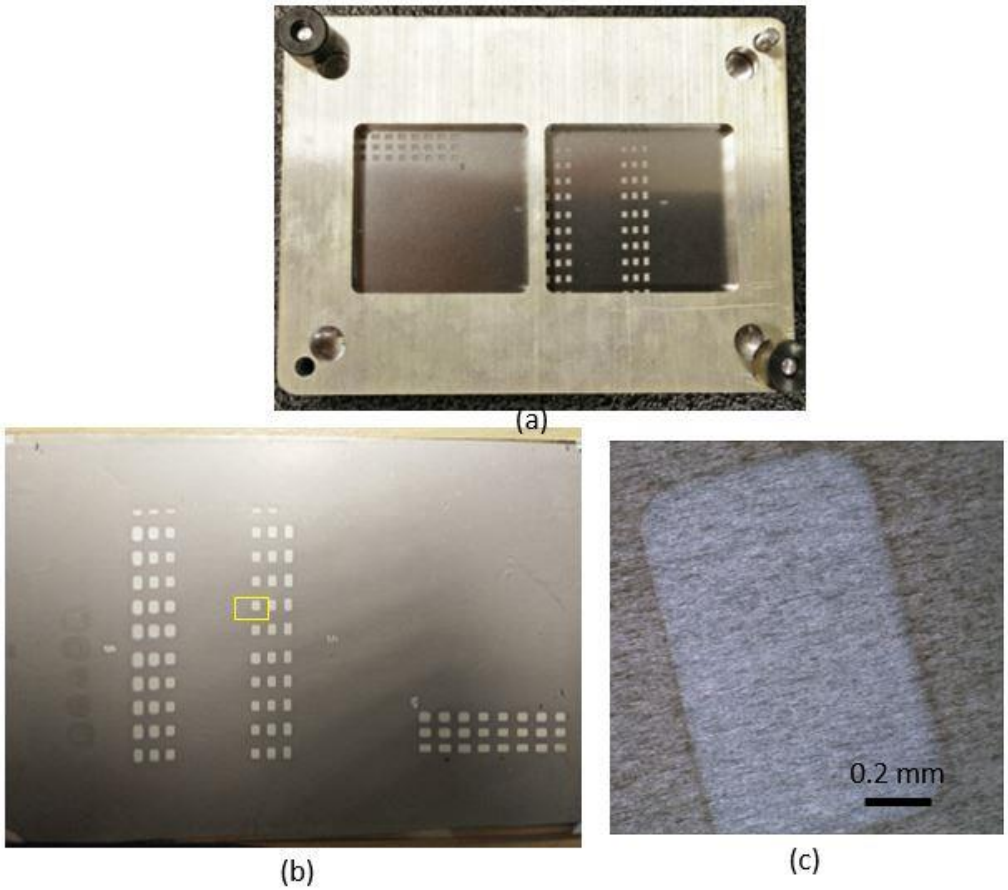

Figure 4.5: (a) Substrate holder arrangement to hold shadow mask to substrate before loading into sputter tool. (b) Pattern after shadow masking 50nm molybdenum onto platinum mask. Region highlighted by yellow box is (c) Optical image of pattern registration of a platinum electrode. The aura of shadow is all around the pattern due to sputter deposition.

Figure 4.5 summarizes pattern registration using shadow mask deposition using sputtering of 50 nm molybdenum using ATC Orion sputter tool at MBI. Unlike

thermal evaporation, sputter deposition is more uniform over large substrate areas. However, this can also lead to poor pattern resolution even if there is very minute gap between substrate and mask. Also, the sputter process tends to heat up the mask due higher kinetic energy of bombarding electrons. This warps the mask on a micrometer scale, enough to cause gaps during deposition to form shadow auras. A way to circumvent this problem would be the usage of bimetal shadow masks, which can withstand this heating effect. Be-Cu shadow masks have shown good pattern resolution results as small as 70 μm [63]. However, the costs and complications associated with fabrication of these bi-metal masks deprioritized their development.

4.2 Controlled laser ablation of titanium – A novel patterning approach

Titanium trace patterning by wet etch methods discussed previously in section 3.5.2 face some inherent issues. Wet etch as a process step, can pose difficulties due to excessive under-cuts due to isotropic nature of wet etch processes [46]. Sample-to-sample variation can be high since there are many variables which can easily be affected. For example, the etchant concentration may deplete upon re-using the etch solution, which may cause poor spatial uniformity in latter samples in a batch-type process. To address this problem, one needs to replenish the right amount of reagents from time to time, which becomes difficult and dangerous for a manually controlled process. Also, constant agitation of the solution is required, and in some cases, a proper temperature control and uniformity in the solution is necessary. Undercutting of titanium traces is also a major issue, given the isotropic nature of wet etch. All these factors can significantly contribute to a less reliable traces.

The etchants needed for titanium etchant usually involve hydrofluoric acid (HF) [41-43], which is especially dangerous for handling, even for an acid. A brief exposure with HF, with solutions even as dilute as 5% can cause HF poisoning [71], which can lead to cardia arrhythmia. These issues reduce the throughput that can be achieved using the wet etch, and coupled with a certain degree of un-abatable hydrogen embrittlement (as discussed in section 3.2.1), warrant for an alternative approach to patterning titanium.

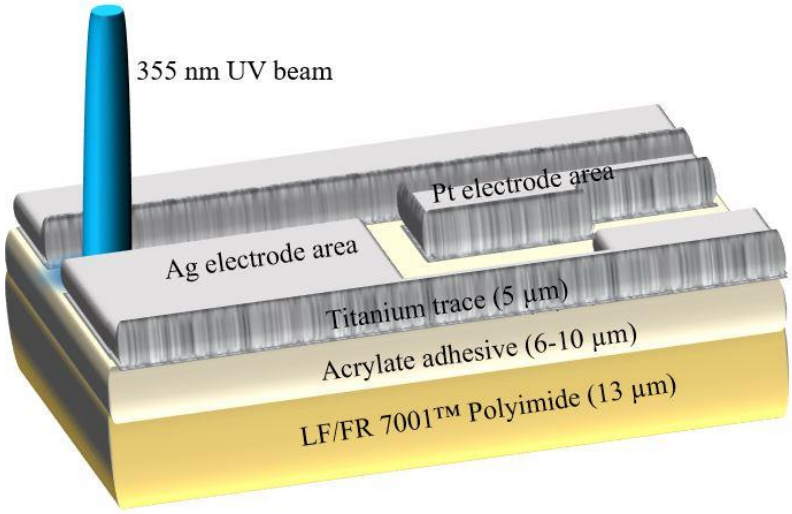

Figure 4.6: Device stack schematic during titanium ablation patterning. The electrode areas are electrically isolated along with their respective traces during laser ablation patterning.

A promising approach involves using the laser, which is currently used by PDT to singulate sensors from the array, to selectively ablate titanium in the form of titanium trace pattern (figure 4.6). The ablated portion of titanium then electrically isolates the silver and platinum electrode areas and routes them to the contact region though conductive titanium traces. However, this approach poses a significant challenge of selectively ablating titanium over the adhesive and polyimide layers underlying it.

Though, the technique of laser ablation pattering is popular in the PCB industry using materials such as copper clad polyimide [74, 75, 77-79], the use of this technique to pattern titanium clad polyimide has not yet been reported in the literature, and requires designing a stable ablation process recipe from the beginning.

This chapter presents a brief description of ablation mechanisms, significant process parameters that influence ablation quality and their optimization to achieve a stable and reliable process, and finally, an outlook into how it can be integrated into the existing process flow.

4.2.1 Theory of laser ablation

From the days when the foundation of laser theory was laid by Einstein [71] to the present day, lasers have immensely contributed to advances in research and have greatly influenced the daily lives of people. The unique properties of laser beams such as coherence, monochromaticity and collimation, makes them very attractive for several research fields. Low power lasers are usually employed in [72, 73] optical fiber communications, data storage, digital recording, printing and many other applications, whereas high power lasers are used for scientific, medical and manufacturing purposes such as weapons, welding, tumor therapy, spectroscopy, etc. This section attempts to employ the use of a high power laser for the purpose of laser ablation and explain the mechanism behind its working. Figure 4.7 illustrates the classifications of lasers that are commercially available.

Commonly available commercial lasers for micromachining metal or polymer films usually belong to molecular gas (CO_2), solid-state crystal (Nd-YAG, 355nm) or excimer (KrF, 193nm) sources [74]. In particular, Nd-YAG lasers are cheaper and popularly used for micro-machining and via drilling for the PCB industry [75].

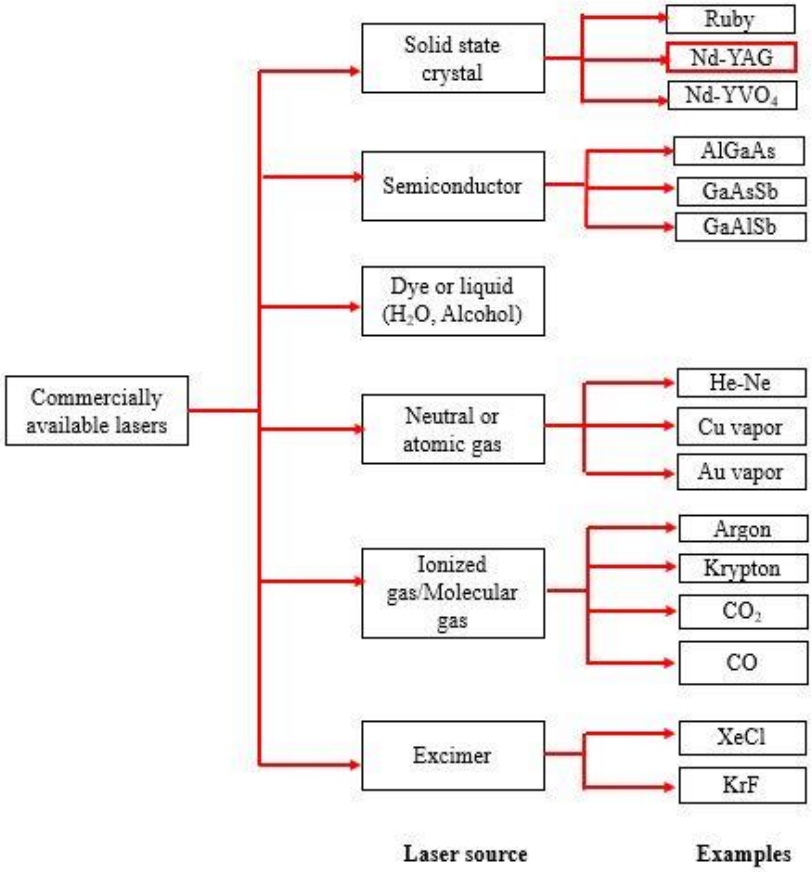

Figure 4.7: Classification based laser source types for some commercially available technologies. The laser used is an NG:YAG laser, highlighted in red.

Laser ablation is essentially the removal of a material (metal, polymer, ceramic, etc.) due to rapid heating and vaporization using the aid of a laser. However, the mechanism in which the material is removed depends upon a number of factors such as the nature of the material (absorption, thermal diffusivity, melting and boiling behavior) and laser parameters (wavelength of the laser source and pulse duration [73].

The peak temperature attained at the ablation site depends on the efficiency of energy delivery. Short and uniform pulses affect smaller volume of material but can

achieve higher peak temperatures whereas, longer pulses result in larger affected area but a lower peak temperature [76]. In case of nanosecond pulsed lasers, the absorbed laser energy first heats up the target metal to its melting point and then vaporizes it, removing the material [76]. However, energy imparted to heating the required specific region depends on heat conduction into the solid during this process.

Laser ablation involves solid-laser interactions and is very complex to realize. However, models exist that are accurate enough to explain the heat transfer during ablation process. The two-temperature thermo-optical model is widely used to model pulsed laser ablation for nanosecond lasers. The heat diffusion equation described in equation 4.1 can be used to model the rate of heating for a nanosecond laser pulse [76].

$$C\frac{\partial T}{\partial t} = \frac{\partial}{\partial z}\left(k\frac{\partial T}{\partial t}\right) + I_a \alpha \exp(-\alpha z) \qquad (4.1)$$

Where T is the temperature of the solid (K), z is the depth into the solid from the surface (along the axis of laser strike) (m), C is the volumetric heat capacity of the solid (J/m^3.K), k is the thermal diffusivity (W/m.K), I_a is the laser intensity at the surface (W/m^2), α is the optical attenuation factor (m^{-1}). In other words, there is enough time for the thermal wave to propagate into the solid during the nanosecond pulse to create a large layer of melted material.

The laser employed for this study was an ESI 5330 uVia laser at MBI, which is a nanosecond pulse-length laser, a frequency tripled Q-switched Nd:YAG crystal

source and an operating wavelength in the UV region (355nm). This laser system is conventionally employed for micro-via drilling in the PCB industry and used for processing copper and polyimide.

The laser supports two beam profiles (gaussian and top-hat), power levels ranging from 0.1 W to 5.8 W for the gaussian and 0.1 W to 2.48 W for the flat-top beam. The flat-top beam is generated from the gaussian beam using beam shaping optics, and offers a uniform power intensity profile and a fixed range of spot-sizes (defined as the spatial diameter of the laser pulse width) from 55 μm to 140 μm. The laser focus piece is mounted on an x-y translational head, which moves the laser at a given translational velocity (a maximum of 400 mm/sec in x or y direction) with respect to a fixed base plate on which the sample to be micro-machined is placed. The peak repetition frequencies (frequency at which the nanosecond pulse repeats itself every second) supported by the laser are from 30 kHz to 70 kHz [77].

The pattern to be ablated is designed in a CAD software such as SolidWorks™, which generates a drawing exchange file format (.dxf). This file is then opened using a CAM software such as SmartCAM™, which assigns a path for the laser to trace and generates a g-code output, a text file containing information of laser co-ordinates and path trace. This g-code is then uploaded into the laser as a text file, and by setting the process parameters (such as power, velocity, etc.), the ablation of the g-code pattern is accomplished on the work-piece. The laser set-up is summarized in figure 4.8. The aim henceforth in this study, is to develop process

parameters and conditions (pre/in-situ/post-processing) to reliably & repeat-ably pattern titanium on polyimide without affecting underlying polyimide.

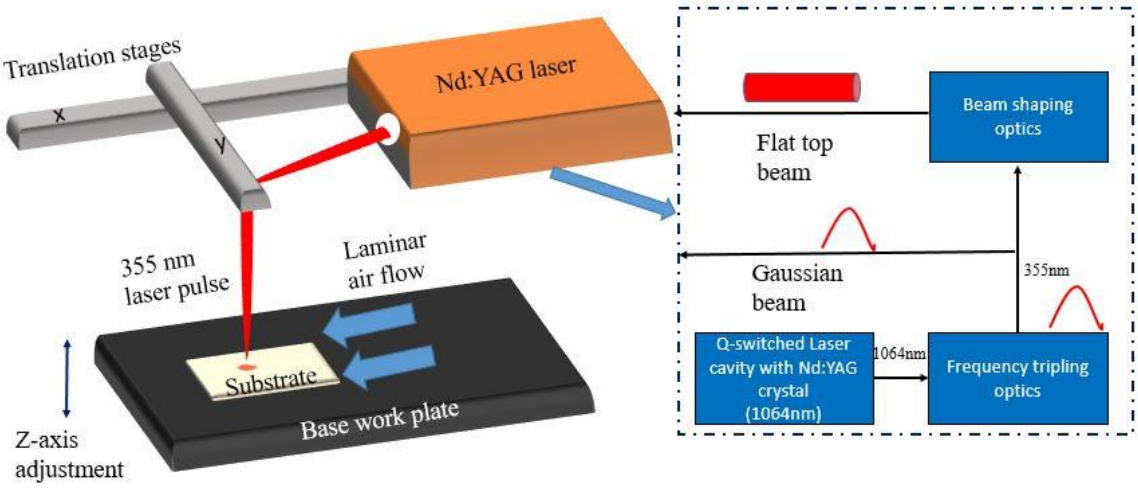

Figure 4.8: Schematic illustrating a conventional set-up of sample on the laser, along with the laser subsystems involved during processing.

4.2.2 Process development

The peak repetition frequency has direct influence on the incident energy/fluence per pulse which was found to decrease with increase in peak repetition frequency, such that rates above 40 kHz were found ineffective in ablating titanium for any power level. Ablation experiments at 40 kHz were found have poor reproducibility and hence a peak repetition frequency of 30 kHz has been used throughout the study. Flat-top beam profile has been chosen for this study for two reasons: (1) it offers a uniform power intensity across a pre-set spot size, thereby having lesser effect on underlying adhesive and polyimide and, (2) unlike gaussian, the spot-size is not prone to z-axis variation. The spot size for the laser in use is

defined only for a top-hat beam since gaussian beam is more ellipsoidal with respect to spatial distribution [77]. The fluence in relation to spot size is given by equation 4.2, where D is the spot size in cm.

$$Fluence(F) = \frac{4(Power)}{\pi D^2}(J / cm^2) \tag{4.2}$$

Increasing the spot size decreases the fluence of incident pulse for a given power level. Also, a bigger spot size requires taking it into account for designing the trace widths and also creates a bigger amount of ablation slag. It was found that a the smallest spot size of 55 μm was best suited for our requirements as it generated the least amount of ablation slag, provided for a bigger power window for experimentation and also had lesser pattern design constraints. A single laser pass resembling a cross pattern was used for the test samples. To characterize the process, SEM images were taken in an FEI Quanta 600 managed by OSU Electron Microscopy Facility.

The first step towards developing a stable recipe for ablation was to determine the threshold fluence of the titanium layer (F_{th}), which is the minimum laser irradiation fluence needed to initiate laser ablation of a material at a given wavelength [78-84]. An experiment was performed to measure the ablation depth as a function of incident fluence at a fixed velocity of 400 mm/sec. The threshold fluence at this velocity was found to be 1.68 J/cm^2 (shown in figure 4.9(b)) below which only

surface heating of titanium is encountered. Above the threshold fluence, the ablation depth of titanium increases approximately linearly with incident fluence until total thickness titanium is ablated at 2.38 J/cm^2. It can be seen from figure 4.9(a) that the adhesive starts to appear for this fluence. However, there is still some residual titanium that needs to be cleared. This titanium may be left over due to uneven melting of the substrate, non-uniform thickness of titanium foil (5 – 6.5μm) or melt re-deposition.

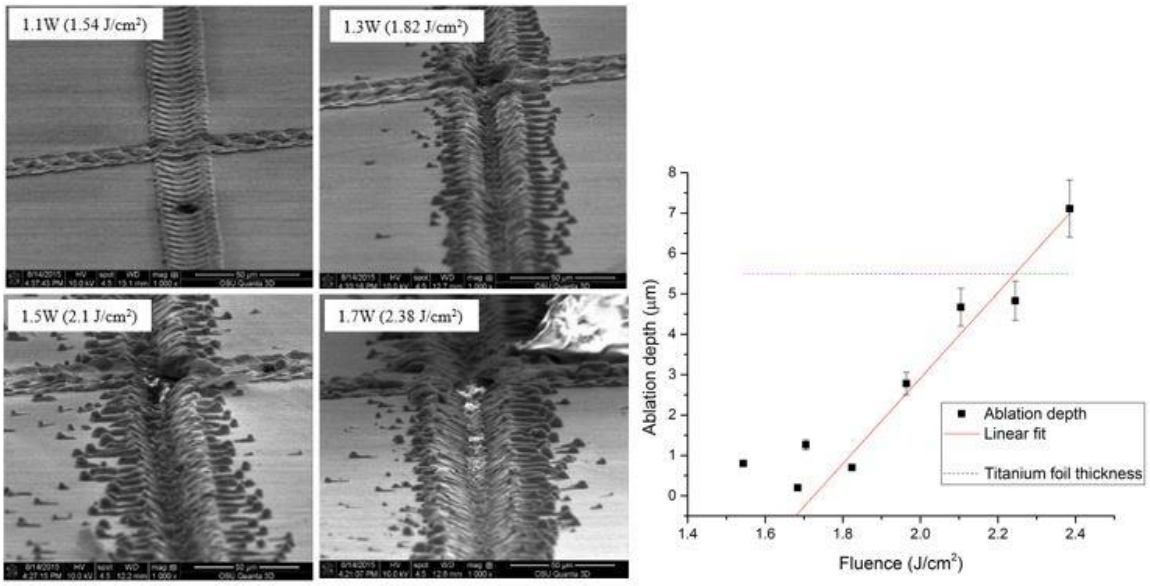

(a) (b)

Figure 4.9: (a) SEM images of a cross pattern, illustrating the increase in ablation depth of titanium on increasing the incident power (or fluence). (b) The graph shows the variation of ablation depth vs. laser fluence. Above the ablation threshold of the titanium, the ablation depth increases in a linear fashion with laser fluence. The x-intercept of the extrapolated line provides the experimental ablation threshold fluence (F_{th}). The depths were measured for a constant translation velocity of 400 mm/sec.

Another parameter that can be experimented with is the translational velocity of the laser. Velocity can influence the bite width of the trace (spatial spacing between one laser pulse to the next) and affect local heating. It can also be seen that threshold fluence strongly depends on the laser velocity and decreases with a decrease in velocity (figure 4.9). This effect is due to increased local heating, which at lower velocities is enough to ablate titanium. The lower thermal conductivity of titanium also contributes to this effect, since heat is not conducted away to prevent local heating. Figure 4.10 shows an approximate inverse linear relationship of ablation depth with laser velocity, which also underlines the possibility of using velocity as a tunable parameter in realizing an optimum recipe. Lower velocities introduce excessive local heating due to lower bite widths. Though this creates better sidewall profiles and lesser outward slag spewing (at low velocities), it ends up melting the underlying adhesive and polyimide layers to the extent of ablating through them for velocities lower than 275 mm/sec (from figure 4.10(b)).

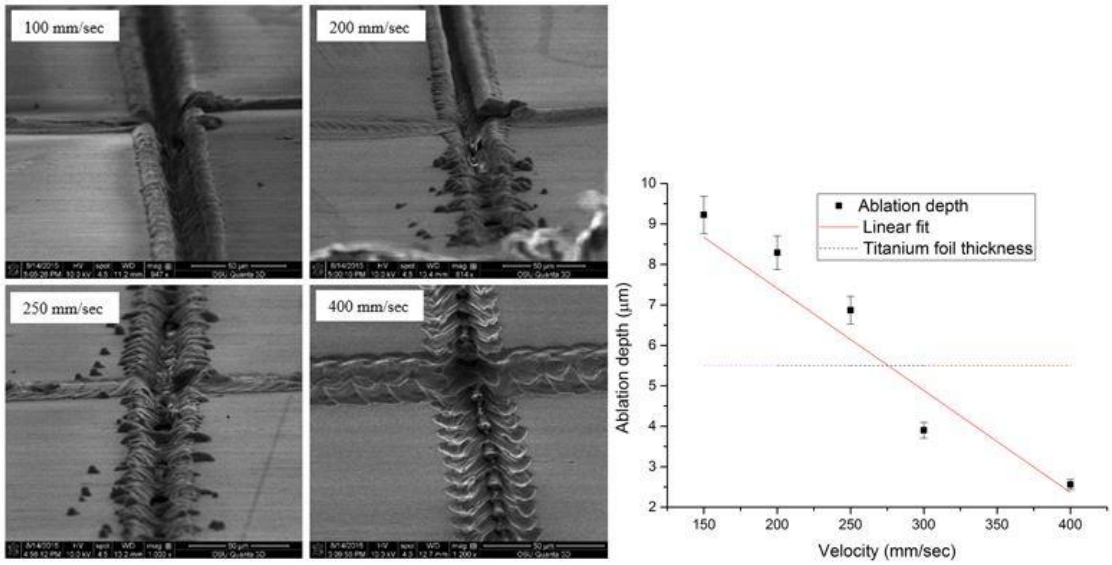

(a) (b)

Figure 4.10: (a) SEM images illustrating decrease in ablation depth of titanium with increasing velocity. This directly translates to a decrease in F_{th} with a decrease in velocity, due to increased local heating. (b) Variation of ablation depth vs. laser velocity where depth varies in an inverse linear fashion with increase in velocity. The depths were measured for a constant fluence of 1.7 J/cm^2 (which yields an F_{th} at 400 mm/sec).

It can also be concluded that as the velocity increases, the ablation threshold for the given velocity increases with Fig 4.10(d) showing surface of titanium very close to ablation threshold for the same fluence setting of 1.7 J/cm^2 . An SEM study of effect of fluence on ablation depth for different velocity setting revealed that the window of controlled ablation depth per pulse existed only for velocities above 300 mm/sec and vanished for lower velocities (i.e. a single pass ablates total thickness of titanium).

From the discussion above, it can be inferred that incident fluence and velocity are important parameters that need to be optimized to achieve selective

ablation of titanium on polyimide. The following second set of experiments were constructed to determine which process parameter (fluence or velocity) showed better and consistent ablation performance. Three different processes were investigated to determine a direction in which the optimum recipe lay, (1) fluence based clean-up process, (2) velocity based clean-up process and (3) velocity based ablation.

Fluence based clean-up process involves a total titanium thickness ablation pass at high fluence (2.38 J/cm^2), followed by a low power clean-up pass (at the ablation threshold of titanium) to remove residual titanium. This resulted in a clean removal of titanium with good electrical isolation across the ablated trace, shown in figure 4.11. However, a significant portion (~7 µm) of adhesive was also removed along with the residual titanium in the second pass. The ablation slag distribution ranged from areas immediately around the trench to distances as long as 30 µm from the trench.

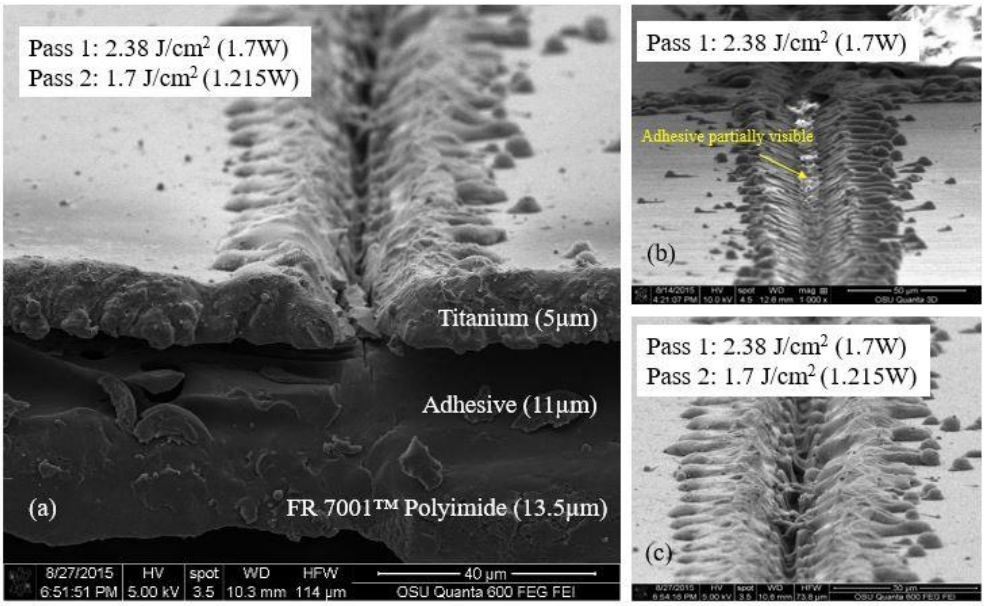

Figure 4.11: (a) Cross-section view of fluence based clean up pass process, (b) top view after a single high power pass, and (c) top view after a low power clean up pass on (b).

Velocity based clean-up process involves a single run with a high power to ablate Ti thickness in one go, but instead combines the clean-up in the same pass using a slightly lower velocity. The clean-up is expected to result from local heating, resulting from the lower velocity. This process requires only one pass (and hence can be expected to have more sample-to-sample uniformity). However, the local heating during the pass is too much for the adhesive layer to take, which usually results in deep pits inside the adhesive (figure 4.12 (b)). The slag spewing is better compared to the previous case due to lower velocity, but however still exists.

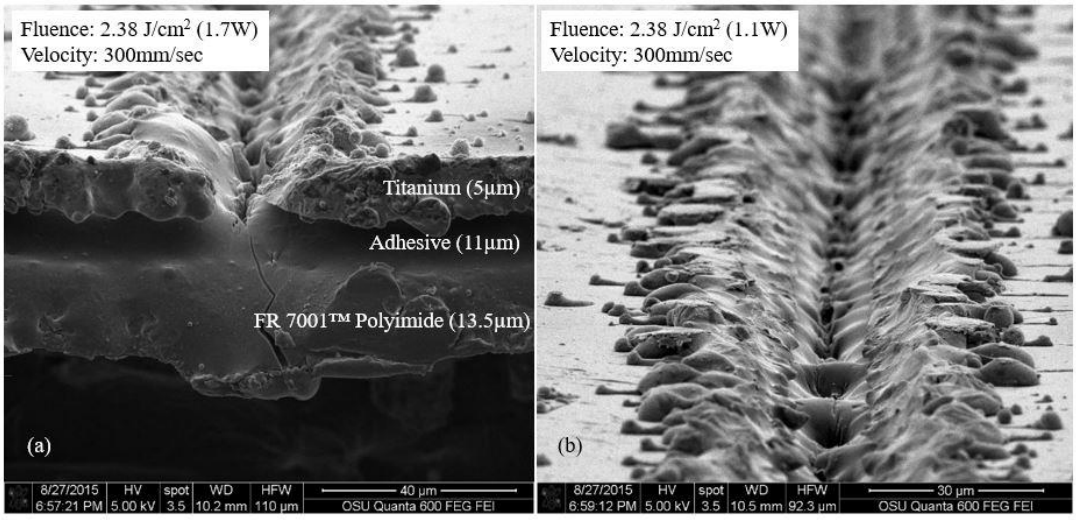

Figure 4.12: (a) Cross-sectional view of velocity based clean-up process (b) top view of velocity based clean-up process

For the process involving velocity based ablation, the fluence is kept constant near the ablation threshold of titanium and velocity is decreased, to facilitate ablation of titanium due to local heating caused by a lower velocity. This method resulted in total ablation of titanium, the adhesive and in some cases, the polyimide underneath. Also, since local heating due to lower velocity is the ablation mechanism used in this method, it appeared to be non-uniform, leaving many hanging bridge shorts (figure 4.13(b)). However, due to the much lower velocity compare to the previous two processes, the slag spew was very less and represented high and steep walls.

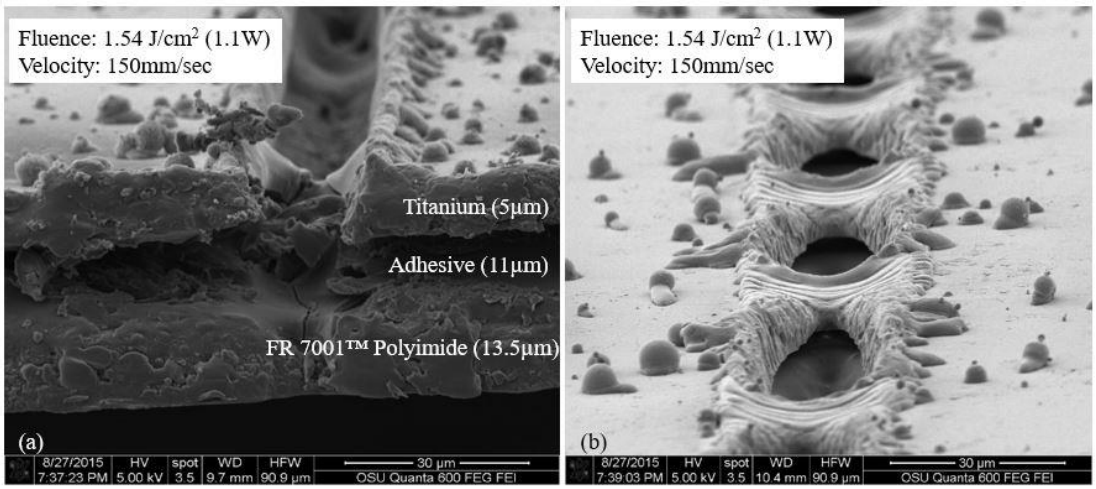

Figure 4.13: (a) Cross-sectional view of velocity based ablation process (b) top view of velocity based ablation process

A fluence based clean-up pass process seemed to yield the best results in terms of repeatability since both velocity based clean-up pass and velocity based ablation processes ablated significantly into the polyimide showing crack formation in their respective cross-sections. Also, both the latter processes resulted in inconsistent ablation since they relied much on local heating, a phenomenon that showed significant spatial process variability. Other process using controlled ablation by multiple passes at lower power and higher velocity did not produce as good a result as the ablation, and was found to be too inconsistent. Processes involving more than 3 passes, even at a very low power setting seemed to ablate completely through the polyimide layer.

The process for fluence based clean-up was optimized by reducing the clean-up pass fluence below the threshold fluence of titanium. At a clean-up fluence of 0.7 J/cm^2, the residual titanium was removed through a controlled ablation of the top 2-3

µm of the adhesive layer (figure 4.14). Patterns over large areas (as large as 3” x 2”) were realized and resulted in successful electrical isolation between traces. A brief summary of the optimized process working mechanism is shown in figure 4.15.

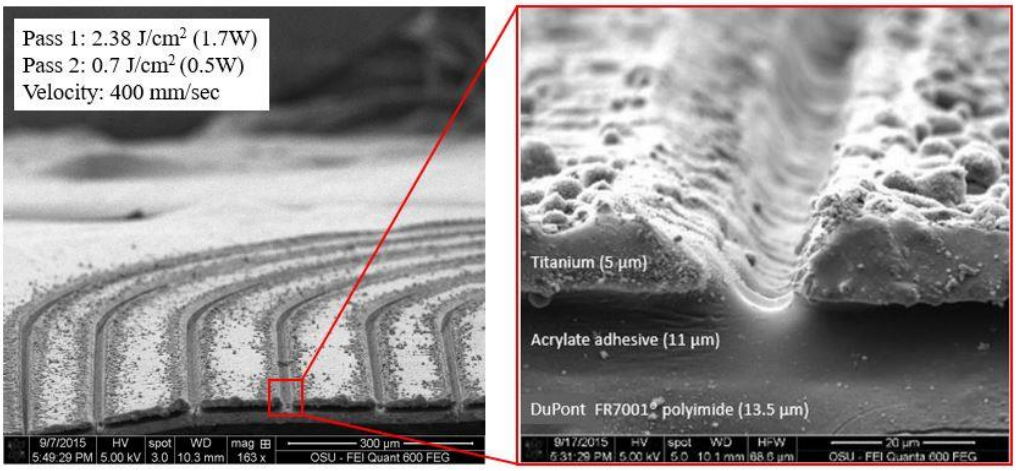

Figure 4.14: Illustrates a zoomed out cross-section SEM image of closely spaced trace patterns and a zoomed version of cross-section, which shows the titanium selectively ablated with most of the adhesive intact.

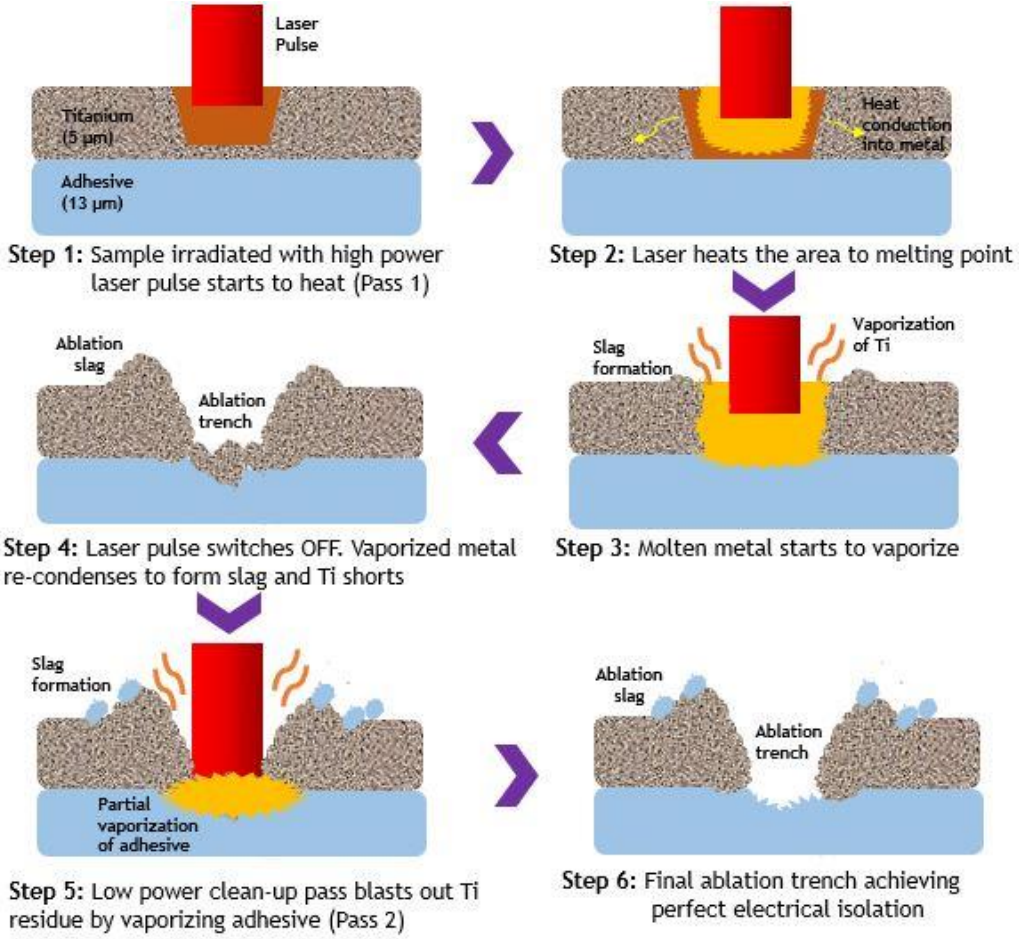

Figure 4.15: Summary of working mechanism of controlled laser ablation of titanium.

4.3 Integrating alternate processes

From the concepts of shadow masking discussed in section 4.1 and controlled laser ablation of titanium discussed in section 4.2, only the latter was found feasible for integration into the existing process flow at the time of study.

It can be described from section 4.2 that laser ablation patterning (LAP) process has been optimized only for a 5 μm titanium foil with no surface treatment. However, attempts to optimize LAP process for a surface treated substrate showed poor results. This was because of a macroscale roughness induced during the pre-clean process, which provided too uneven foil thickness distribution for the pre-existing small process window. The surface reflectivity of the foil also changed after pre-treatment, which could have impacted the energy delivered to the substrate for ablation. Nonetheless, it was required to redesign the process flow to integrate LAP of titanium without a pre-clean.

The existing process design (figure 4.16) involved patterning titanium towards the end of the process flow, i.e. after patterning silver and platinum electrodes. However, trying to use this process flow would result in LAP on a pre-cleaned substrate, which is not feasible as discussed above. Hence, the new process flow would require LAP patterning of titanium before a pre-clean, i.e. before electrode patterning is done. Thus, a new process flow was designed to perform LAP first.

However, this approach would result in subsequent thin film deposition steps shorting electrically isolated titanium traces. An immediate coverlay step was necessary to overcome this problem, in order to protect titanium traces. If the

coverlay step can be performed before a pre-clean, this would also benefit preserving integrity of titanium traces, which are shielded from further wet processing by a strong coverlay. Thus, the coverlay acts as a hard mask in this process for the subsequent process steps.

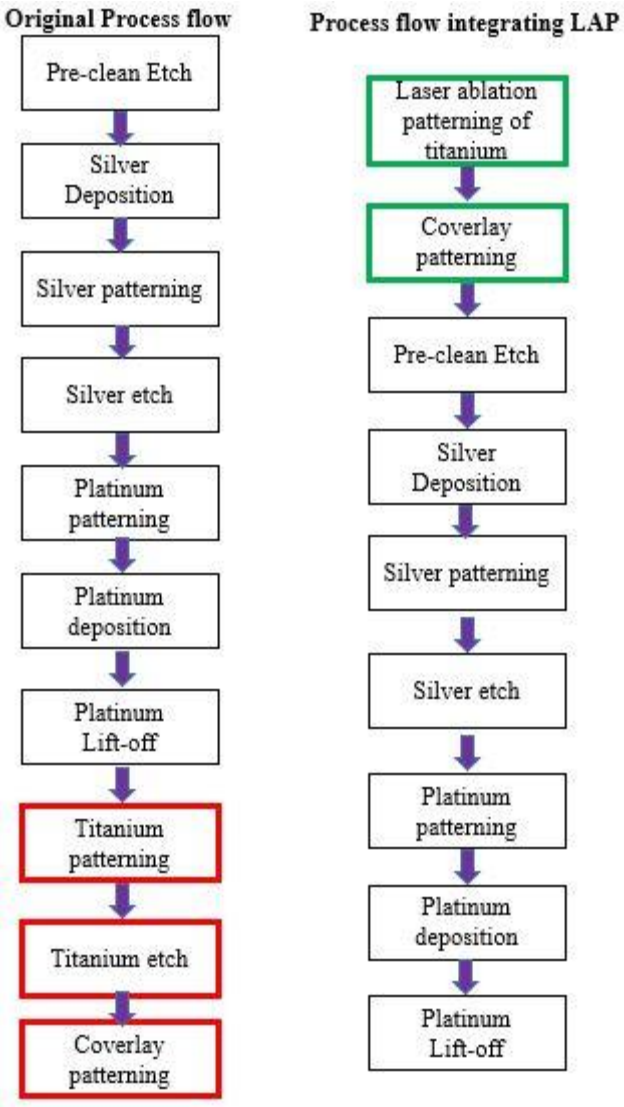

Figure 4.16: Process flow (left) originally discussed in chapter 3 and (right) after integrating LAP. The process steps indicated in red are removed and replaced by process steps in green.

This work focuses on attempts to integrate this process flow and recommends necessary changes that need to be introduced to achieve a stable process.

4.3.1 Coverlay hard mask

Our initial substrate of study is a LAP titanium substrate. The first step involved applying a hard mask or a coverlay that can (i) protect ablated titanium trenches from shorting due to subsequent thin film deposition steps (ii) retain good chemical passivity and durability to withstand subsequent process steps. PI-2525 introduced in section 3.6.2 was used as the coverlay material for this work.

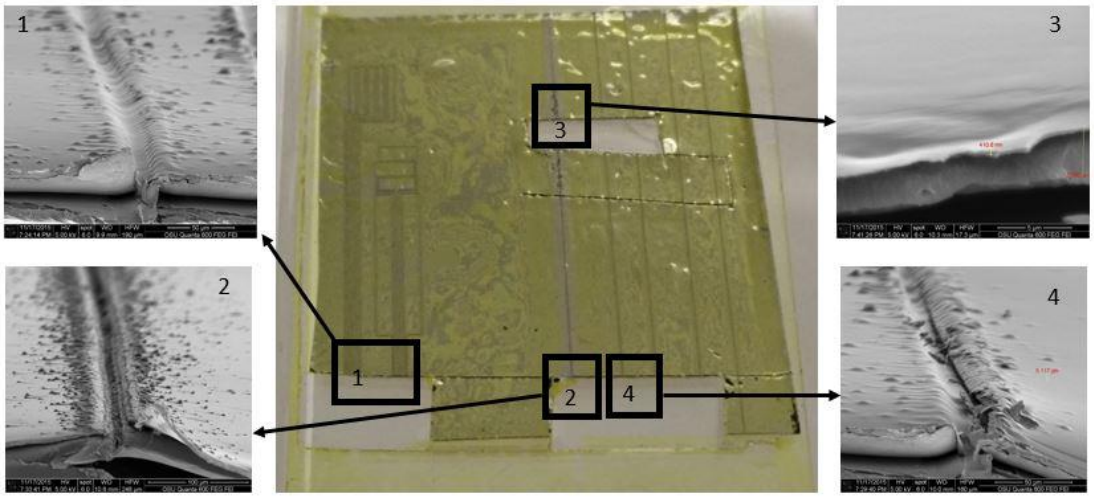

Figure 4.17: LAP processed substrate (center) spin-coated and cured with PI-2525. Images surrounding are the SEM cross-sections of the substrates in their respective indicated regions. Region 1- Good trench coverage of PI-2525 near the edges. Regions 2, 3 & 4 – Poor trench coverage at or near the substrate center due to centrifugal force affecting poor adhesion of PI-2525 to a non-pre-cleaned titanium surface.

PI-2525 was spin-coated on top of a LAP processed substrate as shown in figure 4.17 using spin-coating parameters given in table 3.4. The substrate was then cured at 180^0C for 3 hours. Cross-section SEM images were taken in the regions mentioned in figure 4.17 to test the uniformity of coverlay on a LAP processed substrate.

Region 1, which is close to the periphery was observed to protect the ablation trench with PI-2525. However, regions 2, 3 and 4 were observed to show cracks in the coverlay. The thickness close to the center of the substrate was measured to be ~ 400 nm, much less than the expected thickness of 5μm for a spin speed of 5000rpm. Two reasons can be attributed to this poor uniformity of coating (i) poor adhesion of PI-2525 onto uncleaned titanium foil despite using adhesion promoter (ii) shadowing of features due to titanium ablation slag post processing. A possible scope for future work would be aimed towards improving adhesion of PI-2525 onto titanium foil by increasing concentration of adhesion promoter.

4.3.2 Silver and Platinum electrode patterning

The next aim of the study was to test the durability of cured PI-2525 as a hard mask for subsequent process steps. The coverlay was patterned with PI-2525 on two pre-cleaned substrates using process developed in table 3.4. A 400 nm thick silver layer was first sputtered onto the substrate, which was subsequently patterned with a mask using $NH_4OH:H_2O_2:H_2O$ (8:8:75) etch solution [41, 42]. The second substrate was tested for lift-off conditions using a patterned platinum mask on top of the

patterned coverlay, which was then subsequently sputtered with 50 nm of silver. The patterns resolved on the substrate after silver etch and platinum lift-off patterning are shown in figure 4.18.

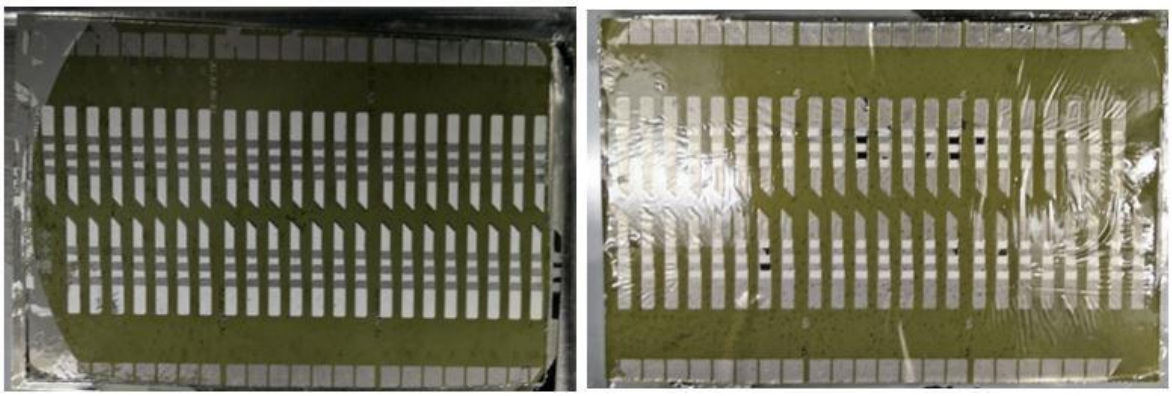

Figure 4.18: (left) PI-2525 hard masked substrate after silver pattern and etch; (right) similar substrate after silver lift-off.

The PI-2525 coverlay was observed to serve as an excellent hard mask by surviving the vicissitudes offered by silver etch solution and lift-off sonication process. Subsequent tests on the coverlay also confirmed its endurance in 50% H_2SO_4 solution for more than 25 min for the purpose of a selective pre-clean.

Hence, it can be concluded the process integration involving hard mask first looks promising. However, the coating and patterning of a PI-2525 based hard mask still needs optimization, due to the rough contours offered by a LAP substrate.

5. Reliability tests and animal studies

Reliability and responsivity are two of the most important factors that contribute to the commercial success of a sensor. This chapter aims to discuss the reliability aspects of the sensor designed and concludes with the results of an animal study conducted to measure the responsivity of the sensors.

5.1 Flex tests

Reliability is the most important aspect of process design with respect to employing a flexible substrate. The challenges which the flexible substrates offer are totally differ from that of rigid substrates used in conventional processes. To endure the vicissitudes that process steps offer such as substrate handling, different processing temperatures and other physical constraints, parameters such as the co-efficient of thermal expansion (CTE), and Young's modulus play an important role [88]. The chemical inertness or reactivity of the flexible substrate are also crucial in determining its compatibility for the chemistry of the process. However, the effect of these parameters takes a backseat if the durability of subsequent layers is compromised.

The purpose of this study is to test the durability of high aspect ratio titanium traces that form the most fragile part of the sensor. Titanium trace failure was observed to be the primary cause of loss of sensor yield, both during processing and in animal studies. Hence, this study attempts to identify the roles of surface preparation and sensor design in determining the durability of the titanium conducting

traces. An acrylic flex tester was fabricated by Tyler Milhem at PDT for this purpose and is shown in figure 5.1.

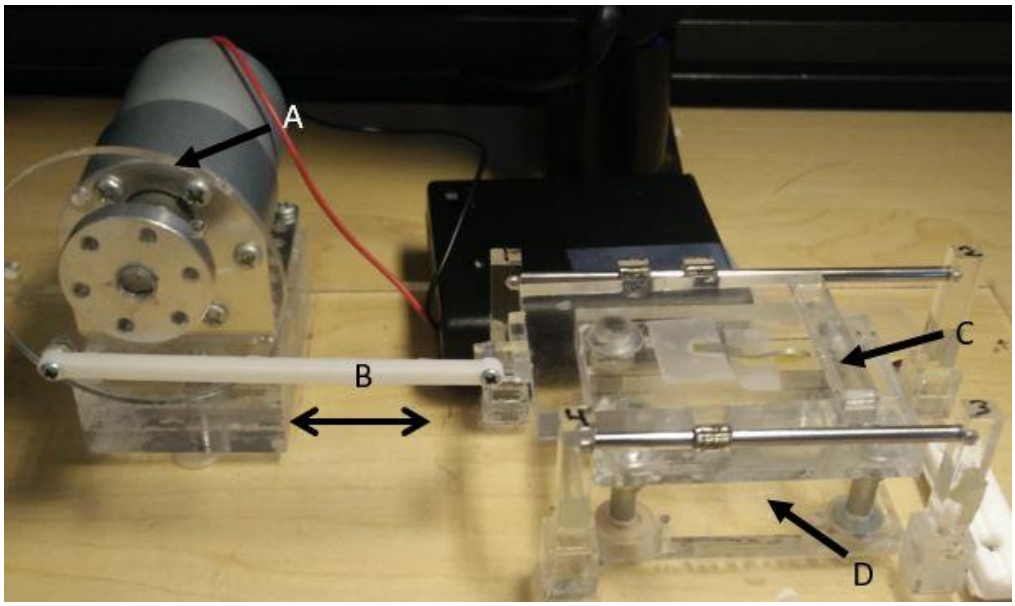

Figure 5.1: Automated flex test fabricated by Tyler Milhem at PDT. Parts labelled: A – rotor, B – shaft with arrow directions showing back and forth motion of the shaft, C – upper acrylic plate moving along with the shaft, D – fixed lower acrylic plate. The sensor to be tested is pinned between plates C and D using a scotch tape.

The flex tester consists of a rotor (A) operated by a battery powered motor of 60 RPM. The rotor is connected through a shaft (B) to the upper acrylic plate (C) which is movable and slides along a steel pin. The rotor blade has circular slots at different radii from the axis to define the length of the slide. The sensor to be tested is taped between its ends between the upper movable plate and the lower fixed plate (D), which moves the bend created in the sensor along its length. The radius of the bend can be adjusted by tightening the screws located below the fixed plate (B).

For this study, a bend radius of 2 mm was used to simulate the extreme bending that the sensor can be subjected to after a subcutaneous implantation. A bend cycle correlates to one back and forth motion of plate C along the entire sensor length and is performed at 60 Hz, i.e. 60 bends per minute.

The durability of different pre-clean and etches as discussed in sections 3.2 and 3.5 are were tested. Five classes of substrates were tested : class 1 – (1:20) HF:H_2O pre-clean followed by a (1:1:20) HF:H_2O_2:H_2O titanium etch, class 2 - (1:1:20) HF:H_2O_2:H_2O pre-clean followed by a (1:1:20) HF:H_2O_2:H_2O titanium etch, class 3 - (1:10:100) HF:HNO_3:H_2O pre-clean followed by a (1:1:20) HF:H_2O_2:H_2O titanium etch, class 4 – 50% solution H_2SO_4 pre-clean followed titanium etch using the same solution, and class 5 – substrates patterned using laser ablation patterning of titanium obtained from Electro Scientific Industries (ESI). Mask revision 25ga Rev I-Dogleg mask was used to pattern the substrates.

From our previous discussion in section 3.2, substrates belonging to classes 1 and 2 were expected to show hydrogen embrittlement whereas classes 2 and 4 show no embrittlement. Figure 5.2 shows a plot of percentage of failure versus number of bend cycles for each sensor class. Class 5 laser patterned substrates do not require any wet pretreatment and hence are not shown in this graph. A sample size of 10 sensors was chosen for each class.

From this graph, the median population for failure lies at 1600 bend cycles for class 4, which is more than double than that of the next reliable class, i.e. class 1. Class 1 and class 2 sensors performed poorly during flex tests partly due to hydrogen

embrittlement, where the failures occurred as cracks along the sensor trace length (region 1). However, sensors which inhibit hydrogen embrittlement showed failure in region 2, which could be attributed to a flaw in sensor design that needs to be addressed. Also, one would expect class 3 sensors to perform better at-least compared to hydrogen embrittled class 1 & 2 sensors. However, the reason class 3 performed poorly during reliability tests was due to lesser thickness of titanium that remained after its pre-clean compared to other pre-cleans. This was verified using a sheet resistance measurement performed on this class 3 of sensors (figure 5.3), which showed a calculated thickness of titanium to be around 1 μm compared to other classes of sensors, which showed a titanium thickness > 2 μm. This is believed to be caused due to higher etch rate of HF and nitric acid pre-clean [43] which eats up significant amount of titanium before the substrate is rinsed.

Class 5 substrates consisting of laser patterned sensors performed exceptionally well with respect to flex tests (shown in figure 5.4) showing more than 350% increase in durability over pre-treated sensors for the same design. All 10 samples that were tested were found to survive more than 3600 bend cycles without any signs of fatigue. These results demonstrate a lot of potential for laser patterned substrates in term of boosting sensor durability.

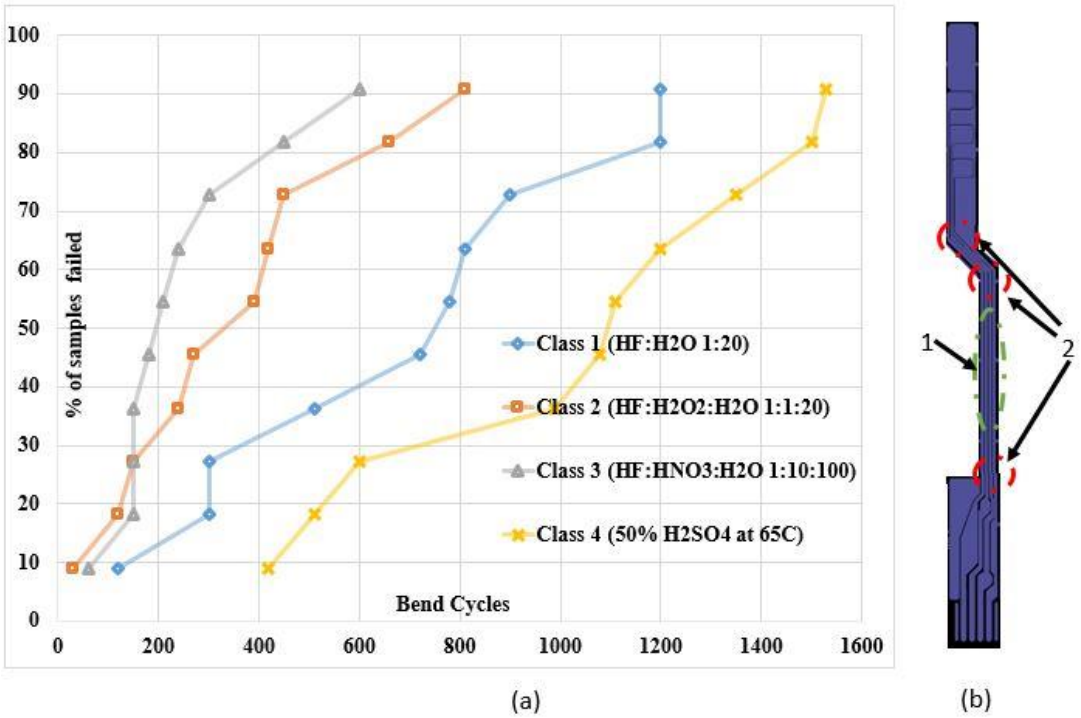

Figure 5.2: (a) Percentage of samples failed plotted versus no. of bend cycles. A sample size of 10 was chosen for each. (b) Schematic of a sensor design of Mask 25ga Rev I-Dogleg, indicating popular locations of failure during bend tests. Region 1 was the most probable location of failure for hydrogen embrittled sensors (class 1 and 2), and region 2 indicates failure locations of class 3 and 4 sensors, which yielded due to stress accumulated near the kinks in the sensor design.

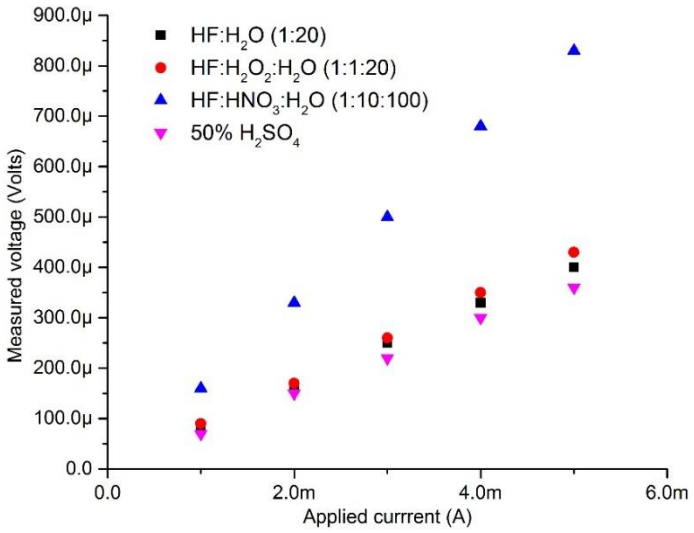

Figure 5.3 Four-point probe measurement of sheet resistances of samples with different pre-cleans. Higher slope of HF and nitric acid based pre-clean shows a higher sheet resistance and hence a lesser titanium thickness, which impacted durability.

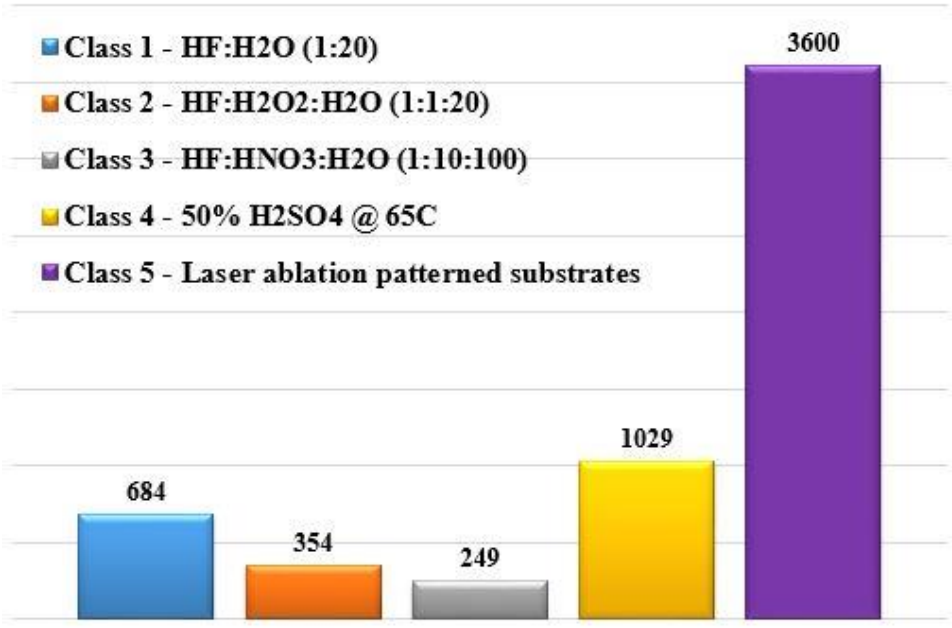

Figure 5.4. Graph showing the mean no. of bend cycles for failure for each pre-treatment in comparison to laser ablation patterned substrates (class 5). Class 5

substrates did not show signs of fatigue even after 3600 bend cycles and displays more than 350% durability compared to conventional pre-treated substrates. Sample size of 10 sensors for each class was considered.

Hence, the results of reliability tests conducted on sensors showed a 50% sulfuric acid pre-clean and etch to show excellent durability. Laser patterned substrates performed the best in terms of durability as they showed no signs of fatigue, even under extreme test conditions and hence look very promising to improve sensor durability.

5.2 Animal studies

The current work fabricated a glucose sensor through the coverlay step. The sensor was then sent to PDT where chloridization was performed followed by GOx and polyurethane diffusion barrier implantation. The sensor was then sterilized for animal studies. An image of the final sensor ready for animal studies is shown in figure 5.5.

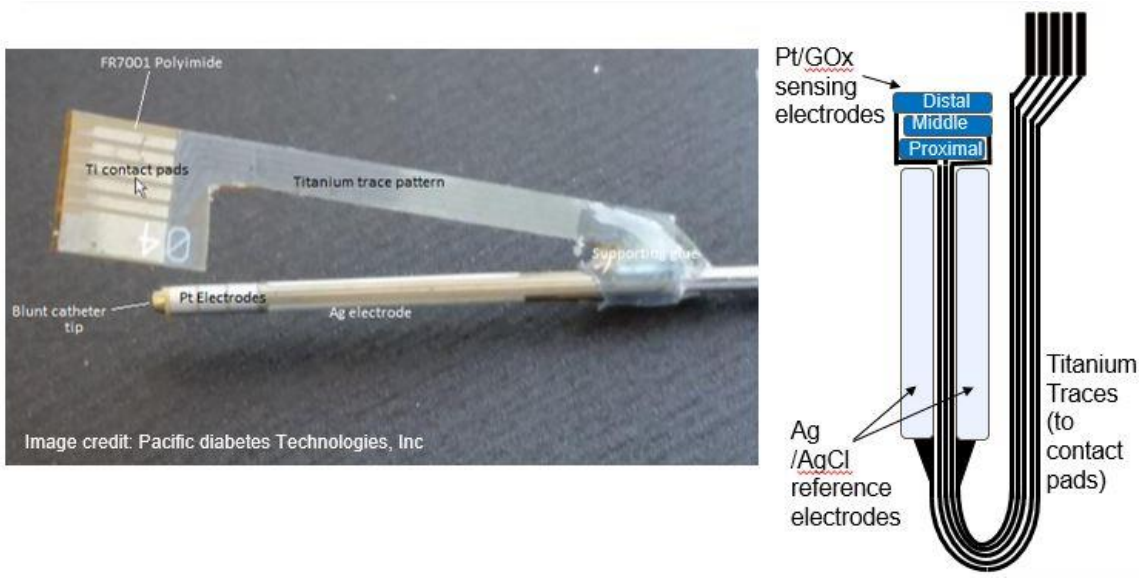

Figure 5.5: (a) A completely fabricated glucose sensor wound around a 21ga catheter ready for animal implantation. (b) Schematic of the sensor before wrapping it around the catheter, with electrodes and traces indicated.

The animal studies were conducted at OHSU. The pig protocol was approved (in writing prior to initiating the study) by the OSU Institutional Animal Care and Use Committee under the guidance of veterinarian Helen Diggs, DVM, ACLAM. The pigs were of the Yucatan mini-pig variety and were not diabetic. The sensors were inserted subcutaneously in the medial abdomen area after the pig had been anesthetized with isoflurane. During the glucose clamp study (the day after the

insertion), the animal was endotracheally intubated and maintained on continuous inhaled isoflurane.

For the purpose of reference, a very accurate glucose meter Hemocue 201 DM® was used for point glucose monitoring. This was done for each point of time marked in figure 5.6 by collecting 0.1 ml of blood sample from an intravenous catheter at the ear vein. Figure 5.6 illustrates glucose current response at three different GOx sensing electrodes of the same sensor.

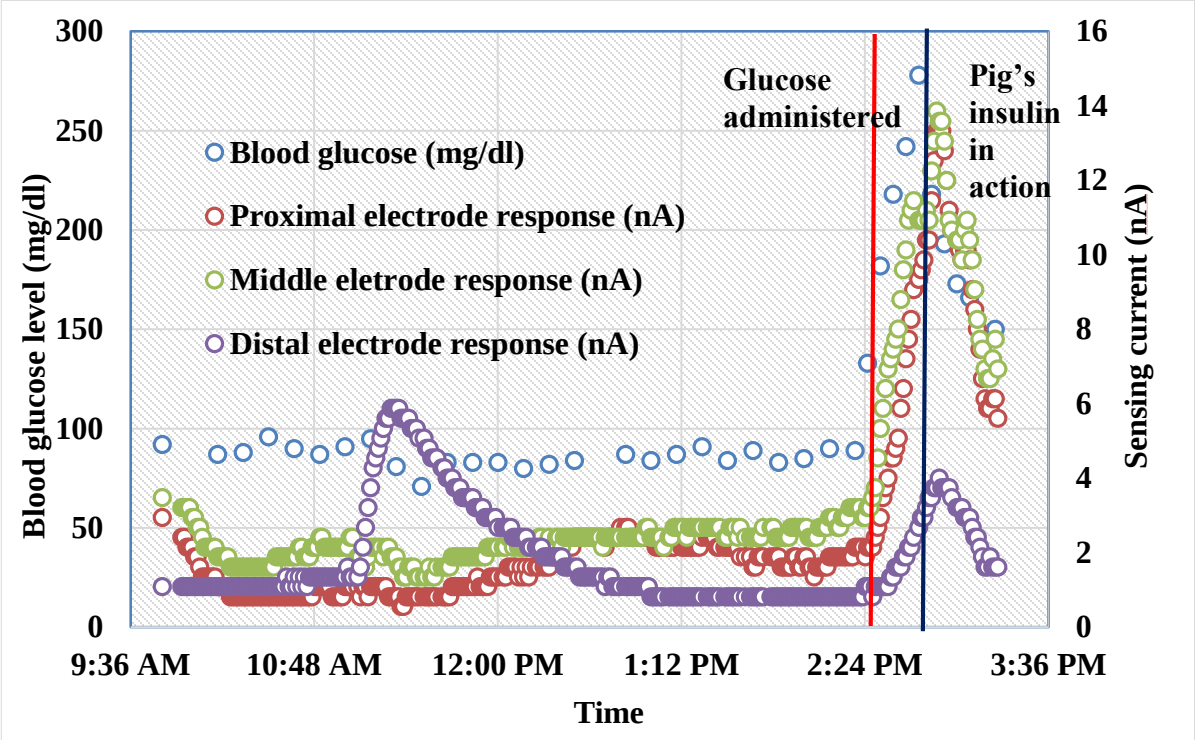

Figure 5.6: Animal study response data showing point blood glucose level data in blue as reference for accurate monitoring and sensed current at (a) proximal (b) middle (c) distal electrode for implanted test sensor shown in figure 5.5.

The pig is administered intravenous glucose at 2:24 PM, which results in ramp up in detected blood glucose level. The drop in glucose level after reaching a peak level is due to action of insulin in processing the administered glucose produced by the pig, which happens at 2:50 PM. A small lag in sensing is inevitable due to time delays between glucose measuring points, which is done manually, and also delay introduced by diffusion barrier on the sensor to allow glucose concentration within the dynamic range of the sensor.

It is advantageous to use three sensing electrodes instead of just one. As seen from for the distal electrode in figure 5.6, a sensing artifact can manifest. The sensing artifact in this sensor originated due to a short circuit in the sensor between the sensing and reference electrodes that produced unpredictable response to blood glucose. However, the other two electrodes work fine and the final data taken is a moving average of the current from each electrode, which smooths out unwanted artifacts.

The fabricated sensor hence showed good responsivity to administered glucose in pig study, thereby achieving the goal of establishing a stable process flow to obtain a working sensor.

6. Conclusion and future work

The work presented in this thesis was able to meet its originally designed objectives, (1) facilitate a successful technology transfer of sensor fabrication process from OSU to PDT and help PDT become self-reliant on having their own process flow, (2) optimize process flows with respect change in mask designs and substrate composition aimed at working toward achieving a sensitive and human implantable device, (3) improvise process flows and recipes to achieve better throughput and yield, and (4) investigate new process flows aimed to reduce the number of process steps and capital investment required by PDT, thereby significantly reducing the cost per sensor.

Durability of sensors have increased tenfold as a result of the current work, facilitating more productive animal studies. Investigation done in this work on alternate process flows such as controlled laser ablation, demonstrate great potential in improving sensor durability further and possibly extending to human studies. Transition to bigger substrates improved throughput by more than a factor of 5, and process optimizations investigated in this work improved sensor yield. Overall, a successful hand over of technology has been achieved in transferring processes from OSU to PDT.

Possible avenues of future work lie in re-investigating shadow masking as a process step alternative to photolithography. Use of bi-metal shadow masks [63] can benefit towards a better feature resolution. Also, investigation towards design

optimization of shadow mask holder can improve uniformity of this process. Perhaps, the most challenging aspect of integrating both silver and platinum shadow masks, is to align platinum shadow mask with a pre-registered silver pattern, which cannot be done manually. This problem can be solved by the use of a shadow mask aligner from Idonus [69], which aligns a shadow mask to a pre-patterned substrate in a similar way to that of a photo-mask aligner.

Another potential and promising avenue of future work involves, integration of controlled laser ablation using process design described in section 4.3. The use of a dry polyimide coverlay by lamination on top of ablated titanium, followed by laser patterning of polyimide foil can eliminate the need for wet processing altogether. To facilitate testing the feasibility of this process flow, PDT has outsourced laser ablation patterning of titanium to ESI. Optimization of this process can save PDT from other process equipment capital investments as most of the process step can be done using a laser.

Bibliography

[1] Heinemann, Lutz, Sylvia Franc, Moshe Phillip, Tadej Battelino, Francisco Javier Ampudia-Blasco, Jan Bolinder, Peter Diem, John Pickup, and J. Hans DeVries. "Reimbursement for continuous glucose monitoring: a European view." *Journal of diabetes science and technology* 6, no. 6 (2012): 1498-1502.

[2] “Estimates of Diabetes and its Burden in the United States” [Online]. Available: http://www.cdc.gov/diabetes/pdfs/data/2014-report-estimates-of-diabetes-and-its-burden-in-the-united-states.pdf

[3] Schuit, F. C., Huypens, P., Heimberg, H., & Pipeleers, D. G. (2001). Glucose sensing in pancreatic β-cells a model for the study of other glucose-regulated cells in gut, pancreas, and hypothalamus. *Diabetes*, *50*(1), 1-11.

[4] Albisser, A. Ml, B. S. Leibel, T. G. Ewart, Z. Davidovac, C. K. Botz, W. Zingg, H. Schipper, and R. Gander. "Clinical control of diabetes by the artificial pancreas." *Diabetes* 23, no. 5 (1974): 397-404.

[5] Heller, Adam, and Ben Feldman. "Electrochemical glucose sensors and their applications in diabetes management." *Chemical reviews* 108.7 (2008): 2482-2505.

[6] Vaddiraju, S., Burgess, D. J., Tomazos, I., Jain, F. C., & Papadimitrakopoulos, F. (2010). Technologies for continuous glucose monitoring: current problems and future promises. *Journal of diabetes science and technology*, *4*(6), 1540-1562.

[7] Kropff, Jort, and J. Hans DeVries. "Continuous glucose monitoring, future products, and update on worldwide artificial pancreas projects." *Diabetes technology & therapeutics* 18.S2 (2016): S2-53.

[8] Dalton, Martin L. "Champ Lyons: an incomplete life." *Annals of surgery* 237.5 (2003): 694-703.

[9] Clark, Leland C., and Champ Lyons. "Electrode systems for continuous monitoring in cardiovascular surgery." *Annals of the New York Academy of sciences* 102.1 (1962): 29-45.

[10] Mann, Charles Kenneth, and Karen K. Barnes. "Electrochemical reactions in nonaqueous systems." (1970).

[11] Hill, John William, Ralph H. Petrucci, and Michael D. Mosher. *General chemistry*. Upper Saddle River, NJ: Pearson Prentice Hall, 2005.

[12] D. Keilin and E. F. Hartree, “The use of glucose oxidase (notatin) for the determination of glucose in biological material and for the study of glucoseproducing systems by manometric methods,” *Biochem. J.*, vol. 42, no. 2, p. 230, 1948.

[13] Moatti-Sirat, D., V. Poitout, V. Thome, M. N. Gangnerau, Y. Zhang, Y. Hu, G. S. Wilson, F. Lemonnier, J. C. Klein, and G. Reach. "Reduction of acetaminophen interference in glucose sensors by a composite Nafion membrane: demonstration in rats and man." *Diabetologia* 37, no. 6 (1994): 610-616.

[14] Gouda, Mudeppa Devaraja, Sridevi Annapurna Singh, AG Appu Rao, Munna Singh Thakur, and Naikankatte Ganesh Karanth. "Thermal inactivation of glucose oxidase mechanism and stabilization using additives." *Journal of Biological Chemistry* 278, no. 27 (2003): 24324-24333.

[15] Sammartano, LAURI J., R. W. Tuveson, and R. Davenport. "Control of sensitivity to inactivation by H2O2 and broad-spectrum near-UV radiation by the Escherichia coli katF locus." *Journal of bacteriology* 168.1 (1986): 13-21.

[16] Tsuge, H., Suzuki, M., Kito, N., Nakanishi, Y., Ohashi, K., & Aoki, K. (1984). Inactivation of glucose oxidase by the cationic detergent, hexadecyltrimethylammonium bromide. *Agricultural and biological chemistry*,*48*(1), 19-28.

[17] Metzger, M., Leibowitz, G., Wainstein, J., Glaser, B., & Raz, I. (2002). Reproducibility of glucose measurements using the glucose sensor. *Diabetes Care*, *25*(7), 1185-1191.

[18] Updike, S. J., Shults, M. C., Gilligan, B. J., & Rhodes, R. K. (2000). A subcutaneous glucose sensor with improved longevity, dynamic range, and stability of calibration. *Diabetes Care*, *23*(2), 208-214.

[19] Liang, Yin, Habiba Najafi, and F. M. Matschinsky. "Glucose regulates glucokinase activity in cultured islets from rat pancreas." *Journal of Biological Chemistry* 265.28 (1990): 16863-16866.

[20] Prabhu, V. G., L. R. Zarapkar, and R. G. Dhaneshwar. "Electrochemical studies of hydrogen peroxide at a platinum disc electrode." *Electrochimica Acta* 26.6 (1981): 725-729.

[21] Sato, T. "Silver, silver chloride electrodes." U.S. Patent No. 3,834,373. 10 Sep. 1974.

[22] Janz, George J., and David JG Ives. "Silver, silver chloride electrodes." *Annals of the New york Academy of Sciences* 148.1 (1968): 210-221.

[23] Tapsak, M. A., Rhodes, R. K., Shults, M. C., & McClure, J. D. (2007). *U.S. Patent No. 7,226,978*. Washington, DC: U.S. Patent and Trademark Office.

[24] "Chloride test-blood:MedlinePlus" [Online]. Available: https://www.nlm.nih.gov/medlineplus/ency/article/003485.html [Accessed: 10-Mar-2016]

[25] Haynes, William M., ed. *CRC handbook of chemistry and physics*. CRC press, 2014.

[26] Matthews, David J. *Fabrication of a flexible glucose sensing catheter for human implantation* (Masters thesis). Retrieved from OSU Scholars Archive [Online] Address: http://hdl.handle.net/1957/45164

[27] Du, X., Durgan, C.J., Matthews, D.J., Motley, J.R., Tan, X., Pholsena, K., Árnadóttir, L., Castle, J.R., Jacobs, P.G., Cargill, R.S., Ward, W.K., Conley Jr., J.F., and Herman, H.S., 2015. Fabrication of a flexible amperometric glucose sensor using additive processes. *ECS Journal of Solid State Science and Technology*, *4*(4), pp.P3069-P3074.

[28] Bianchi, G., F. Mazza, and T. Mussini. "Catalytic decomposition of acid hydrogen peroxide solutions on platinum, iridium, palladium and gold surfaces." *Electrochimica Acta* 7.4 (1962): 457-473.

[29] Zeis, R., Lei, T., Sieradzki, K., Snyder, J., & Erlebacher, J. (2008). Catalytic reduction of oxygen and hydrogen peroxide by nanoporous gold. *Journal of Catalysis*, *253*(1), 132-138.

[30] Brunette, D. M., Tengvall, P., Textor, M., & Thomsen, P. (Eds.). (2012).*Titanium in medicine: material science, surface science, engineering, biological responses and medical applications*. Springer Science & Business Media.

[31] Lütjering, Gerd, and James Case Williams. *Titanium*. Vol. 2. Berlin: Springer, 2003.

[32] Basame, Solomon B., and Henry S. White. "Scanning electrochemical microscopy of native titanium oxide films. Mapping the potential dependence of spatially-localized electrochemical reactions." *The Journal of Physical Chemistry* 99.44 (1995): 16430-16435.

[33] Vogt, K. W., Kohl, P. A., Carter, W. B., Bell, R. A., & Bottomley, L. A. (1994). Characterization of thin titanium oxide adhesion layers on gold: resistivity, morphology, and composition. *Surface science*, *301*(1), 203-213.

[34] Packham, David Ernest, ed. *Handbook of adhesion*. John Wiley & Sons, 2006.

[35] Molitor, P., V. Barron, and T. Young. "Surface treatment of titanium for adhesive bonding to polymer composites: a review." *International Journal of Adhesion and Adhesives* 21.2 (2001): 129-136.

[36] Briant, C. L., Z. F. Wang, and N. Chollocoop. "Hydrogen embrittlement of commercial purity titanium." *Corrosion Science* 44.8 (2002): 1875-1888

[37] Groeneveld, T. P., E. E. Fletcher, and A. R. Elsea. "Review of literature on hydrogen embrittlement." *Contract Number NAS8-20027, Battelle Memorial Institute, Columbus, Ohio* (1966).

[38] Iwaya, Y., Machigashira, M., Kanbara, K., Miyamoto, M., Noguchi, K., Izumi, Y., & Ban, S. (2008). Surface properties and biocompatibility of acid-etched titanium. *Dental Materials Journal*, *27*(3), 415-421.

[39] Brauer, E., R. Gruner, and F. Rauch. "Kinetics and Mechanism of Hydrogen Diffusion in Hydrides of Titanium, Zirconium and TiNi0. 5." *Berichte der Bunsengesellschaft für physikalische Chemie* 87.4 (1983): 341-345.

[40] Beachem, C. D. "A new model for hydrogen-assisted cracking (hydrogen “embrittlement”)." *Metallurgical transactions* 3.2 (1972): 441-455.

[41] Williams, Kirt R., and Richard S. Muller. "Etch rates for micromachining processing." *Microelectromechanical Systems, Journal of* 5.4 (1996): 256-269.

[42] Williams, Kirt R., Kishan Gupta, and Matthew Wasilik. "Etch rates for micromachining processing-Part II." *Microelectromechanical Systems, Journal of* 12.6 (2003): 761-778.

[43] Donachie, Matthew J. *Titanium: a technical guide*. ASM international, 2000

[44] Nelson, Howard G. "Hydrogen and advanced aerospace materials." (1988).

[45] ASTM D3359. "Standard Test Methods for Measuring Adhesion by Tape Test." (2005).

[46] Madou, Marc J. *Fundamentals of microfabrication: the science of miniaturization*. CRC press, 2002.

[47] “Shipley’s Microposit™ S1800™ series” [Online]. Available : http://cmnst.ncku.edu.tw/ezfiles/23/1023/img/127/s1800seriesDataSheet.pdf [Accessed 10-March-2016]

[48] “Dual layer photoresist processing” [Online]. Available: https://snf.stanford.edu/SNF/processes/process-modules/photolithography/lift-off-lol-procedures/liftoff [Accessed 10-March-2016]

[49] Fjelstad, Joseph. *An Engineer's Guide to Flexible Circuit Technology: Materials, Design, Applications, Manufacturing*. Electrochemical Publications, 1997.

[50] Figura, Daniel, and Johanna Bartel. "Fabrication of high aspect ratio SU-8 structures using UV lithography and megasonic-enhanced development." *ECS Transactions* 25.31 (2010): 29-35.

[51] del Campo, Aránzazu, and Christian Greiner. "SU-8: a photoresist for high-aspect-ratio and 3D submicron lithography." *Journal of Micromechanics and Microengineering* 17.6 (2007): R81.

[52] Nemani, K. V., Moodie, K. L., Brennick, J. B., Su, A., & Gimi, B. (2013). In vitro and in vivo evaluation of SU-8 biocompatibility. *Materials Science and Engineering: C*, *33*(7), 4453-4459.

[53] Keller, S., Blagoi, G., Lillemose, M., Haefliger, D., & Boisen, A. (2008). Processing of thin SU-8 films. *Journal of micromechanics and microengineering*, *18*(12), 125020.

[54] Stopperan, Jahn J. "Printed circuit assembly with fine pitch flexible printed circuit overlay mounted to printed circuit board." U.S. Patent No. 5,719,749. 17 Feb. 1998.

[55] Richardson, R. R., J. A. Miller, and William M. Reichert. "Polyimides as biomaterials: preliminary biocompatibility testing." *Biomaterials* 14.8 (1993): 627-635.

[56] Feger, Claudius. "Curing of polyimides." *Polymer Engineering & Science*29.5 (1989): 347-351.

[57] Myllymaa, S., Myllymaa, K., Korhonen, H., Lammi, M. J., Tiitu, V., & Lappalainen, R. (2010). Surface characterization and in vitro biocompatibility assessment of photosensitive polyimide films. *Colloids and Surfaces B: Biointerfaces*, *76*(2), 505-511.

[58] "Product Bulletin PI-2525, PI-2555 & PI-2474, HD-Microsystems" [Online]. Available:http://www.hdmicrosystems.com/HDMicroSystems/en_US/products/non_photodefineable/2500_dry_etch.html

[59] Jensen, Ronald J., John P. Cummings, and Harshadrai Vora. "Copper/polyimide materials system for high performance packaging." *Components, Hybrids, and Manufacturing Technology, IEEE Transactions on* 7.4 (1984): 384-393.

[60] Kazarian, Sergei G., and KL Andrew Chan. "ATR-FTIR spectroscopic imaging: recent advances and applications to biological systems." *Analyst*138.7 (2013): 1940-1951.

[61] Maurer, M. L., A. C. Tooker, and S. H. Felix. *Characterization of polyimide via FTIR analysis*. No. LLNL-TR-659320. Lawrence Livermore National Laboratory (LLNL), Livermore, CA, 2014.

[62] Pryde, C. A. "FTIR studies of polyimides. II. Factors affecting quantitative measurement." *Journal of Polymer Science Part A: Polymer Chemistry* 31.4 (1993): 1045-1052.

[63] "Shadow Masks- Stanford Nanofabrication Facility" [Online]. Available: https://snf.stanford.edu/SNF/processes/other-resources/shadow-masks

[64] Takano, Nao, Lianne M. Doeswijk, Marc AF van den Boogaart, Janko Auerswald, Helmut F. Knapp, Olivier Dubochet, Thomas Hessler, and Jürgen Brugger. "Fabrication of metallic patterns by microstencil lithography on polymer surfaces suitable as microelectrodes in integrated microfluidic systems." *Journal of Micromechanics and Microengineering* 16, no. 8 (2006): 1606.

[65] Apanius, Matt, Pankaj B. Kaul, and Alexis R. Abramson. "Silicon shadow mask fabrication for patterned metal deposition with microscale dimensions using a novel corner compensation scheme." *Sensors and Actuators A: Physical* 140.2 (2007): 168-175.

[66] Brugger, J., Andreoli, C., Despont, M., Drechsler, U., Rothuizen, H., & Vettiger, P. (1999). Self-aligned 3D shadow mask technique for patterning deeply recessed surfaces of micro-electro-mechanical systems devices. *Sensors and Actuators A: Physical*, *76*(1), 329-334.

[67] Handbook, Metals. "Vol. 1." *Properties and Selection: Irons, Steels, and High-Performance Alloys* (1990): 758-79.

[68] Baer, Thomas M., and Mark S. Keirstead. "Nd-YAG laser." U.S. Patent No. 4,653,056. 24 Mar. 1987.

[69] “Mask aligner-Idonus” [Online]. Available: http://www.idonus.com/index.php?menu=products&submenu=shadow_mask_aligner

[70] Takase, I., Kono, K., Tamura, A., Nishio, H., Dote, T., & Suzuki, K. (2004). Fatality due to acute fluoride poisoning in the workplace. *Legal medicine*,*6*(3), 197-200.

[71] Einstein, Albert. "Zur quantentheorie der strahlung." *Physikalische Zeitschrift*18 (1917).

[72] Sadoqi, M., S. Kumar, and Y. Yamada. "Photochemical and photothermal model for pulsed-laser ablation." *Journal of thermophysics and heat transfer*16.2 (2002): 193-199.

[73] Bozsóki, István, Bálint Balogh, and Péter Gordon. "355nm nanosecond pulsed Nd: YAG laser profile measurement, metal thin film ablation and thermal simulation." *Optics & Laser Technology* 43.7 (2011): 1212-1218.

[74] Illyefalvi-Vitéz, Zsolt. "Laser processing for microelectronics packaging applications." *Microelectronics Reliability* 41.4 (2001): 563-570.

[75] Van Steenberge, Geert, Peter Geerinck, Steven Van Put, Jan Van Koetsem, Heidi Ottevaere, Danny Morlion, Hugo Thienpont, and Peter Van Daele. "MT-compatible laser-ablated interconnections for optical printed circuit boards." *Lightwave Technology, Journal of* 22, no. 9 (2004): 2083-2090.

[76] Stafe, M., Negutu, C., Puscas, N. N., & Popescu, I. M. (2010). Pulsed laser ablation of solids. *Rom. Rep. Phys*, *62*(4).

[77] Zhang, H., Simenson, G., Hainsey, R., Barsic, D., Howerton, J., Crowther, W., & Leonard, P. (2013). *U.S. Patent No. 8,379,679*. Washington, DC: U.S. Patent and Trademark Office.

[78] Zakariyah, Shefiu S., Paul P. Conway, David A. Hutt, David R. Selviah, Kai Wang, Hadi Baghsiahi, Jeremy Rygate, Jonathan Calver, and Witold Kandulski. "Polymer optical waveguide fabrication using laser ablation." In *Electronics Packaging Technology Conference, 2009. EPTC'09. 11th*, pp. 936-941. IEEE, 2009.

[79] Shin, B. S., J. Y. Oh, and H. Sohn. "Theoretical and experimental investigations into laser ablation of polyimide and copper films with 355-nm Nd: YVO 4 laser." *Journal of materials processing technology* 187 (2007): 260-263.

[80] P. B. Johnson and R. W. Christy. Optical constants of transition metals: Ti, V, Cr, Mn, Fe, Co, Ni, and Pd, *Phys. Rev. B* **9**, 5056-5070 (1974)

[81] Tang, Guang, and Amin Abdolvand. "Structuring of titanium using a nanosecond-pulsed Nd: YVO4 laser at 1064 nm." *The International Journal of Advanced Manufacturing Technology* 66.9-12 (2013): 1769-1775.

[82] Gittard, Shaun D., and Roger J. Narayan. "Laser direct writing of micro-and nano-scale medical devices." *Expert review of medical devices* 7.3 (2010): 343-356.

[83] Miller, P. R., Aggarwal, R., Doraiswamy, A., Lin, Y. J., Lee, Y. S., & Narayan, R. J. (2009). Laser micromachining for biomedical applications. *Jom*, *61*(9), 35-40.

[84] Vogel A, Venugopalan V. Mechanisms of pulsed laser ablation of biological tissues. Chem Rev 2003;103(2):577–644. [PubMed: 12580643]

[85] Liu X, Du D, Mourou G. Laser ablation and micromachining with ultrashort laser pulses. IEEE JQuant Electron 1997;33(10):1706–1716.••Thorough discussion of the physics of ablation with ultrashort pulsed lasers.

[86] Sutter, E. M. M., and G. J. Goetz-Grandmont. "The behaviour of titanium in nitric-hydrofluoric acid solutions." *Corrosion science* 30.4 (1990): 461-476.

[87] Seiji Ban, Yukari Iwaya, Hiroshi Kono, Hideo Sato, Surface modification of titanium by etching in concentrated sulfuric acid, Dental Materials, Volume 22, Issue 12, December 2006, Pages 1115-1120, ISSN 0109-5641, http://dx.doi.org/10.1016/j.dental.2005.09.007

[88] Wong, William S., and Alberto Salleo, eds. *Flexible electronics: materials and applications*. Vol. 11. Springer Science & Business Media, 2009.

[89] White, S. F., Turner, A. P., Schmid, R. D., Bilitewski, U., & Bradley, J. (1994). Investigations of platinized and rhodinized carbon electrodes for use in glucose sensors. *Electroanalysis*, *6*(8), 625-632.

[90] Mullen, W. H., Churchouse, S. J., Keedy, F. H., & Vadgama, P. M. (1986). Enzyme electrode for the measurement of lactate in undiluted blood. *Clinica chimica acta*, *157*(2), 191-198.

[91] Mascini, M., and G. Palleschi. "Design and applications of enzyme electrode probes." *Selective Electrode Rev* 11 (1989): 191-264.

[92] Adams, Ralph N. "Electrochemistry at solid electrodes." (1969).

[93] Klueh, U., Liu, Z., Ouyang, T., Cho, B., Feldman, B., Henning, T. P., & Kreutzer, D. (2007). Blood-induced interference of glucose sensor function in vitro: implications for in vivo sensor function. *Journal of diabetes science and technology*, *1*(6), 842-849.

[94] Cengiz, Eda, and William V. Tamborlane. "A tale of two compartments: interstitial versus blood glucose monitoring." *Diabetes technology & therapeutics* 11.S1 (2009): S-11.

[95] O'Neal, D. N., Adhya, S., Jenkins, A., Ward, G., Welsh, J. B., & Voskanyan, G. (2013). Feasibility of adjacent insulin infusion and continuous glucose monitoring via the Medtronic Combo-Set. *Journal of diabetes science and technology*, *7*(2), 381-388.

[96] Castle, Jessica R., and W. Kenneth Ward. "Amperometric glucose sensors: sources of error and potential benefit of redundancy." *Journal of diabetes science and technology* 4.1 (2010): 221-225.

[97] Cunningham, David D., and Julie A. Stenken, eds. *In vivo glucose sensing*. Vol. 174. John Wiley & Sons, 2009.

[98] Schmelzeisen-Redeker, G., Staib, A., Strasser, M., Müller, U., & Schoemaker, M. (2013). Overview of a novel sensor for continuous glucose monitoring. *Journal of diabetes science and technology*, *7*(4), 808-814.